Centre for Computational Geostatistics (CCG)
Guidebook Series Vol. 3

Guide to SAGD (Steam Assisted Gravity Drainage) Reservoir Characterization Using Geostatistics

C.V. Deutsch
J.A. McLennan

Centre for Computational Geostatistics (CCG)
Guidebook Series

Volume 1. Guide to Geostatistical Grade Control and Dig Limit Determination

Volume 2. Guide to Sampling

Volume 3. Guide to SAGD (Steam Assisted Gravity Drainage) Reservoir Characterization Using Geostatistics

Volume 4. Guide to Recoverable Reserves with Uniform Conditioning

Volume 5. User's Guide to Alluvsim Program

Published by Centre for Computational Geostatistics
3-133 Markin/CNRL Natural Resources Engineering Facility,
Edmonton, AB, Canada T6G 2W2

http://www.uofaweb.ualberta.ca/ccg/

TABLE OF CONTENTS

ABSTRACT

The application of SAGD will become increasingly important in northern Alberta because of the vast resources/reserves accessible with this production mechanism. Quantitative reservoir characterization of McMurray formation facies and petrophysical properties is required for uncertainty assessment, well placement and production performance prediction. This guidebook was launched to address this need. We plan on expanding this documentation and the associated programs to ultimately provide a comprehensive toolbox for characterizing McMurray-type formations. At present, this is just a "taste" of what is to come. Members of the Centre for Computational Geostatistics (CCG) have full access to the report and associated presentations, programs and some help. All others are encouraged to join the CCG.

1 INTRODUCTION

Conventional crude oil reserves in Canada have been declining since the late 1960's. At the same time, Canadian offshore ventures are very costly to develop. Canada, threatened with a growing requirement for funds to purchase foreign oil, became more reliant on Alberta's immense heavy oil and bitumen resources, in particular, the Athabasca oil sands deposit (also referred to as the McMurray formation). Located in Northern Alberta, the Athabasca oil sands deposit spans 40,000 square kilometers and contains 140 billion cubic meters or one trillion barrels of original bitumen-in-place. This amount comprises two-thirds of Alberta's total oil reserves and 20% of Canada's.

In the past thirty years, oil sands have gone from 2% to 30% of Canada's total annual oil production. Syncrude Canada Ltd. and Suncor Inc., using surface mining techniques up to depths of approximately 130 meters, are currently extracting and producing approximately 22% of this 30% just North of Fort McMurray. However, a mere 10% of the Athabasca oil reserve, that is, only 14 billion cubic meters, is located sufficiently close to the surface to allow the continued use of economical surface mining methods. The demand for innovative oil sands extraction technology to recover the deeper oil sands is high. Expanded production of oil sands bitumen will be essential in maintaining Alberta's role as the major Canadian source of crude oil in the 21st century.

1.1 TIMELINE

Government, researchers and industry have undertaken many steps since the late 1960's to meet the demand for new oil sands extraction processes. Refer to Figure 1.1 for an illustration of an applicable timeline. In 1974, the Alberta government created a crown corporation with the specific mandate of, in cooperation with researchers and industry, developing new oil sands exploitation technologies: the Alberta Oil Sands Technology and Research Authority (AOSTRA). One of the main targets of AOSTRA was that part of the Athabasca oil sands that could not be recovered using surface mining techniques. In 1986, the Alberta Department of Energy (ADOE) took over AOSTRA's role in developing oil sands technology; then, in August 2000, ADOE's oil sands research initiatives and programs were consolidated by the Alberta Energy Research Institute (AERI).

In 1978, Dr. Roger Butler, Chemical Engineering Ph.D. from the Imperial College of Science and Technology (1951) and holder of the Endowed Chair of Petroleum Engineering at the University of Calgary from 1983 to 1995, introduced the concept of Steam Assisted Gravity Drainage (SAGD). AOSTRA, the Alberta petroleum industry and government quickly supported SAGD as a promising innovation in oil sands extraction technology. Today, it is proposed that more than one-third of the Athabascan oil sands' bitumen-in-place can be recovered using SAGD.

In 1984, the Underground Test Facility (UTF) was initiated by AOSTRA as an in-situ SAGD bitumen recovery facility. The facility was owned and operated by ten industrial

participants and received ample government support. The SAGD process and its commercial viability have been confirmed at this site. Currently, at least 20 oil companies are invested in SAGD pilot and commercial projects across the world that total near $1 billion.

During the mid 1990's, many organizations worked to bridge the gap between industrial challenges and research and development (R&D) involving innovative bitumen-in-place extraction and treatment technology. For example, the Canadian Oil Sands Network for Research and Development (CONRAD) was created in 1994. The Petroleum Technology Alliance of Canada (PTAC) was founded in 1996. Similarly, the CANMET Western Research Centre (CWRC), the Advanced Separation Technologies institution (AST), the National Centre for Upgrading Technology (NCUT) and the Alberta Department of Energy (ADOE)/Alberta Research Council (ARC) Core Industry (AACI) were also created in the 1990's. SAGD is a major part of all of these organization's transactions and goals.

1.2 THE STEAM ASSISTED GRAVITY DRAINAGE (SAGD) PROCESS

SAGD is a thermal in-situ heavy oil recovery process. The procedure is applied to multiple well pairs. The well pairs are drilled horizontal, parallel and vertically aligned with each other; their length and vertical separation are on the order of 1 kilometer and 5 meters, respectively. The upper well is known as the "injection well" and the lower well is known as the "production well". The process begins by circulating steam in both wells so that the bitumen between the well pair is heated enough to flow to the lower production well. The freed pore space is continually filled with steam forming a "steam chamber". The steam chamber heats and drains more and more bitumen until it has overtaken the oil-bearing pores between the well pair. Steam circulation in the production well is then stopped and injected into the upper injection well only. The cone shaped steam chamber, anchored at the production well, now begins to develop upwards from the injection well. As new bitumen surfaces are heated, the oil lowers in viscosity and flows downward along the steam chamber boundary into the production well by way of gravity. Figure 1.2 illustrates the concept with a typical well pair.

Steam is always injected below the fracture pressure of the rock mass. Also, the production well is often throttled to maintain the temperature of the bitumen production stream just below saturated steam conditions to prevent steam vapor from entering the well bore and diluting oil production – this is known as the SAGD "steam trap". The SAGD process is able to economically recover 55% of the original bitumen-in-place. There are many other engineering considerations for SAGD such as recovery rate, thermal efficiency, the capability and economics of drilling horizontal well pairs, steam quality, steam injection rate, steam pressure, minimizing sand production, reservoir pressure maintenance and water intrusion; however, their importance is not key to the purpose of this report, which is to describe how to characterize a potential SAGD reservoir using geostatistics.

SAGD offers a number of advantages in comparison with conventional surface mining extraction techniques and alternate thermal recovery methods. For example, SAGD offers significantly greater per well production rates, greater reservoir recoveries, reduced water treating costs and dramatic reductions in SOR.

1.3 THE UNDERGROUND TEST FACILITY (UTF)

The Underground Test Facility (UTF) was initiated in 1984 by AOSTRA, later known as ADOE and currently the AERI. The UTF site is located approximately 60km North-West of Fort McMurray, Alberta, Canada, see Figure 1.3. This is just a few kilometers West of Syncrude Canada Ltd. and Suncor Inc.'s surface mining operations. Drilling the horizontal wells and conducting the SAGD tests from underground meant less capital cost and minimal environmental impact. The purpose of this facility is to validate SAGD's physical process, commercial viability and ancillary operations, e.g., drilling horizontal wells. The UTF consists of two vertical shafts 3.3m in diameter penetrating 140m of overburden, 20m of oil sands and 15m of limestone. Within the solid limestone formation, a horseshoe-shaped horizontal tunnel 5m wide and 4m high was excavated. From these tunnel walls, horizontal wells were drilled upward through the limestone sequence then horizontal through the lower pay zone of the oil sands. Figure 1.4 illustrates the setup.

There were multiple phases to the UTF operation. The first phase in 1987, "Phase A", sought to validate only the physical process of SAGD. Three horizontal well pairs, horizontally separated by 25m and 60m in length, were drilled for this phase. The test was successful. The second phase, "Phase B", aimed to prove the SAGD process on a commercial scale. For this phase, three well pairs, horizontally and vertically separated by 70m and 4m, respectively, and 600m in length, were drilled from underground into the base of the oil sands pay zone. These wells were successfully operated for approximately 10 years at better than predicted production outputs. UTF's "B Wells" also successfully exhibited the steam trap mechanism. By the mid 1990's, horizontal well drilling and completion had gained much experience in drilling from the surface; "Phase D" involved drilling two horizontal SAGD well pairs 650m in length and 6m in vertical separation from the surface with a slant-drilling rig. This phase was only partially successful. One well pair was successfully completed to its specifications; but problems were encountered in placing the liner in the second well pair. However, the two SAGD well pairs were still put into operation successfully. In 1997, the second well pair was repaired and production significantly improved.

1.4 GEOLOGY OF THE ATHABASCA OIL SANDS

About 100 million years ago, streams containing sand and mud, flowed from the Rocky Mountains in the West and from the Precambrian Shield in the East into the Prairie Provinces such as Alberta and Saskatchewan. The stream runoff formed a massive inland sea. The sand and mud was spread relatively flat throughout the sea, except on the

shores where sand preferentially accumulated. These sediments were covered by other sediments, buried and lithified. Although there is debate, popular opinion among geologists suggests that the oil came from somewhere else, more specifically, highly organic Cretaceous shale in the southern portion of the Alberta Sedimentary Basin. The deposit's cap rock consists mostly of marine shale, and at times tidal flat sediments, known in the Athabasca region as the "Cleanwater Formation".

The Athabascan oil sands are composed of approximately 70% sand and clay, 10% water and anywhere from 0 to 18% heavy oil or bitumen. Unlike conventional oil, the oil sands contain a mixture of bitumen, sand, clay and water. A thin film of water, which contains trace amounts of clay, iron, vanadium and titanium, surrounds each sand particle. The viscous oil called bitumen then surrounds the water skin and sand particle. The oil sands must be specifically treated in order to remove the bitumen from the sand. Syncrude, for example, first removes the majority of the sand and clay via a hot water washing process, and then the resulting froth is diluted with a hydrocarbon mixture that settles water and solids and suspends the viscous bitumen.

Figure 1.5 shows a few of the geological specifications and statistics applicable to the UTF region. There are several companies that have invested in the Athabasca oil sands deposit, each with a different lease property and, therefore, slightly different geological specifications.

1.5 GEOSTATISTICAL CHARACTERIZATION OF POTENTIAL SAGD RESERVOIRS

Geological heterogeneities are impossible to exactly predict between wells. Uncertainty is an unavoidable characteristic of any geological model, that is, the unique true distribution of lithofacies and petrophysical properties between wells will remain unknown. Geostatistics allows the construction of multiple realizations that can be combined into a model of uncertainty. This geological uncertainty is transferred into production uncertainty, that is, uncertainty in production variables such as the cumulative SOR and oil production rate over time.

The main advantage of using geostatistics is the capability to access production uncertainty on the basis of geological uncertainty. Multiple geostatistical realizations of lithofacies and petrophysical properties, conditional to exploratory core hole data, are constructed to assess geological uncertainty. These realizations are then input into the "transfer function", that is, flow simulation, which provides realizations of SOR and oil production rate. Access to production uncertainty allows better SAGD developmental decisions to be made such as the number and location of horizontal well locations. The value of additional delineation information such as infill wells or seismic data can also be assessed.

Using geostatistics, it is possible to identify regions of a reservoir with the greatest SAGD potential, aid in selecting the optimal number of SAGD wells to put into

production and assess the value of additional delineation information. A geological ranking system that is correlated to production variables such as SOR and oil production rate can be used to choose optimal well locations. An analysis of production uncertainty, derived from geological uncertainty and flow simulation, will aid in the selection of the optimal number of SAGD wells. The entire process can be repeated with more or different conditioning data to assess the value of additional or different information.

Although there are many sources of production uncertainty, geological uncertainty is perhaps the most significant contributor.

This report is intended to be a guide to SAGD reservoir characterization using geostatistics. The main steps of the geostatistical study are (1) geological structure and gridding analysis, (2) preliminary statistical analysis, (3) variography, (4) construction of multiple realizations, (4) post-processing and ranking these realizations for flow simulation. Further work entails flow simulation on selected realizations, calibration of flow responses to geological ranking and an uncertainty analysis. These main steps are very clear and unambiguous; however, there are several details that need to be addressed along the way.

Each detail and step of the geostatistical procedure will be described and carried out on some data in this guidebook. The guidebook will grow in time to become more comprehensive.

1.6 FIGURES

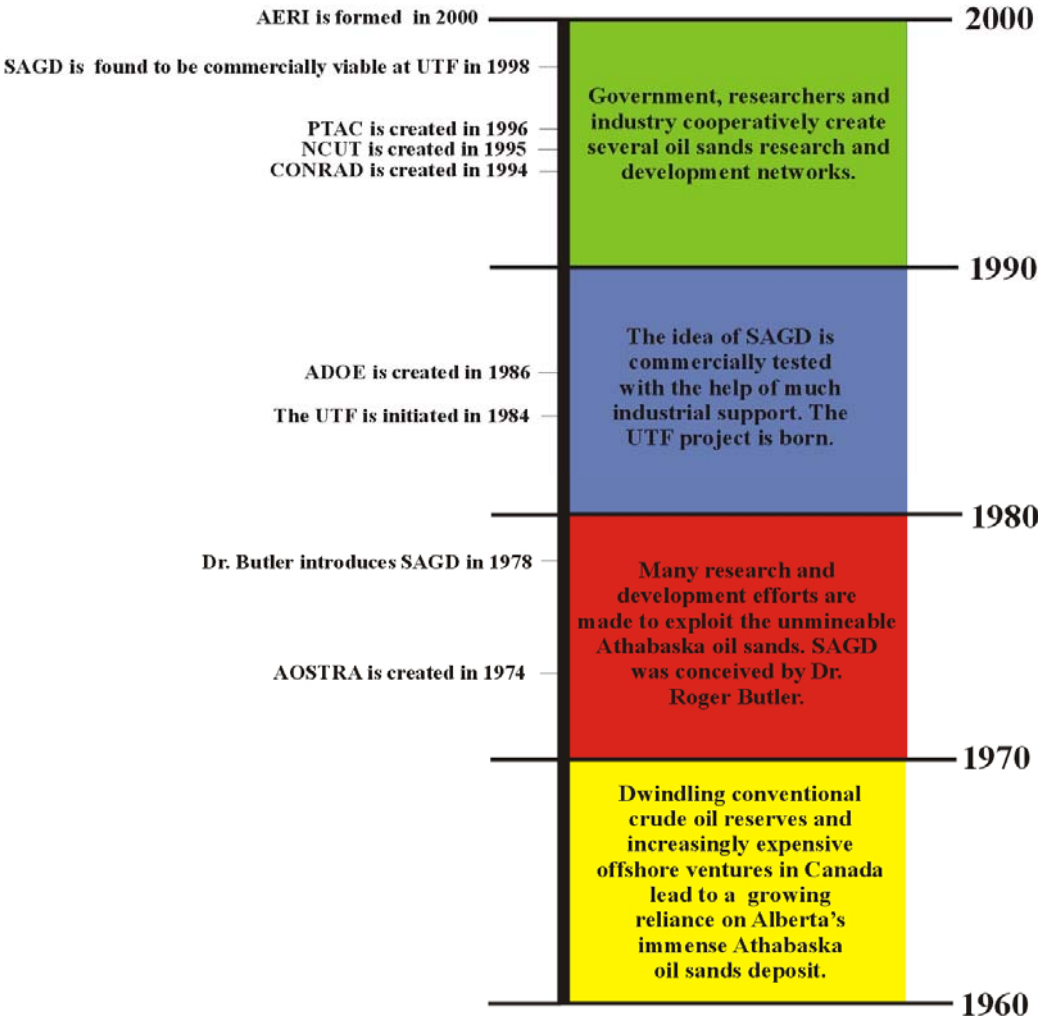

Figure 1.1 – SAGD Timeline. Highlights concerning the growth of SAGD technology. The colored right side of the vertical bold line describes four 10 year decades from 1960 to 2000. On the left are some specific dates within the decade blocks.

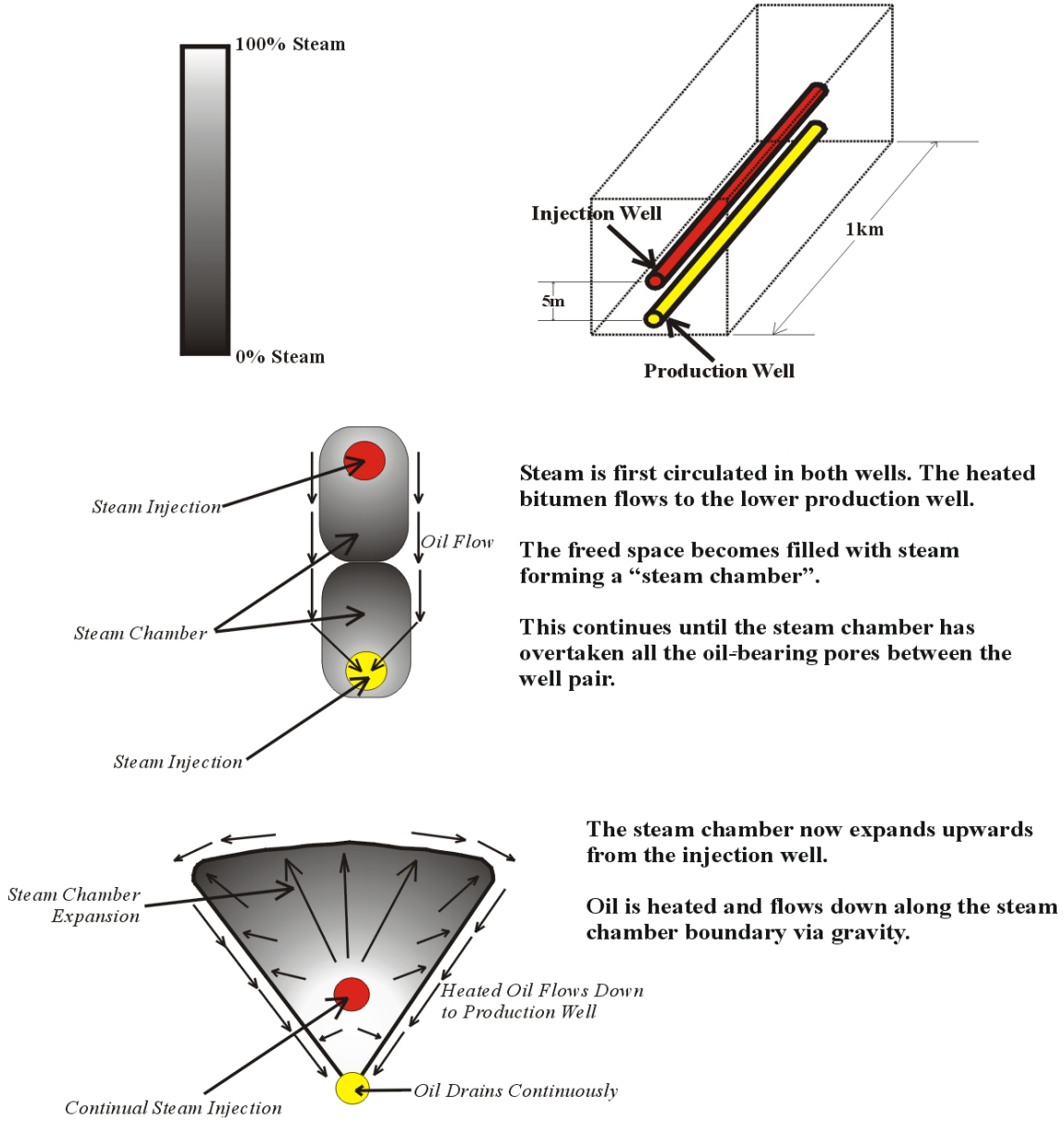

Figure 1.2 – The Steam Assisted Gravity Drainage (SAGD) Process. Schematic illustration of the physical SAGD process. Steam concentration is depicted on the grayscale shown in the top left; the setting, including the horizontal well dimensions, is shown in the top right. The middle illustrates the initial stage of SAGD when steam is injected into both wells and the steam chamber begins to form. The bottom shows the overriding SAGD mechanics when steam is injected into the injection well only and a cone shape steam chamber develops from the injection well anchored at the production well.

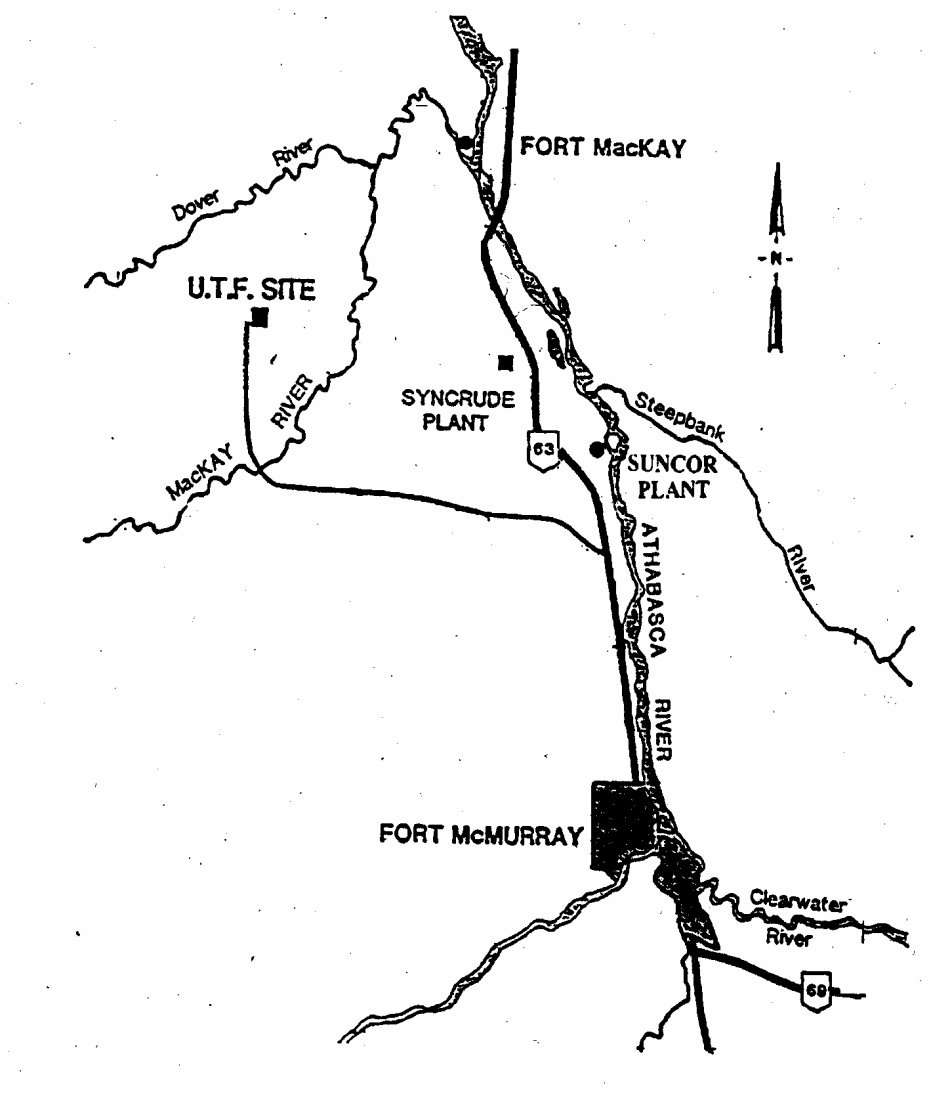

Figure 1.3 – UTF Location. Map showing the location of the Underground Test Facility (UTF). (Source: *Pilot Testing of Post-Steam Bitumen Recovery from Mature SAGD Wells in Canada*, 1998)

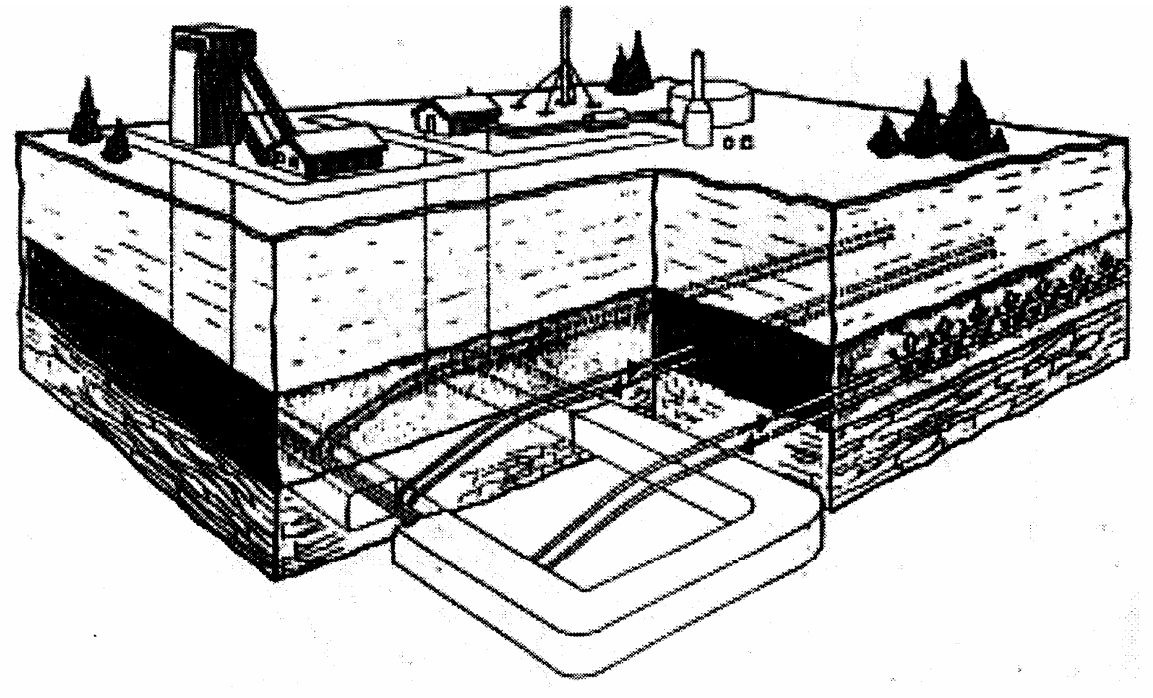

Figure 1.4 – UTF. Schematic illustration of the Underground Test Facility (UTF) in its preliminary stages. (Source: *Pilot Testing of Post-Steam Bitumen Recovery from Mature SAGD Wells in Canada*, 1998)

Parameter	Value
Depth from Surface	125 to 175m
Net Pay Thickness	15 to 20m
Sand Porosity	35%
Sand Permeability	5 to 12 Darcy
Bitumen Saturation	85%
Bitumen Viscosity (70^0C)	5×10^6 cp
Weight % Bitumen	16%
API Gravity	8^0

Figure 1.5 – UTF Geology. Summary of some important geological parameters applicable to the UTF site.

2 THE EXAMPLE

Synthetic data modeled after real data are considered for a potential Steam Assisted Gravity Drainage (SAGD) project. The reservoir dimensions and exploratory core hole data certainly fall within the range of actual projects.

The idea is to some horizontal SAGD well pairs at optimum locations. Additional delineation information will improve SAGD well pair planning by decreasing the production uncertainty, that is, fewer well pairs in better locations would need to be drilled for the same production performance. A balance must be struck between the cost of additional delineation information and the cost of lost production opportunity.

The McMurray formation's geological structure is fairly well known. This deterministic knowledge, combined with our geostatistical analysis of the available core hole data, allow for an improved understanding of the geological model. However, it is the geological uncertainty in facies and petrophysical that contribute the most to uncertainty in production performance.

The primary production variables depend on the distribution of facies, for example, shale and oil-bearing sand, porosity and other reservoir characteristics such as sand connectivity. Geostatistics is used with vertical core hole data (and available seismic) to extrapolate these reservoir characteristics into a full geological model and quantify the uncertainty associated with these extrapolations.

The connectivity of the geostatistical realizations can be calculated to give an appreciation of the production potential (and uncertainty) at different locations in the reservoir. This "static" connectivity can be calculated without resorting to full flow simulation. Nevertheless, flow simulation is required to assess dynamic reservoir performance.

Computer resource demands to perform flow simulation is high. The calculations are complex and require detailed input rock, fluid and pressure properties. We limit the flow simulation input by selecting only a few geostatistical realizations to input into the flow simulator. The selection of these realizations is done via a geological ranking or geological "goodness" system. The production responses can also be calibrated to this geological measure in order to infer the flow responses for all realizations at all locations. Of course, this entails some additional production uncertainty.

An analysis of the production uncertainty will allow us to determine the optimum number and location of SAGD well pairs for a specified production goal.

2.1 THE DATA

There are 20 exploration core holes that populate a regular 400 x 400m grid, see Figure 2.1. There are 4 core holes in the Easting direction and 5 core holes in the

Northing direction spanning an area 1600m East-West by 2000m North-South. The core holes are vertical measurements reported at 10cm depth increments to avoid losing important vertical heterogeneity. The data start where a reliable oil-bearing facies such as sand or interbedded sand is observed. Similarly, they stop where consistent impermeable shales are observed. Therefore, the top and bottom of the McMurray formation and the top and bottom of our model is not the same. Figure 2.2 shows a schematic Elevation-Easting section through the reservoir showing the relative positions of these surfaces and the core holes.

Because the data follow a regular grid specification, declustering for representative statistics is not necessary.

For each 10cm increment, there are eight variable values: *Nch* – the core hole number (shown in Figure 2.1), *X* – the Easting coordinate, *Y* – the Northing coordinate, *Z* – the elevation coordinate, *Fcs* – the facies type code (there are four facies with codes from 1 to 4), *Por* – the porosity as a percent, *OilSat* – the oil saturation as a percent, and *GasSat* – the gas saturation as a percent. Figure 2.3 illustrates these seven variable values for core hole number 9 (*Nch* = 9).

The core hole data was formatted into an ASCII file compatible with the GSLIB software. In ASCII format, the first lines need to contain (1) a title, (2) the number of columns and (3) a label for each of the columns. Figure 2.4 shows the first lines of the ASCII data file used in this example. The title of the data file is “Core Hole Data”, the number of columns is eight (each variable is placed in a separate column) and the column labels are the same as the variable names discussed in the previous paragraph. The remaining lines contain the values of the eight variables.

2.2 GEOSTATISTICAL METHODOLOGY

All of the geostatistical modeling is done using GSLIB related software. The output models from GSLIB are also in ASCII format. For visualization and validation, the geostatistical models were imported into the GoCad software.

The main steps for geostatistical modeling are (1) create top, bottom and thickness structure models, (2) establish a suitable reservoir grid and vertical coordinate system, (3) determine the basic statistical characteristics of the data variables, (4) establish a 3-Dimensional model of covariance/correlation within the reservoir structure model for each variable, and (5) create multiple realizations of each variable conditional to all available data.

After the main geostatistical modeling is complete and multiple realizations of each variable have been created, there are additional steps that need to be taken to characterize the reservoir for SAGD potential. These are (1) post-processing for geological ranking (2) model extraction and regridding for flow simulation, (3) perform flow simulation for SOR and oil production rate, (4) calibrate SOR and oil production rate to the geological

ranking measure and (5) decide on the number and placement of SAGD wells based on an uncertainty analysis.

The purpose of this report is to describe a geostatistical procedure to characterize potential SAGD reservoirs. Although flow simulation is part of the overall SAGD characterization procedure, it will not be performed on the example presented in this guidebook

The main steps of the geostatistical SAGD reservoir characterization procedure are now outlined. Subsequent sections will describe each step in detail and illustrate the results using the example.

2.2.1 STRUCTURE MODELING

The first step in any reservoir modeling process is to establish the large scale geological structure. A top, bottom and thickness model are required to define the limits of the hydrocarbon bearing formation and our subsequent reservoir "volume". These surfaces, however, are impossible to predict without uncertainty. A geostatistical procedure will be used to quantify the uncertainty in extrapolating the available surface elevation data. The established or reservoir volume is then filled with an appropriate grid network, which is then populated with variables such as lihtofacies, porosity and permeability.

2.2.2 GRIDDING AND THE VERTICAL COORDINATE SYSTEM

The reservoir volume must be gridded to conform to large scale geological structure and available software. Geostatistical software, including GSLIB, largely implements Cartesian-based grids. The number and size of cells is a balance between computational resources and the required detail of heterogeneity.

A stratigraphic vertical coordinate that makes it possible to calculate natural measures of correlation and preserve the overall geological structure must be decided on. Such stratigraphic coordinates capture our deterministic knowledge of the overall structural correlation within the reservoir volume accounting for structural deformation, differential compaction, erosion and onlap geometry.

2.2.3 BASIC STATISTICAL CHARACTERISTICS

It is helpful to investigate some of the basic statistical relationships of the variables that will be subsequently extrapolated throughout the reservoir model. Histograms can illustrate the basic behavior of certain variables and validate data collection practices. For example, a histogram of porosity will be bimodal when there are low porosity shales and higher porosity sands.

2.2.4 FACIES MODELING

Once the structure modeling is complete with an appropriate grid system, the lithofacies are modeled. Multiple 3-D realizations of the facies type codes are created using indicator simulation. The amount of exploratory core hole data allows the use of a locally varying mean.

There are a variety of facies modeling techniques broadly grouped into object-based modeling and cell-based modeling. Indicator simulation is a cell-based technique that has proven applicable when it is not possible to infer simple clean shapes for object-based modeling.

A number of inputs are required to run the lithofacies simulation. The simulation needs the original core hole data with the column of facies type codes, a 3-D grid specification, a 3-D variogram model for each of the four facies types and a 3-D proportion trend model.

2.2.5 PETROPHYSICAL PROPERTY MODELING

The procedure is similar to facies modeling. Multiple 3-D realizations of porosity are created using the original core hole data, a 3-D grid specification, 3-D variogram models and 3-D trends.

The fact that the characteristics of petrophysical properties vary depending on which lithofacies they are found in needs to be dealt with. The final model of each petrophysical property will, therefore, be derived by (1) creating a 3-D variogram model within each facies, (2) creating a 3-D trend model within each facies and (3) simulate each cell accounting for the collocated facies type and trend value.

2.2.6 POST PROCESSING AND CONNECTIVITY

Each set of structure, facies and petrophysical property parameter realizations constitute a single “geological realization”. These multiple geological realizations are then used for calculating various resource assessment parameters. The geological uncertainty is directly transferred into resource parameter uncertainty, which is the fluctuation of the calculated output parameter.

Conventional resource assessment parameters are not completely satisfactory for characterizing a potential SAGD reservoir. We would like to know where and how much bitumen is going to be heated and potentially recovered by the SAGD process. These SAGD specific transfer functions are constructed with “connectivity” calculations.

2.2.7 MODEL REGRIDDING, RANKING, SAGD FLOW SIMULATION AND ANALYSIS

Although favorable SAGD areas can be located in the reservoir based on the connected resource assessment, practice dictates a regularly spaced SAGD well pair configuration so that potential reserves all have a chance to be recovered. For a potential SAGD reservoir, the transfer of geological uncertainty into dynamic production is vital. It is linked via flow simulation. Model regridding and ranking are two preliminary steps that need to be described and implemented before flow simulation. The results provide key engineering decision support.

A few preliminary procedures need to be performed on the selected location scenarios before they can be passed through as input into the flow simulator. For instance, the input scenario needs to be re-scaled to provide the detail necessary for flow simulation. The selected locations are, therefore, extracted from the reservoir model and then used as conditioning data for a finer grid simulation. It is these finely gridded versions that are input into flow simulation.

Not all of the finely gridded realizations of are passed through to flow simulation. This would require too many computing resources. Instead, a few are chosen to span the reservoir's SAGD potential. This requires a ranking parameter that is correlated to the production characteristics. The ranking parameter could be a measure of connected resources.

Flow simulation transfers geological uncertainty into production performance uncertainty. The inputs are the selected geological models at locations based on the geological ranking system, after extraction and regridding. The outputs are SOR, oil production rate and other performance measures.

The SOR production outputs can be calibrated to the geological ranking measure. This allows the flow responses to be estimated at all locations for all realizations. This calibration is the link between geological uncertainty and production performance.

If the geological ranking measure is well correlated to the production outputs, it becomes possible, on the basis of the geological ranking measure, to identify areas with the greatest SAGD potential.

Uncertainty in SAGD well production is linked to underlying geological uncertainty. Flow simulation production outputs such as SOR and oil production rate, and their calibration to the geological ranking measure, provide the link from geological uncertainty to production. This link is the key to estimating production decisions such as assessing the number of SAGD well pairs to meet a certain production target.

Additional core hole data or seismic data will decrease production uncertainty. Another geostatistical simulation exercise could be carried out to address the reduction of uncertainty due to additional delineation data. The cost of increasing the core hole density

is easily quantified (number of additional core holes multiplied by the cost of a core hole). The cost of uncertainty is, perhaps, drilling too many SAGD well pairs for the needed production or having to quickly establish new well pairs for greater production.

2.3 FIGURES

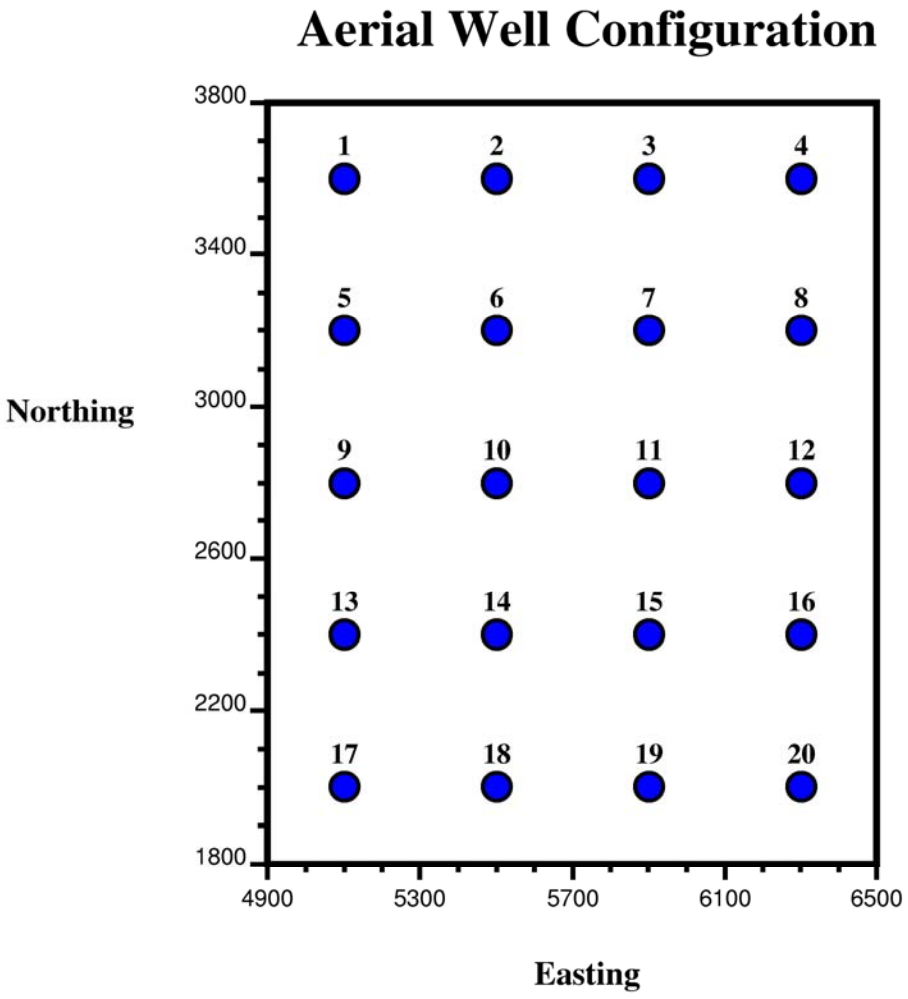

Figure 2.1 – Aerial Well Configuration. Plan view of the 20 exploratory core holes. The blue circles represent each core hole; the number is the core hole number. The core holes are spaced 400m apart in the East-West and North-South directions.

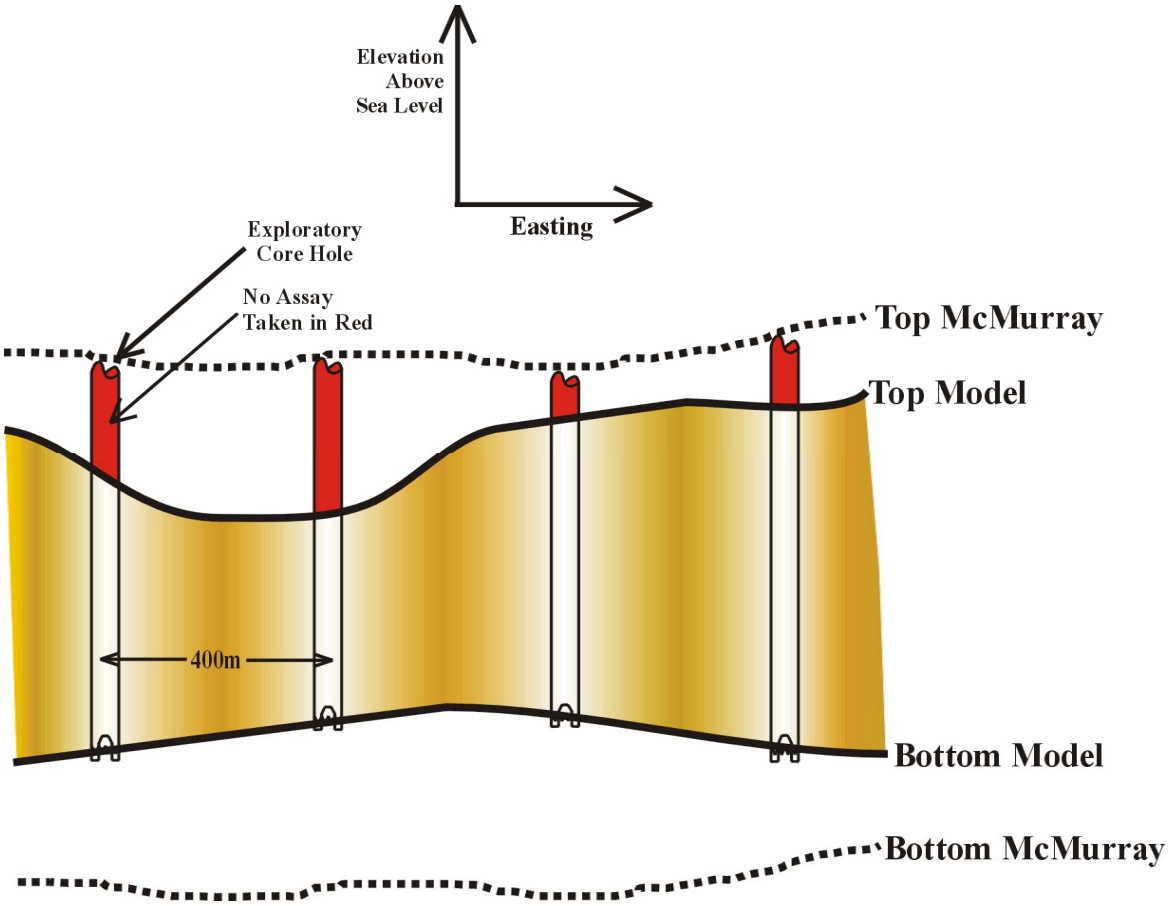

Figure 2.2 – McMurray Formation and Model Top and Bottom. Schematic Elevation-Easting section showing the relative position of the top and bottom surfaces of the McMurray formation and our structural model as well as the exploratory core holes. The red region of the core hole is where no assays were taken. The core holes are aligned with the elevation above sea level.

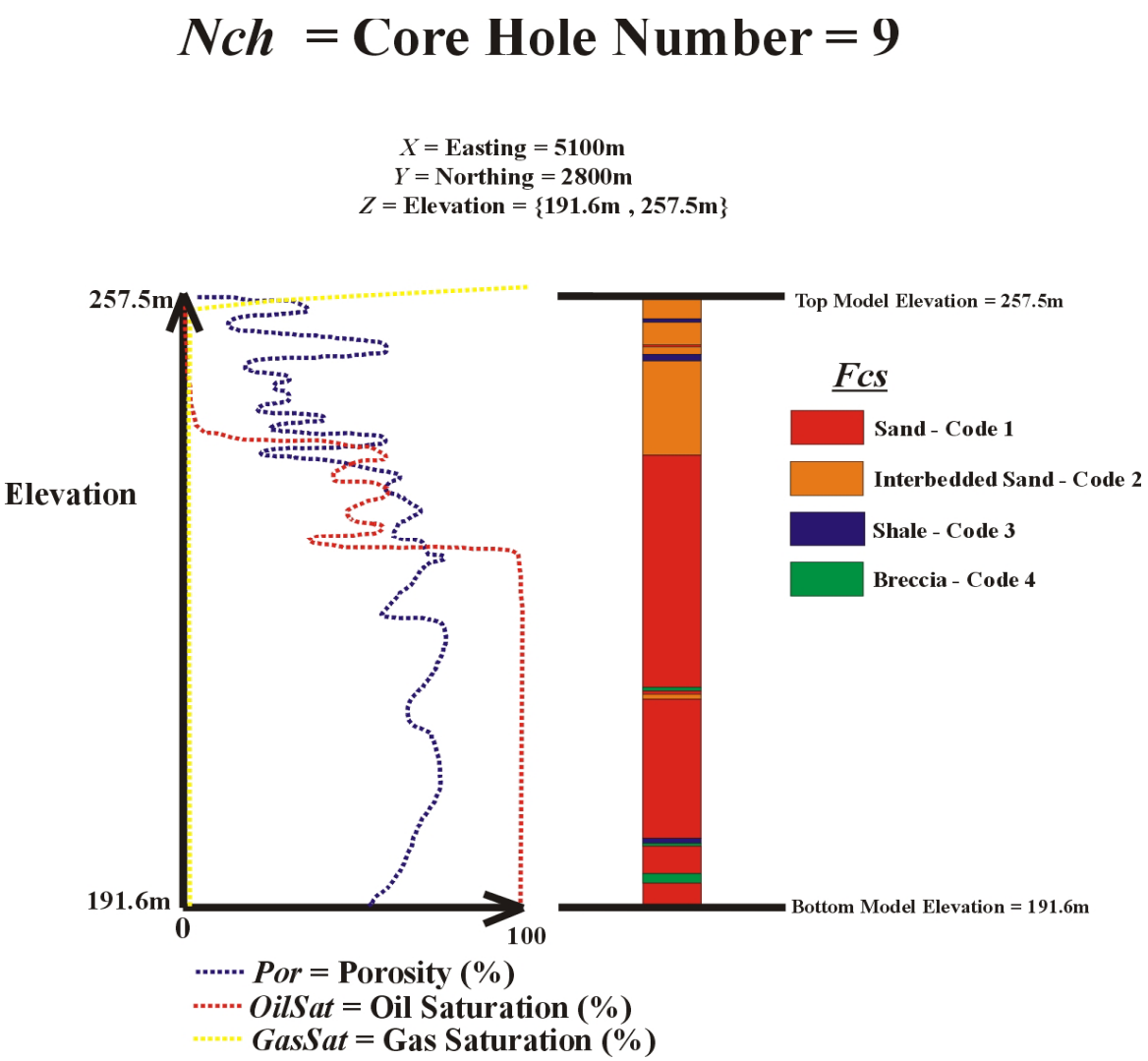

Figure 2.3 – Core Hole Number 9 Variable Values. An illustration of the seven variables and their values within core hole number 9. The *X* (Easting) and *Y* (Northing) values are 5100m and 2800m, respectively; the *Z* (Elevation) value changes each 10cm increment from 191.6m to 257.5m. To the right, the value of *Fcs* (the facies type code) is shown for all *Z*. To the left, the continuous variables *Por* (porosity in percent), *OilSat* (oil saturation in percent) and *GasSat* (gas saturation in percent) are shown for all *Z*.

```
Core Hole Data
8 [number of columns]
Nch     = Core Hole Number
X       = Easting
Y       = Northing
Z       = Elevation
Fcs     = Facies Type Code
Por     = Porosity in Percent
OilSat  = Oil Saturation
GasSat  = Gas Saturation
16 6300.000  2400.000  247.83  1  0.051  0.000  0.000
16 6300.000  2400.000  247.73  1  0.051  0.000  0.000
16 6300.000  2400.000  247.63  1  0.051  0.000  0.000
16 6300.000  2400.000  247.53  1  0.051  0.000  0.000
16 6300.000  2400.000  247.43  1  0.051  0.000  0.000
16 6300.000  2400.000  247.33  1  0.051  0.000  0.000
16 6300.000  2400.000  247.23  2  0.051  0.000  0.000
16 6300.000  2400.000  247.13  2  0.051  0.000  0.000
16 6300.000  2400.000  247.03  2  0.051  0.000  0.000
16 6300.000  2400.000  246.93  2  0.051  0.000  0.000
16 6300.000  2400.000  246.83  2  0.051  0.000  0.000
16 6300.000  2400.000  246.73  2  0.051  0.000  0.000
16 6300.000  2400.000  246.63  2  0.051  0.000  0.000
16 6300.000  2400.000  246.53  2  0.051  0.000  1.000
16 6300.000  2400.000  246.43  2  0.324  0.000  1.000
16 6300.000  2400.000  246.33  1  0.324  0.000  1.000
16 6300.000  2400.000  246.23  1  0.324  0.000  1.000
16 6300.000  2400.000  246.13  1  0.324  0.000  1.000
16 6300.000  2400.000  246.03  1  0.324  0.000  1.000
16 6300.000  2400.000  245.93  1  0.324  0.000  1.000
16 6300.000  2400.000  245.83  1  0.324  0.000  1.000
16 6300.000  2400.000  245.73  1  0.324  0.000  1.000
16 6300.000  2400.000  245.63  1  0.324  0.000  1.000
16 6300.000  2400.000  245.53  1  0.324  0.000  1.000
16 6300.000  2400.000  245.43  1  0.324  0.000  1.000
16 6300.000  2400.000  245.33  1  0.324  0.000  1.000
16 6300.000  2400.000  245.23  1  0.324  0.000  1.000
16 6300.000  2400.000  245.13  1  0.324  0.000  1.000
16 6300.000  2400.000  245.03  1  0.324  0.000  1.000
16 6300.000  2400.000  244.93  1  0.324  0.000  1.000
16 6300.000  2400.000  244.83  4  0.324  0.000  1.000
16 6300.000  2400.000  244.73  4  0.324  0.000  1.000
16 6300.000  2400.000  244.63  4  0.324  0.000  1.000
16 6300.000  2400.000  244.53  4  0.324  0.000  1.000
16 6300.000  2400.000  244.43  1  0.324  0.000  1.000
16 6300.000  2400.000  244.33  1  0.324  0.000  1.000
16 6300.000  2400.000  244.23  1  0.324  0.000  1.000
16 6300.000  2400.000  244.13  1  0.324  0.000  1.000
16 6300.000  2400.000  244.03  1  0.324  0.000  1.000
16 6300.000  2400.000  243.93  1  0.324  0.000  1.000
16 6300.000  2400.000  243.83  1  0.324  0.000  1.000
16 6300.000  2400.000  243.73  1  0.324  0.000  1.000
16 6300.000  2400.000  243.63  3  0.324  0.000  1.000
16 6300.000  2400.000  243.53  3  0.324  0.000  1.000
16 6300.000  2400.000  243.43  3  0.324  0.000  1.000
.  .          .          .       .  .      .      .
.  .          .          .       .  .      .      .
.  .          .          .       .  .      .      .
.  .          .          .       .  .      .      .
.  .          .          .       .  .      .      .
.  .          .          .       .  .      .      .
```

Figure 2.4 – The ASCII Core Hole Data File. An illustration of the main data file in ASCII format for geostatistical modeling using the GSLIB software.

3 STRUCTURE MODELING

The reservoir top and bottom are not flat and the reservoir thickness is not constant. Before geostatistical modeling of facies and petrophysical property modeling, the top and bottom surfaces of the reservoir need to be defined; thickness is the difference between the top and bottom.

Any method used to extrapolate the 20 core hole top and bottom elevations will involve uncertainty. By using geostatistics, we can quantify this uncertainty and carry it through the rest of the geostatistical characterization procedure to assess its impact on SAGD production performance. A 2-D variogram model is established using the 20 available elevation data for the top and bottom surfaces. Multiple realizations of the elevations at unsampled locations are then created. The fluctuation of these extrapolated values from realization to realization defines the structural uncertainty. To properly account for structural uncertainty in SAGD performance, each realization of the reservoir top and bottom structure is passed through the entire SAGD geostatistical procedure.

3.1 THE CONDITIONING DATA

There are 20 core hole top and bottom elevations. Figure 3.1 shows both sets of data. The top elevation data are where the first assay is taken in reliable oil bearing facies such as sand or interbedded sand, and the bottom elevation data are located just above the lower dominant impermeable shale facies.

3.2 VARIOGRAPHY

Before performing geostatistical estimation and simulation at the unsampled locations, we need to quantify the spatial correlation of the top and bottom structures. Semi-variogram calculation and modeling gives us a mathematically positive-definite correlation or covariance for all distances and directions and incorporates our knowledge about the spatial characteristics of the surfaces we are modeling.

Some implementation details: First, the variograms are calculated using the normal score values of the elevation data so that any subsequent variogram sills are 1 and in anticipation of using Gaussian geostatistical techniques for stochastic simulation. Second, after a sensitivity study, it is found that the omnidirectional variogram adequately represents all directional variograms. Third, due to the limited number of core holes, only three experimental semi-variogram points can be reliably calculated. This is often the case in hydrocarbon reservoirs where the cost of drilling exploration core holes or wells is high.

The top and bottom surface variogram models both have no nugget effect, 1 nested structure and are isotropic; the difference is in their ranges. Given in equation form, the top and bottom surface variogram models are $\gamma(\mathbf{h}) = 1.0 \cdot Guass_{a=1200}(\mathbf{h})$ and

$\gamma(\mathbf{h}) = 1.0 \cdot Guass_{a=400}(\mathbf{h})$, respectively. Smooth Gaussian type variogram structures are used to account for the inherent smoothness of the top and bottom surfaces. The final calculated and modeled surface variograms are presented in Figure 3.2.

3.3 SIMULATION

Multiple geostatistical realizations of the top and bottom surface elevations that honor all the available data are created using the *sgsim* program from the GSLIB package. The *sgsim* program implements Sequential Gaussian Simulation. 100 realizations are constructed for each surface. Although the realizations can be built at an arbitrary resolution, a 50 x 50m aerial grid is used. Therefore, there are 32 cells in the Easting (*X*) direction and 40 cells in the Northing (*Y*) direction for a total of 1,280 cells in each model. The next section describes the details and considerations involved in making this grid definition decision.

Figure 3.3 summarizes the top and bottom surface realizations. The 50th realization of each set of 100 is shown with the original conditioning data. Notice the original data is honored and the smoothness imparted into the distribution of estimates due to the smooth Gaussian variogram model. At each of the 1,280 locations, there are 100 realizations of what the top/bottom elevation could possibly be. The average at each location is calculated and also shown (labeled “Cell Averages”) in this figure.

By subtracting the bottom elevation from the top elevation, the thickness of the reservoir is obtained. This gives us 100 realizations of the thickness at each location. A histogram and map of the cell average thickness is shown in Figure 3.4. The average thickness ranges from 48.1 to 72.0m with an average of 61.2m.

Figure 3.5 shows the 10th top and bottom elevation realizations with the 20 conditioning core holes. The orientation of the picture is consistent with the previous Figures in this Section. It is apparent that thicker zones reside in the Northern area of the reservoir. Also, notice that the derrick locations where the top of the McMurray formation exists does not coincide with the model top surface elevations and the bottom of the core holes where the bottom of the McMurray formation exists, are at a greater depth than the model bottom surface elevations.

3.4 STRUCTURAL UNCERTAINTY

The structure of the reservoir affects SAGD production performance. For example, oil production is generally more optimal with a SAGD production well aerially located in a thicker part of the reservoir. By simulating the top and bottom surfaces multiple times, we have access to the reservoir’s structural uncertainty. Each realization of the structure is passed through the entire subsequent geostatistical SAGD reservoir characterization process. Part of the SAGD production uncertainty will, therefore, be due to the uncertainty in reservoir structure.

3.5 FIGURES

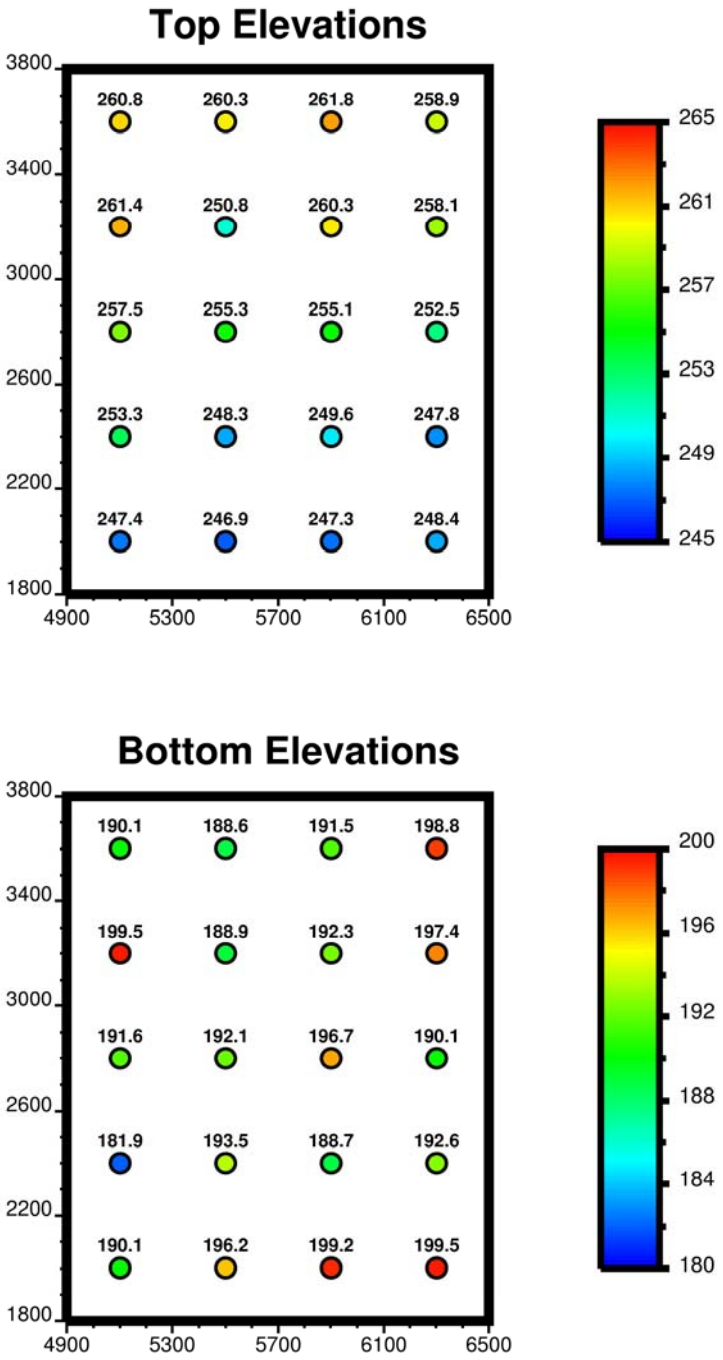

Figure 3.1 – Core Hole Top and Bottom Elevations. Plan view of the 20 core hole top and bottom elevation data. The *X* and *Y* locations can be derived from the inscribed field scale; the corresponding top and bottom elevations are color coded according to a cold-hot, that is, blue-red, color scale to the right as well as printed above each location.

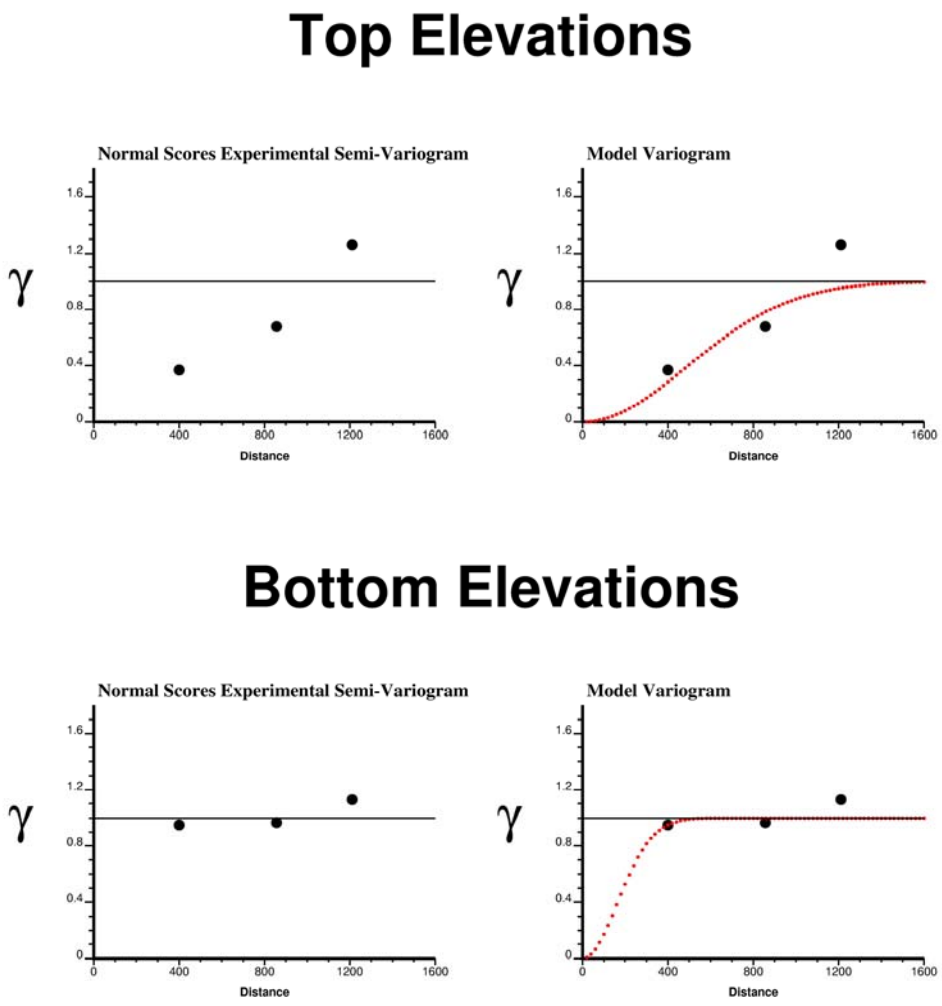

Figure 3.2 – Surface Variograms. Calculated and modeled top and bottom surface variograms. For each surface, the experimental points are shown to the left and the models over top of the experimental points are shown to the right. The calculated variograms are represented as black dots and the models as broken red lines.

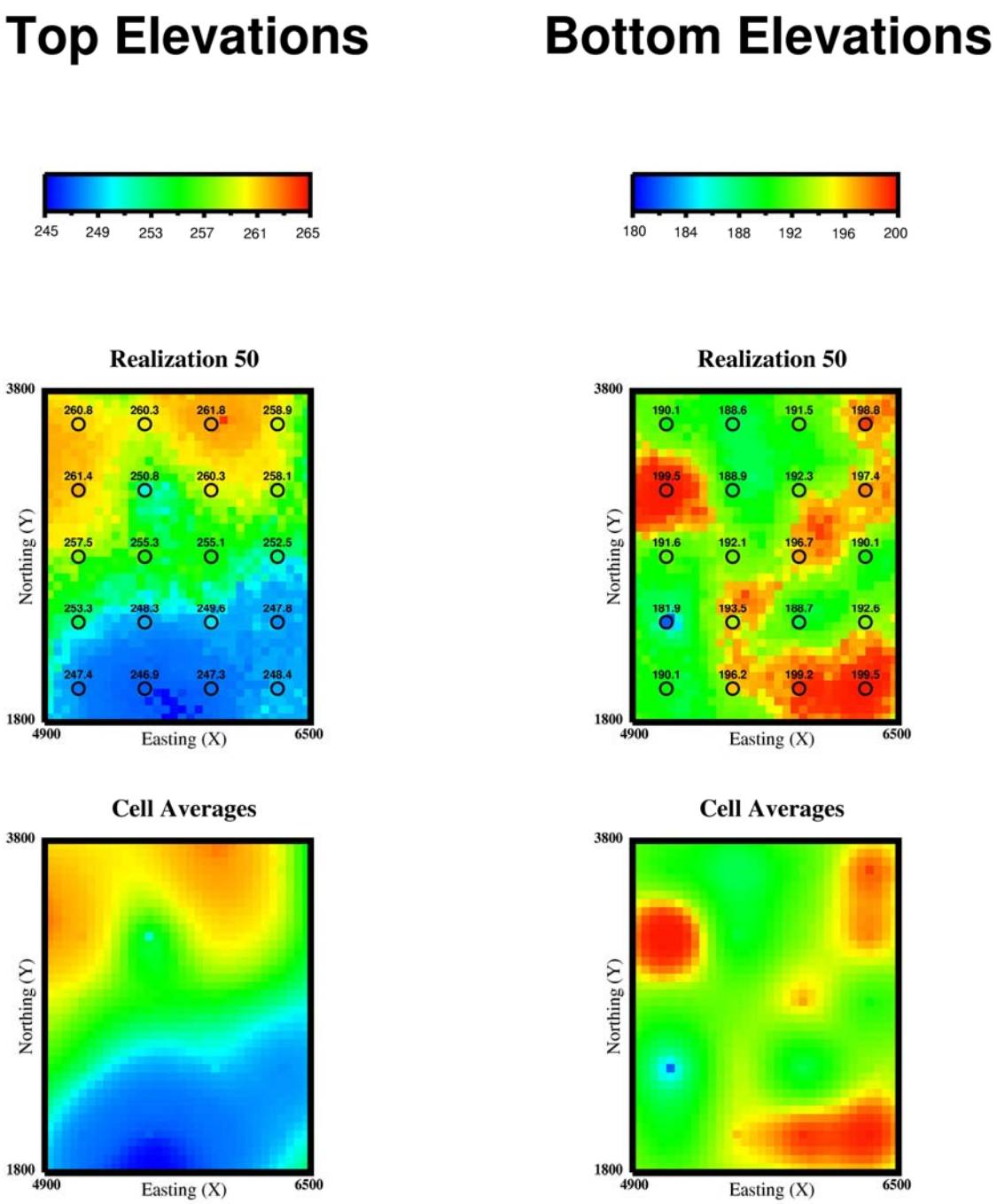

Figure 3.3 – Surface Simulation. A summary of the 100 top and bottom surface realizations. The top elevation models are shown to the left and the bottom elevation models are shown to the right. The same blue-red color scale used in Figure 3.1 is used and shown at the top of this figure. The 50th top and bottom realizations are shown as well as the top and bottom surface cell averages.

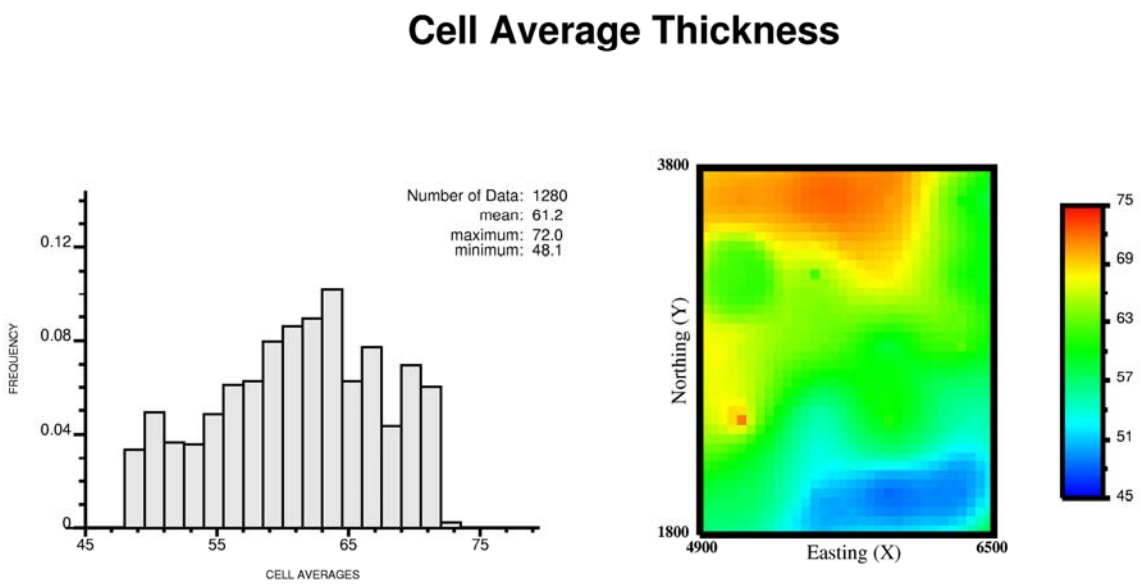

Figure 3.4 – Thickness. A summary of the structural thickness realizations. A histogram and map of the thickness cell averages is shown.

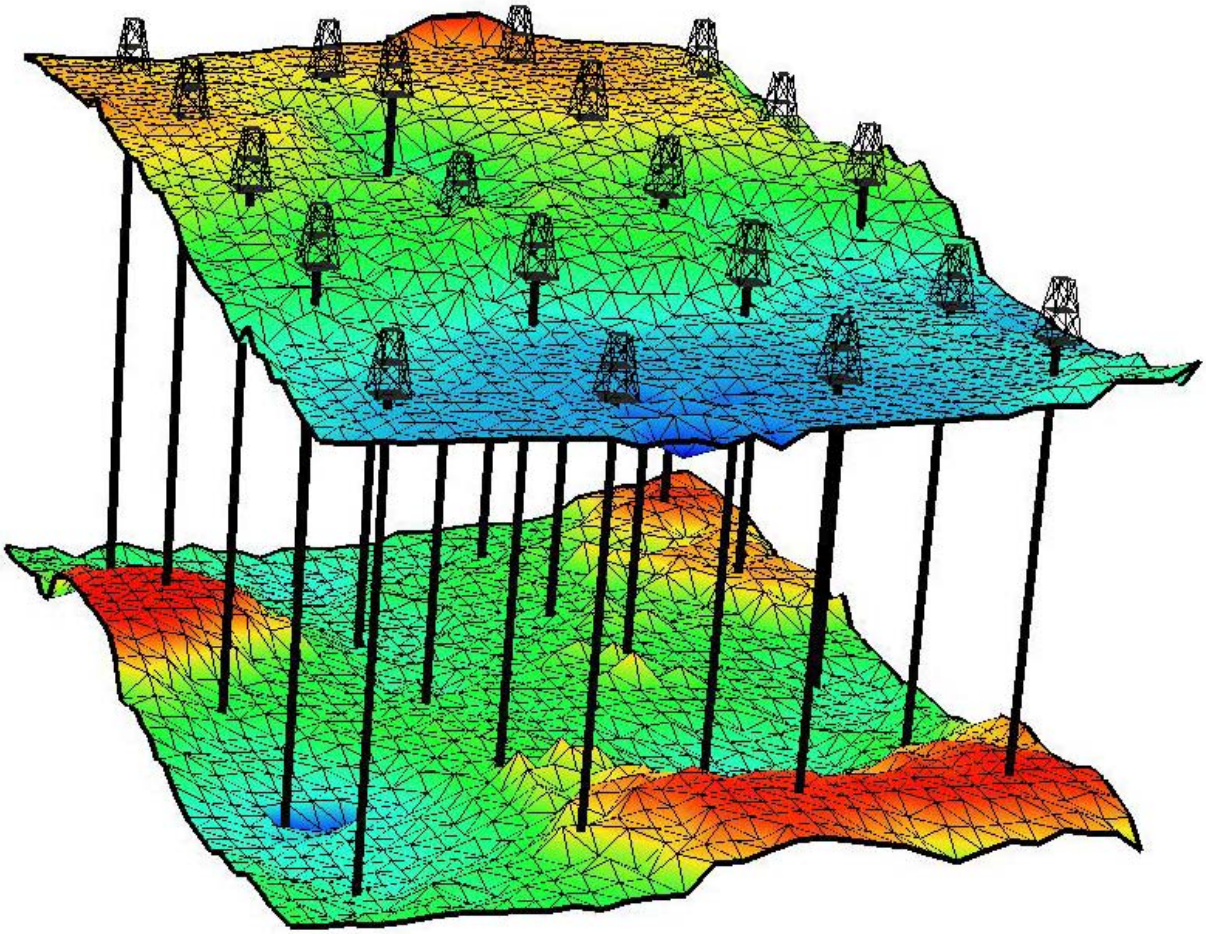

Figure 3.4 – Surface Visualization. A GoCad screen capture of the 10th top and bottom surface realizations with the 20 conditioning core holes. The orientation is consistent with Figures 2.1 and 2.2 and will be the same for subsequent GoCad screen captures.

4 GRIDDING AND THE VERTICAL COORDINATE SYSTEM

Now that the structure has been modeled, an appropriate grid system for lithofacies and petrophysical properties must be established. In choosing a grid specification, there are many considerations. The grid network should facilitate subsequent geostatistical operations, be an appropriate size and incorporate any deterministic geological knowledge.

Figure 4.1 shows the grid system used in our SAGD reservoir characterization procedure. An Easting, Northing and Elevation section through the grid network are all shown. The 1st top and bottom surface realizations are used. The details of the grid and the considerations explored during its construction are presented below.

4.1 GRIDDING

The basic topology used in most geostatistical reservoir modeling is Cartesian, defined by either corner-point or cell-centered aerial and isochore vertical grids. Corner-point and cell-centered grids are used because of their compatibility with geostatistical operations and flow simulation. Since all cells constitute the same volume, scaling operations for geostatistical simulation and flow simulation are straightforward. While tetrahydra-based gridding schemes used for triangulated grids in visualization software such as GoCad are extremely flexible with complex surfaces, they are more computationally expensive and complicated to scale. The aerial and isochore vertical grids in Figure 4.1 are cell-centered.

There are a number of considerations in choosing the grid size. An overriding consideration is the ultimate goal of the project. For example, smaller grid sizes or larger cell sizes better suit reservoir volumetric or dimensional studies; however, when additional geological detail is required, a higher resolution is needed. Another consideration is the computer resources used to store, manipulate and visualize the final model. The chosen grid size is generally a balance between the required geological detail and the available computer resources. With this in mind, we chose to use 50 x 50m aerial cell sizes and 0.5m vertical cell sizes. This amounts to 32 cells in the *X* (Easting) direction, 40 cells in the *Y* (Northing) direction and, depending on the thickness, anywhere from 110 to 190 cells in the *Z* (Elevation) direction for a total of, at most, 243,200 cells per model. We will down scale these models when needed.

4.2 VERTICAL COORDINATE SYSTEM

Reservoirs are made up of a sequence of genetically related strata or layers. In our state of incomplete geological knowledge, a layer is defined as a significant homogeneous reservoir unit that can be correlated between multiple well data over a significant aerial extent of the reservoir. The surfaces that separate these layers each

correspond to a particular time period and depositional setting. Multiple layers, each with their own structural grid specification, need to be defined in a geostatistical study when the nature of the geological heterogeneities changes significantly.

The goal is to (1) implement geostatistical calculations such as horizontal variography within each layer's natural or original geological correlation structure, which is not always the same as the layer's existing geological correlation structure and (2) preserve the existing geological correlation structure in the final numerical model. A layer's original or natural geological correlation structure changes over time due to various structural deformation processes such as differential compaction and erosion that result in missing strata and/or strata filling in existing topography. A stratigraphic vertical coordinate that restores or flattens the layer's structure must be considered for directional geostatistical calculations.

Each layer's "existing" structure can be defined by an existing top and existing bottom surface. In realizing that these existing surfaces, via various structural deformations, are likely different from the layer's "natural" top and bottom surface structures (at the time of deposition) and that, therefore, the directional correlation of the lithofacies and petrophysical properties may not conform to the existing top and bottom surface structure, additional correlation surfaces may be required to establish the natural layer specific correlation style, in which to perform geostatistical calculations. The correlation grids are created from geological understanding of the depositional setting of the reservoir; the vertical coordinate is defined as the relative distance between the correlation top and correlation base surface. Such stratigraphic vertical coordinates make it possible to calculate natural measures of horizontal correlation and preserve the existing geological correlation structure in the final numerical model.

For our SAGD reservoir example, we do consider that the correlation grids are flat. Minimal structural deformation has taken place since the Athabasca oil sands were deposited. However, because the sand deposited filled empty channels at the bottom of the reservoir and accumulated in spots along the sides of the channels, the top surface is not flat and the thickness is not constant.

The stratigraphic vertical coordinate is flat. This simple vertical coordinate is consistent with the style of correlation and will account for the space filling at the base and accumulation at the top. Horizontal variography and other directional geostatistical calculations are, therefore, done within this correlation structure.

4.3 FIGURES

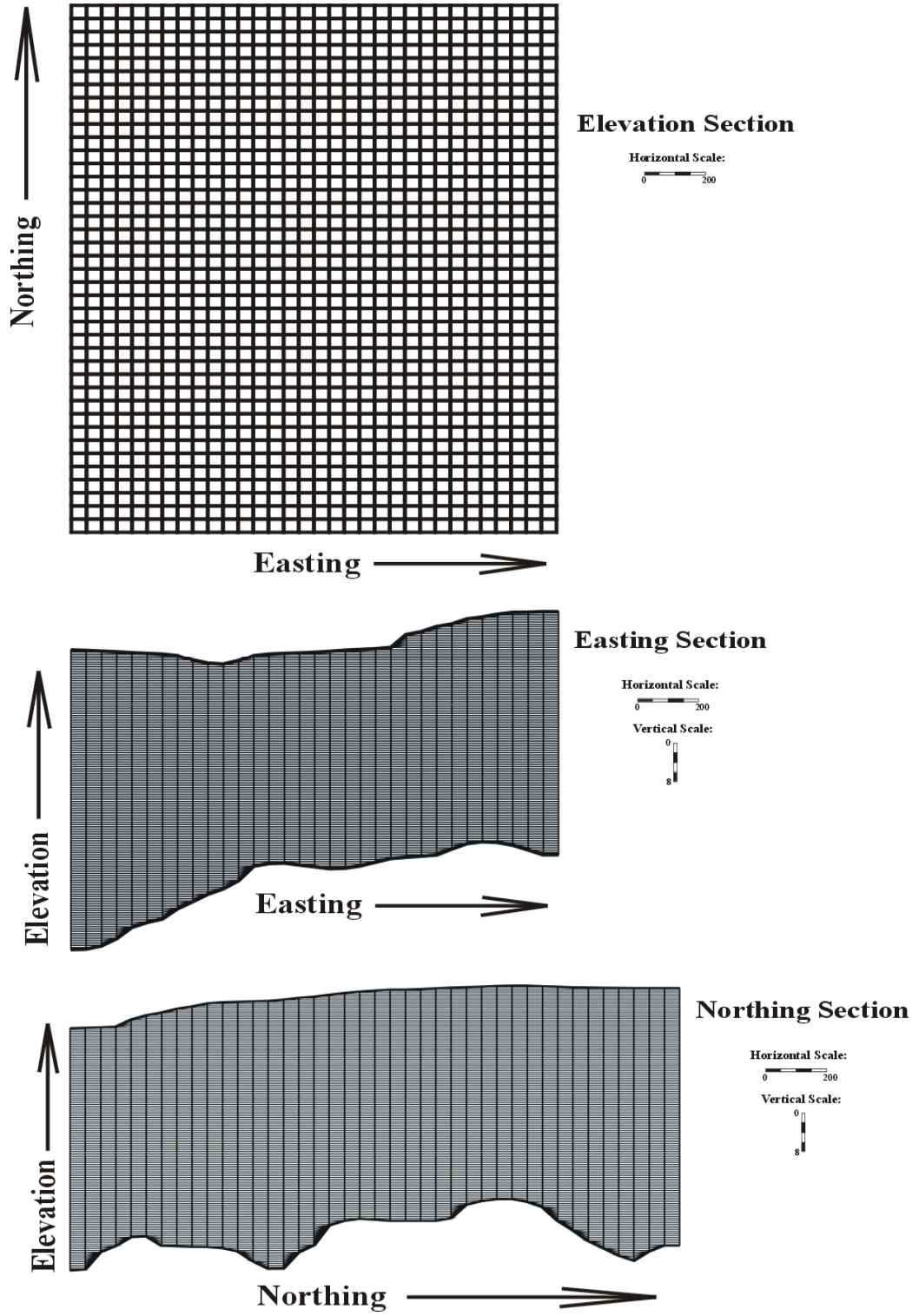

Figure 4.1 – Grid Specification. An illustration of the 3-D grid specification. An Easting, Northing and Elevation section through the grid structure is shown. The horizontal and vertical scale is the same for all sections. The top and bottom elevation surfaces were extracted from the first structure realization.

5 BASIC STATISTICAL CHARACTERISTICS

It is useful to explore some basic statistical characteristics of the data variables prior to geostatistical modeling. Geostatistical simulation requires a prior understanding of the data and representative statistics.

The lithofacies variable was regridded to 10cm increments down the length of each of the exploratory core holes. The histogram of the facies types is shown in Figure 5.1. There are four facies types, each with its own binary code: Sand – 1, interbedded sand – 2, shale – 3 and breccia – 4; the proportion of sand, interbedded sand, shale and breccia is approximately 0.51, 0.22, 0.18 and 0.09, respectively. Subsequent facies simulation models should reproduce these proportions within appropriate stochastic fluctuations.

The porosity variable was scaled to a constant 10cm resolution down the length of each core hole. The histogram of porosity is shown in Figure 5.2. It shows a tri-modal type behavior. The first mode is in the form of a spike near 0% porosity corresponding to samples taken from impermeable shale. Centered at about 10% porosity, the second mode represents samples taken mostly from interbedded sand. The third mode, centered at about 35% porosity, represents porosity in the sand facies. The average porosity is about 21%.

The tri-modal behavior of the porosity histogram is better understood by observing the histogram of porosity within each facies. Figure 5.3 shows four histograms of the porosity variable, each one within a different lithofacies. The average porosity within the sand, interbedded sand, shale and breccia facies is 32%, 15%, 3% and 20%, respectively. All of the histograms exhibit a single mode/spike centered at the average porosity in each corresponding facies. Notice the relationship between the locations of these by-facies modes with those of the tri-modal global porosity histogram. From this relationship and from the varying shape of the histograms, it is apparent that porosity behavior is dictated largely by lithofacies. Porosity is not stationary over the entire reservoir as a whole.

5.1 FIGURES

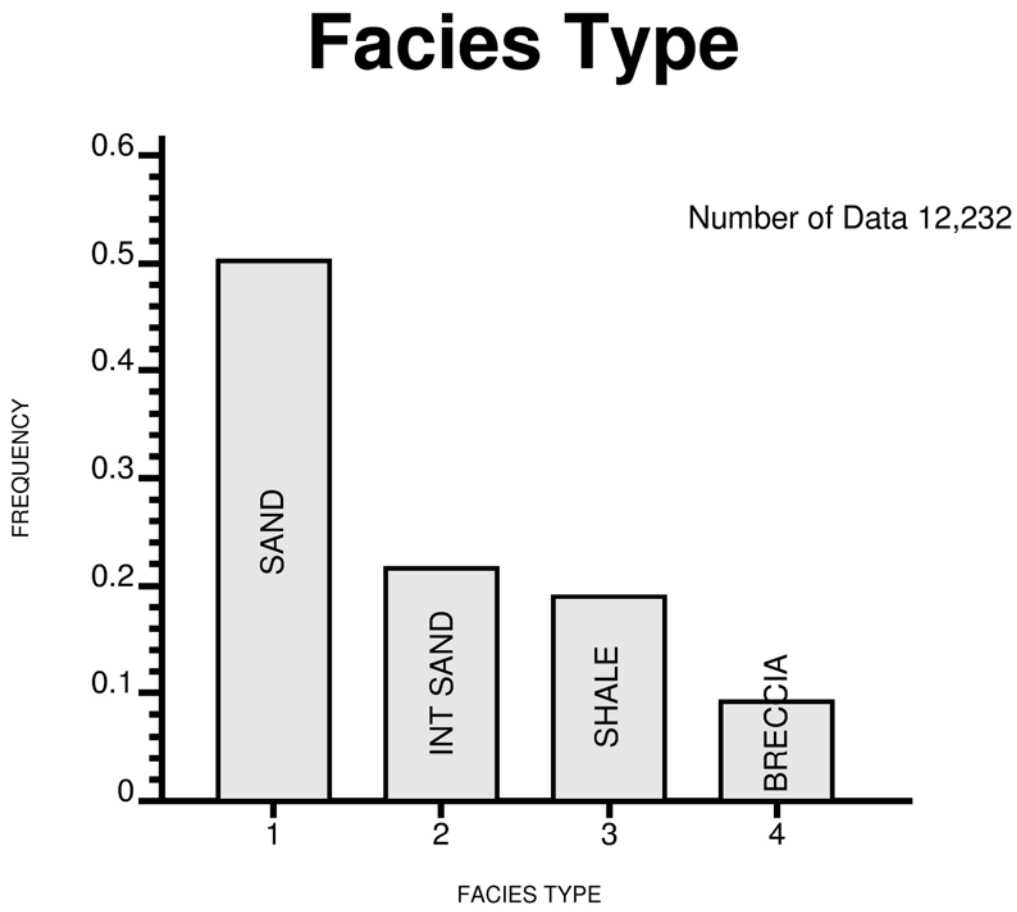

Figure 5.1 – Facies Type Histogram. A histogram of the facies type variable. The four facies, sand, interbedded sand, shale and breccia are equal to 1, 2, 3 and 4, respectively.

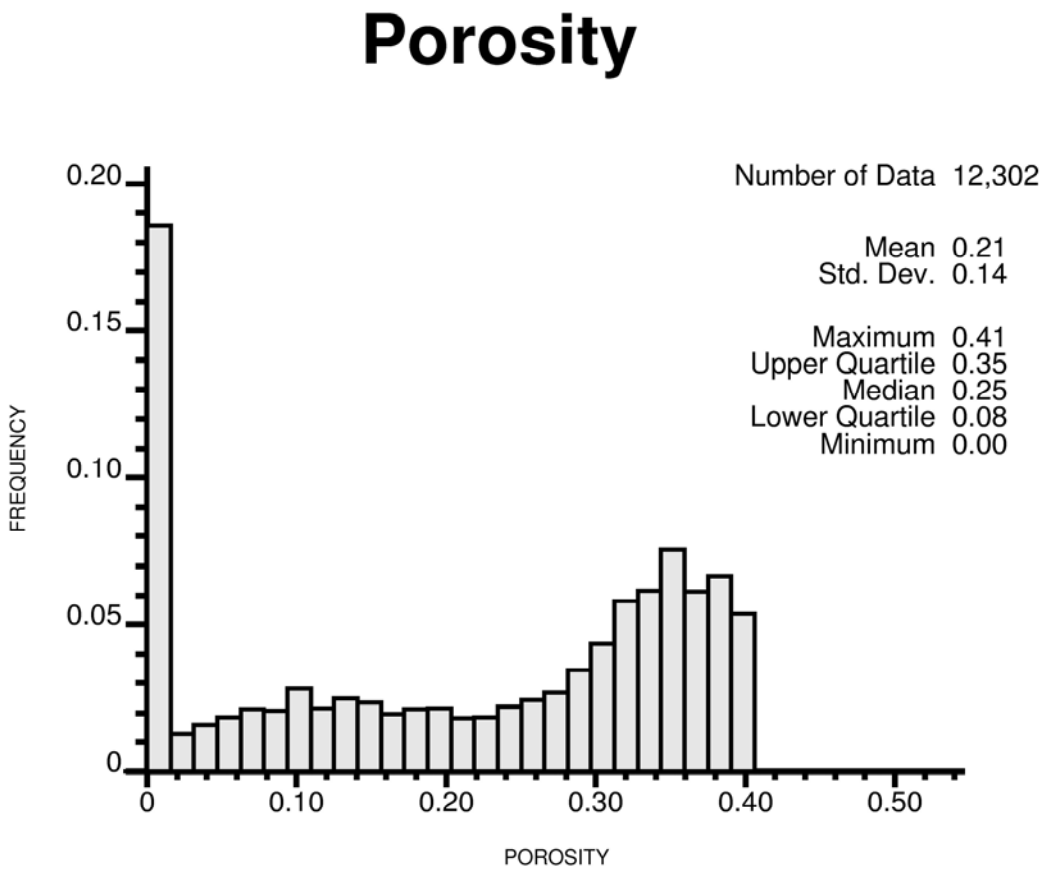

Figure 5.2 – Global Porosity Histogram. A histogram of the porosity variable.

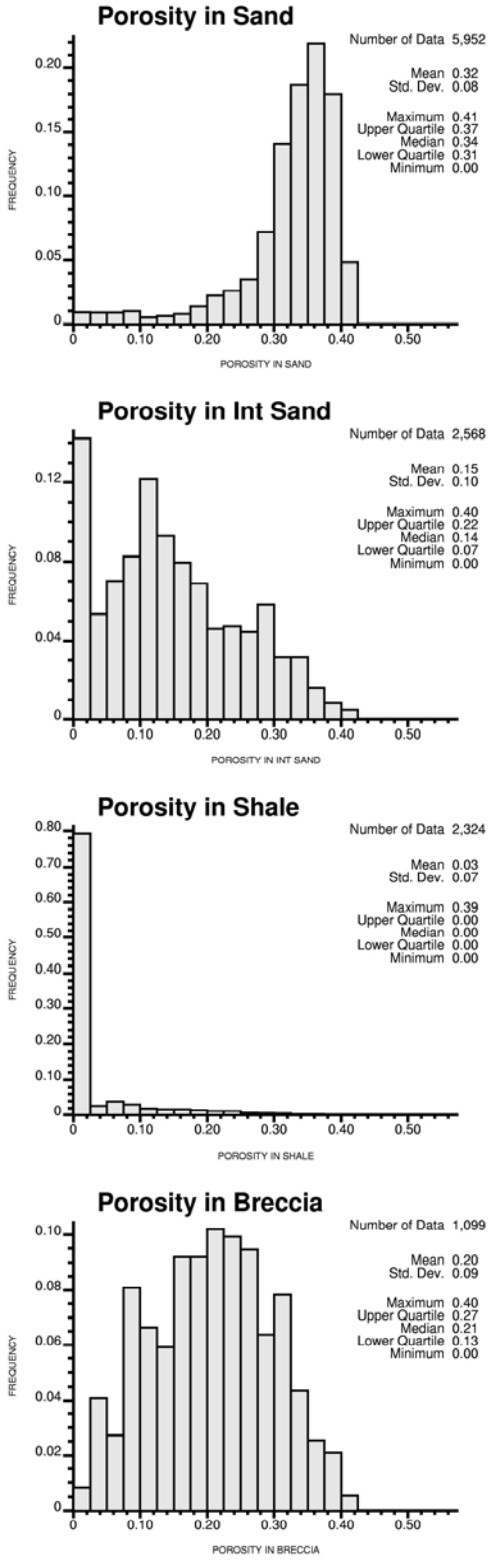

Figure 5.3 – Facies Type Porosity Histograms. A histogram of the porosity variable within each of the four lithofacies. Notice the relationship to the global porosity histogram.

6 FACIES MODELING

The structure has been modeled, an infill grid system with an appropriate vertical coordinate has been established and the basic statistical characteristics of the SAGD variables have been explored. We are now ready to extrapolate the lithofacies and porosity to unsampled locations. This section describes the process used to create multiple cell-based geostatistical realizations of the facies for subsequent use in porosity/permeability modeling and reservoir management.

Facies types are only modeled when they have significant control on important petrophysical properties. In exploring the basic statistical characteristics of our porosity and facies data, it was found that porosity is largely dependant on lithofacies, see Figure 5.3. If this were not the case, facies modeling would be of little benefit since the geological uncertainty would not be reduced and the resulting models would have no more predictive power.

The main steps for cell-based geostatistical facies modeling include (1) gathering and formatting the relevant conditioning data (2) establishing aerial and vertical trends and combining them into a 3-D proportion/trend model (proportion and mean are interchangeable terms when speaking about facies code distributions), (2) assembling a licit 3-D variogram model of spatial correlation for each facies type, (4) stochastically constructing the facies realizations and (5) validation. Each step will now be described in detail and implemented on the example.

6.1 THE LITHOFACIES CONDITIONING DATA

There are four facies types used in the SAGD reservoir characterization example, each with a separate code. Figure 6.1 shows each lithofacies' code and the color scheme applied throughout the remainder of this report. The lithofacies variable is available along the length of the exploratory core holes in 10cm increments. The conditioning global facies proportions are shown in Figure 5.1.

6.2 FACIES TREND MODELING

All conventional geostatistical algorithms including kriging and variography depend on an assumption of stationarity, which assumes the spatial statistics such as the mean or variogram value, are location independent. Trends are non-stationarities. Prior to implementing any variant of indicator simulation, we must account for these location-dependant statistics with a 3D model of the mean.

Virtually all depositional settings show facies trends due to climate change, space-filling, structural deformation, pressure and so on during the time of deposition. For example, breccia units in the Athabasca oil sands are found primarily at lower elevations corresponding to times when water eroded sediment off the top of the extensive ridges

and channels across Alberta and Saskatchewan. Such facies trends should be included as conditioning information in subsequent stochastic indicator simulation. Our final geological model must reproduce locally varying facies proportions as well as the global facies proportions.

If previous geological knowledge is reliable enough to deterministically model the trend, this should be done. If little reliable geological knowledge is known, a data-driven statistical approach could be used if the trends are clear; otherwise, no trend should be modeled..

The methodology for creating a 3-D proportion trend model consists of building a 1-D vertical trend and a 2-D aerial trend and then combining them into a final 3-D proportion trend model. Figure 6.2 illustrates this methodology for the 4 facies types. The proportion trends are different for each facies; however, the methodology is the same.

6.2.1 THE VERTICAL TRENDS

Building the vertical trends can be broken into a two step procedure. The first step is to visualize the varying proportions along the established stratigraphic vertical coordinate. The second step is to create 1-D vertical proportion trend models on the basis of these visualizations.

Refer to Figure 6.3 for the application of this two step procedure to the 4 facies types. After a small sensitivity study, we chose to calculate the lithofacies proportions within 1m bins (10 samples per core hole per bin) along the vertical coordinate. Plotting the center of each elevation bin versus the calculated proportions (left side of Figure 6.3) provides the visualization needed to infer the final vertical proportion models. Multiple control points are established on these cross-plots and linear interpolation is used between the control points to inform all elevations. The final 1-D vertical proportion models are the connected lines (right side of Figure 6.3).

There is unavoidable subjectivity associated with trend modeling, that is, when establishing the control points, it is important to separate deterministic features from stochastic features. The variations of the calculated vertical proportions from our final linear 1-D models are considered to be stochastic. Our final 1-D vertical proportion models do not account for these small-scale stochastic features, but our final simulated realizations will.

6.2.2 THE HORIZONTAL TRENDS

The aerial proportion maps or horizontal trends for lithofacies are created by some type of extrapolation algorithm with the proportion of each facies over the vertical extent of the exploratory core holes as conditioning data. The amount of detail to be modeled by the extrapolation procedure is, again, a function of our degree of knowledge concerning the separation of deterministic features and stochastic features in the conditioning data. If

in doubt, it is better to infer less detail than mistakenly incorporate more into the trend model.

To create the aerial proportion maps for the SAGD example, a kriging algorithm is used. There are 4 sets of conditioning data – one set for each lithofacies. Within each set there is one value per core hole location, which is the proportion of the corresponding facies over the vertical extent of that core hole. Variography is first performed with these conditioning data. The output cells measure 50m a side. The resulting smooth kriged maps and corresponding variograms used to create them are shown in Figure 6.4. These maps are the aerial proportions that will be combined with the vertical proportion models in Figure 6.3, to create the 3-D proportion trend models, see Figure 6.2.

6.2.3 COMBINING THE VERTICAL AND HORIZONTAL TRENDS

Now that the 1-D vertical proportion trend and the 2-D aerial proportion trend for each lithofacies have been constructed, we are ready to combine them into 3-D proportion trend models. Although there are various ways to achieve this combination, we will use a scaling procedure that assumes conditional independence between the two trends.

The 3-D trend value for each location for each facies is calculated as the aerial trend multiplied by the vertical trend divided by the global facies proportion at each location for each facies. The scaling procedure takes the following equation form:

$$proportion(X,Y,Z) = \frac{areal\_proportion(X,Y) \bullet vertical\_proportion(Z)}{global\_proportion}$$

This scaling procedure is implemented for each of the four facies. The final 3-D proportion trend model will be honored by subsequent sequential indicator simulation, that is, the vertical trend and the form of the aerial trend should be reproduced by lithofacies realizations within the bounds of appropriate stochastic fluctuations.

The final 3-D proportion trend models are now investigated. Figure 6.5 illustrates the sections through each 3-D trend model that will be used. These 3-D trend model sections for the (1) sand, (2) interbedded sand, (3) shale and (4) breccia facies are illustrated in Figures 6.6 to 6.9, respectively. The mathematical scaling procedure can be observed within each 3-D facies proportion trend model. The vertical scale is exaggerated on the elevation sections by a factor of 5.

6.3 FACIES VARIOGRAPHY

Lithofacies often exhibit different continuity in different directions. Before implementing any variant of indicator simulation, we must first quantify the spatial correlation/covariance structure of each facies type in all directions.

The main challenge in obtaining reliable variograms is the horizontal direction; there are often too few exploratory core holes to calculate a reliable horizontal variogram. Conventional variogram modeling is usually not enough in these cases – analogue data such as anisotropy ratios or seismic calibrations and/or expert judgment is needed. The vertical resolution, however, almost always permits a reliable vertical variogram to be calculated.

Horizontal and vertical indicator variograms are calculated and modeled for each facies. Only 3 experimental semi-variogram values can be calculated for the experimental horizontal variograms. The experimental vertical variograms are well informed. The variography results are shown in Figure 6.10.

6.4 FACIES SIMULATION

We have so far gathered all the available lithofacies conditioning data and created a 3-D model of locally varying proportions and spatial correlation for each facies code. This completes the preliminary facies modeling steps necessary to implement stochastic simulation for creating multiple realizations of the facies types.

sisim_lm (sequential indicator simulation with a locally varying mean) from the GSLIB package is now used to create 100 3-D geostatistical realizations of the facies type codes.

A few notes concerning the grid specification are now appropriate. We want the output facies realizations to populate a grid resolution of 50 x 50m aerially and 0.5m vertically. The field spans 1600m, 2000m and 95m in the Easting, Northing and Elevation directions from the 3-D *X*-*Y*-*Z* point: 4900m, 1800m, 175m. This entails 32 x 40 x 190 cells in the Easting (*X*), Northing (*Y*) and Elevation (*Z*) directions, respectively, amounting to 243,200 cells per facies realization. These same grid specifications must be used for the 3-D proportion trend models for the *sisim_lm* program. In anticipation of this constraint, the vertical proportion trends were constructed at a 0.5m resolution resulting in 190 $vertical\_proportion(Z)$ values and the aerial proportion trends were constructed at a 50 x 50m resolution resulting in 1,280 $areal\_proportion(X,Y)$ values, corresponding to the same 243,200 cell locations. The facies realizations at this 32 x 40 x 190 grid specification are then clipped according to the top and bottom structure models created in the “Structure Modeling” section, that is, if a particular facies code realization is above the top structure model or below the bottom structure model, it is excluded from the final numerical model. In anticipation of this step, the top and bottom structure model grids were also created at a 50 x 50m aerial resolution.

Figure 6.11 shows the 50th of the 100 equal-probable facies realizations. Notice the general form of the vertical and horizontal trend is reproduced. For example, relative to the vertical coordinate, there are significant volumes of simulated sand populating the middle of the reservoir, the vertical proportion trend model of sand predicts this. The same section locations used to visualize the 3-D proportion trend models are used to visualize the 50th lithofacies realization in this figure.

A geostatistical reservoir model consists of a set of different parameters including (1) the top and bottom structure defining each stratigraphic layer, (2) the facies types within each layer and (3) the petrophysical properties such as porosity within each facies type and within each layer. A reservoir model consists of a single realization of each parameter. The point is that multiple facies realizations are not created for one top and bottom structure model; rather, one facies model is associated to each top and bottom structure realization.

Figures 6.12 and 6.13 aid in visualizing the facies conditioning data and the simulation results, in particular, the 10^{th} facies realization. The conditioning facies core hole data in Figure 6.12 shows the predominance of sand facies within the Northern part of the reservoir where it is thickest and shale facies within the Southern part of the reservoir where it is thinnest. The cross sections shown in Figure 6.13 show that the simulated facies data honor the conditioning core hole data.

6.5 VALIDATION

Reservoir modeling consists of several interrelated steps, each with the potential of producing incorrect results. It is necessary to check or validate stochastic models as much as possible before using them in subsequent modeling. To completely validate multiple geostatistical realizations is impossible; however, there are many basic checks that can be used to identify problems and inconsistencies.

Cross validation is the most popular way to validate a set of estimates. The result is a set of collocated true values and estimated distributions of uncertainty; validation is based on their agreement. The concept of cross validation can also be used to check simulation. Simulation creates distributions of what the attribute of interest could possibly be at unsampled locations. In validating these distributions of uncertainty, cross validation compares the actual fraction of simulated values falling within a specified probability interval vs. the probability interval. The accuracy and precision of these local models of uncertainty could also be quantified.

Many other checks and tests can be applied to validate geostatistical models consisting of multiple realizations. We can validate the facies code realizations in several ways. The original facies conditioning data, global facies proportions, locally varying facies proportions and the model of spatial correlation should all be reproduced within appropriate stochastic fluctuation. Although not done in the example, the theory of cross validation for indicator variables can be applied to validate the constructed facies realizations.

We now check that the simulated output reproduces the conditioning data at their locations, the global facies proportions, the local facies proportions, and the facies variograms. To check that the conditioning data are honored, a program is used to check that the simulated output is the same as the original conditioning data values at the original conditioning data locations. A histogram of the simulated facies codes is created

and compared to the histogram of original binary facies codes (Figure 5.1) to check global proportion reproduction. The vertical and aerial proportions are then calculated for each facies and compared to the original ones (Figure 6.3 and 6.4) used to condition the simulation. Finally, the horizontal and vertical indicator variograms are calculated and compared to the originals (Figure 6.10) used in the simulation. To save time, a script is created to do these operations on every facies realization – in the end it is the average of these checks over all realizations that is compared to the original parameters. By doing this, we found that (1) the original conditioning data are honored, (2) the global facies proportions are reproduced, (3) the general form of the vertical and horizontal trend is reproduced and (4) the original 3-D variogram models are reproduced.

6.6 FACIES UNCERTAINTY

It was previously mentioned that the structural parameters of the final geological model will affect SAGD production performance. Moreover, the distribution of facies within each top and bottom structure model will also affect SAGD production performance. The uncertainty in the distribution of facies, which is the fluctuation from realization to realization, like the structural uncertainty, must, therefore contribute to the final uncertainty in production performance. Each realization of the facies within the corresponding realization of the top and bottom structure realization is passed through the entire geostatistical SAGD reservoir characterization procedure. The combined contribution of structural uncertainty and facies distribution uncertainty to SAGD production uncertainty can, therefore, be quantified in terms of production performance.

6.7 FIGURES

Facies Type	Binary Code
SAND	1
INTERBEDDED SAND	2
SHALE	3
BRECCIA	4

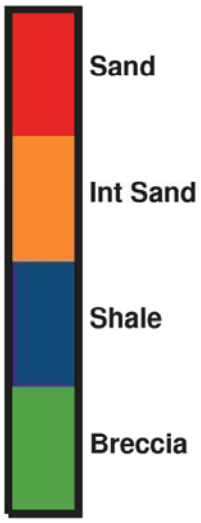

Figure 6.1 – Facies Conditioning Data. An illustration of the lithofacies conditioning data. A chart showing the code associated to each facies type and a color bar showing the color associated to each facies type is presented.

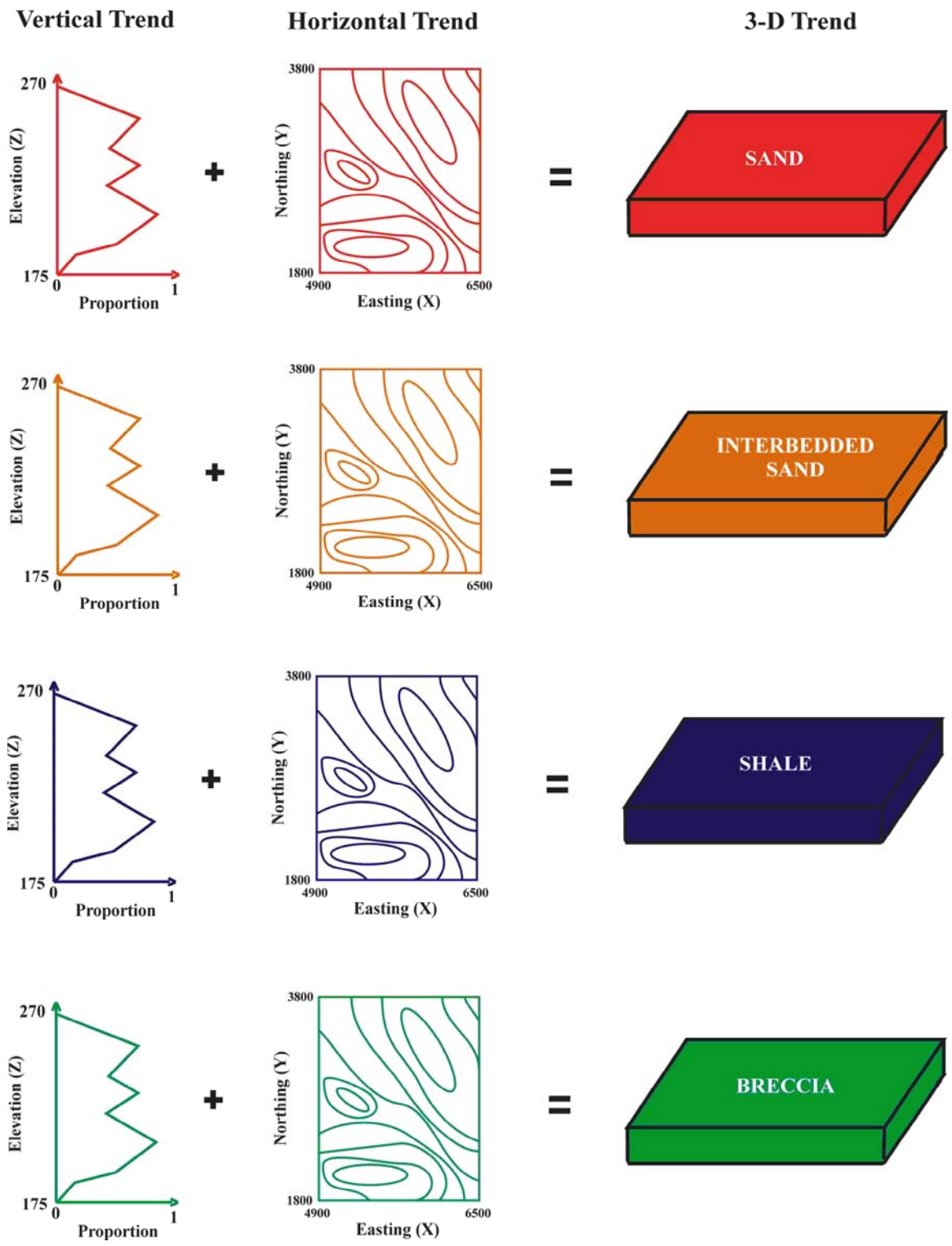

Figure 6.2 – Facies Trend Modeling Methodology. An illustration of the methodology used to build a 3-D proportion trend for each facies type. The same color scheme used in Figure 6.1 is used in this figure to show that a separate 3-D trend model is created for each facies.

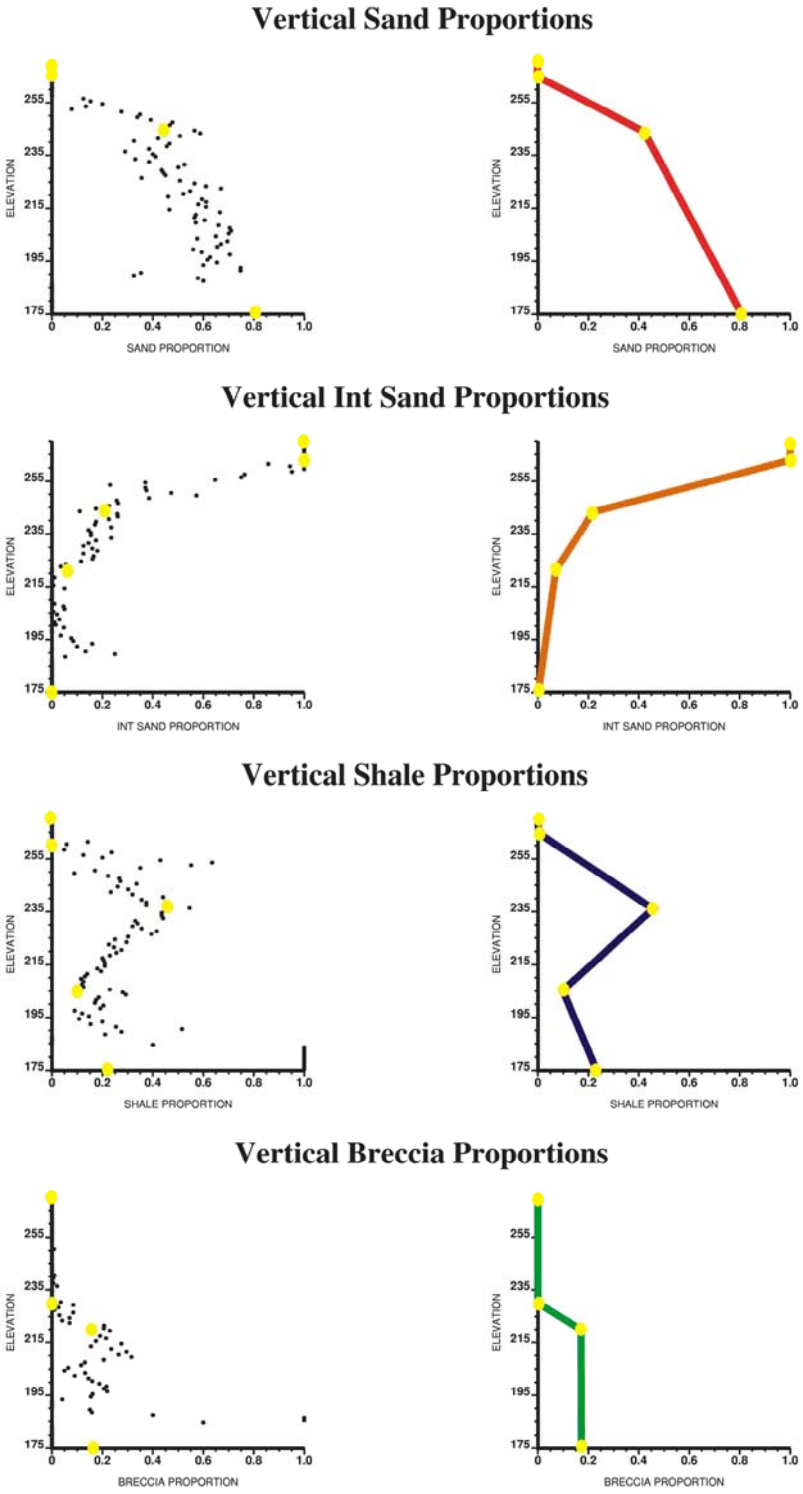

Figure 6.3 – Vertical Facies Trends. An illustration of the cross-plots and the control points used to infer the vertical proportion trend for each facies. The cross-plots on the left show the center of each elevation bin vs. the calculated facies proportions and are used for visualizing the trends. The control points are shown on these cross-plots in yellow. Linearly interpolating between these control points allows us to create the final 1-D vertical proportion trend models shown on the right.

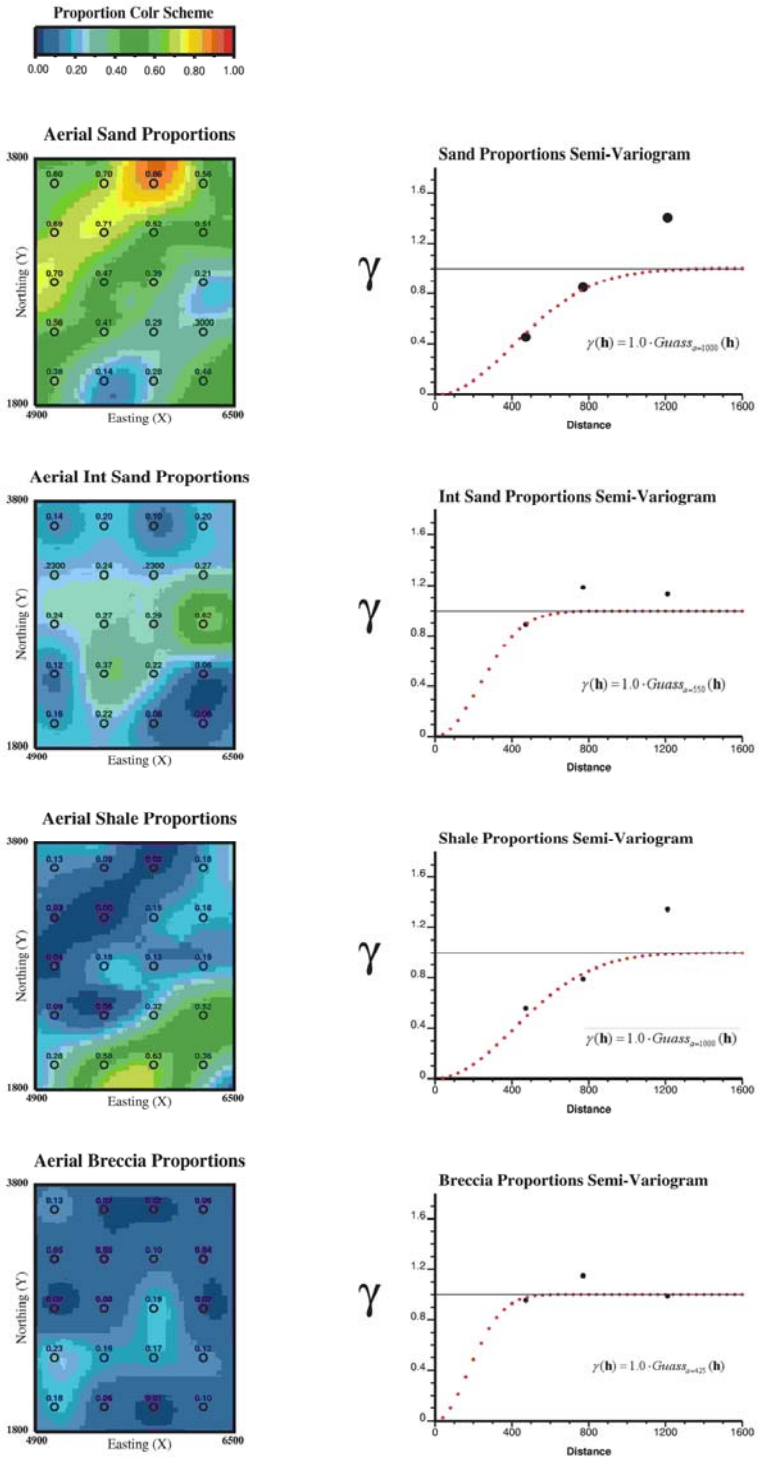

Figure 6.4 – Horizontal Facies Trends. An illustration of the smoothly kriged aerial proportion maps for each facies. The conditioning vertical facies proportion data are superimposed on top of the aerial proportion maps on the left. Both the conditioning data and the kriged values follow the color scheme shown at the top left. The right side of the figure shows the variogram (in graphical and equation form) used to create the corresponding aerial proportion maps.

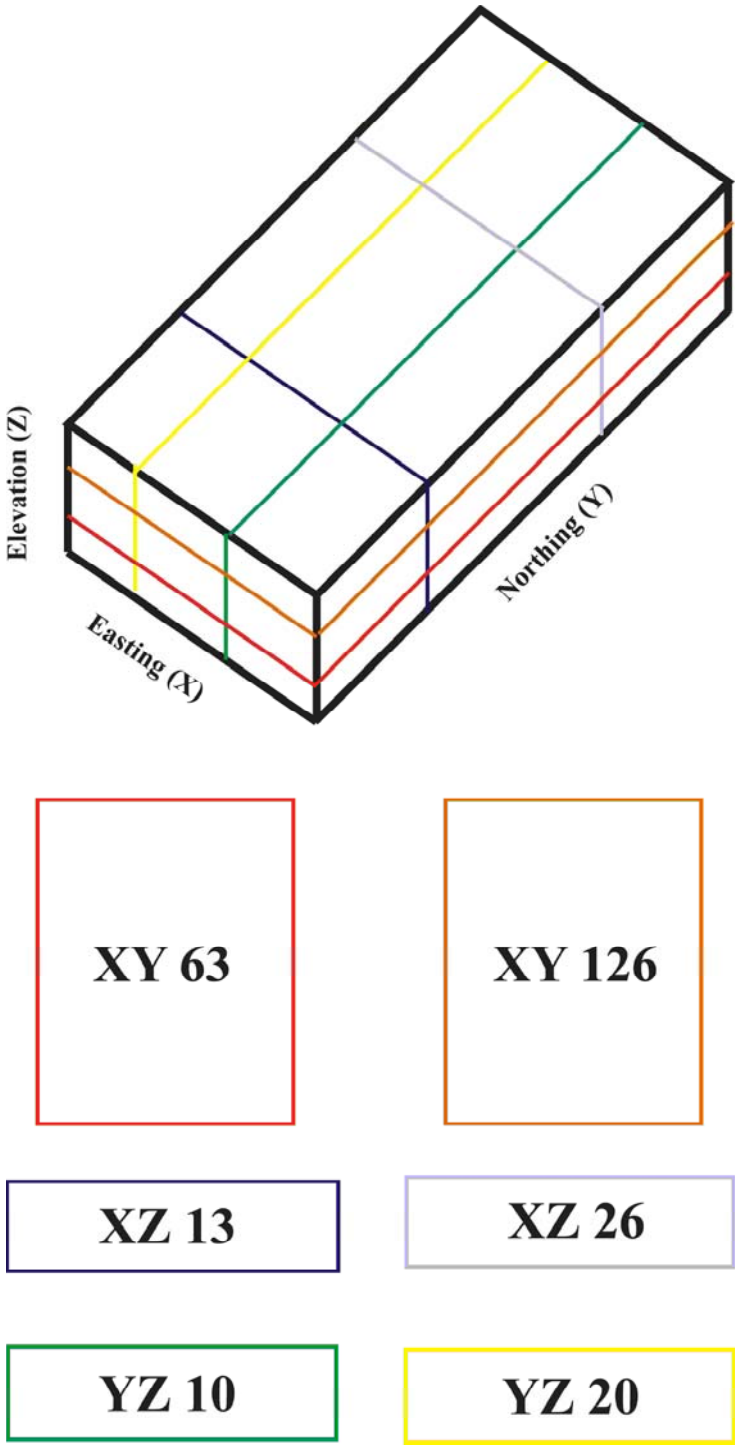

Figure 6.5 –Section Locations. A color coded illustration of the section locations implemented to visualize the 3-D proportion trend model for each facies type. The trend models are composed of 32, 40 and 190 cells in the Easting (*X*), Northing (*Y*), and Elevation (*Z*) directions, respectively. These sections will be illustrated for each facies in the next 4 figures.

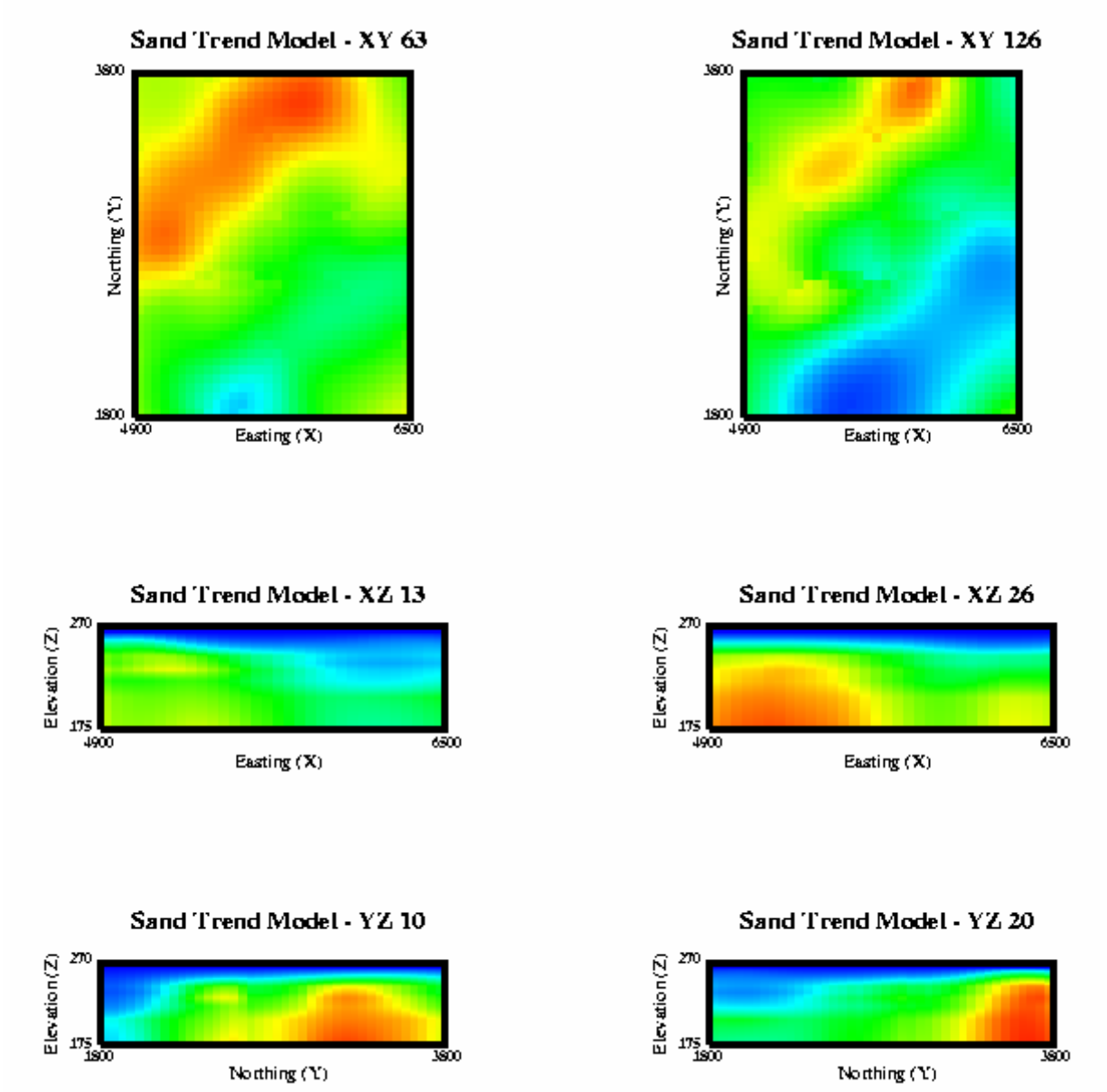

Figure 6.6 – Sand Trend Model. Two *XY*, *XZ* and *YZ* sections through the trend model of proportions for the sand facies. The same proportion color scheme shown in Figure 6.4 is used in this figure.

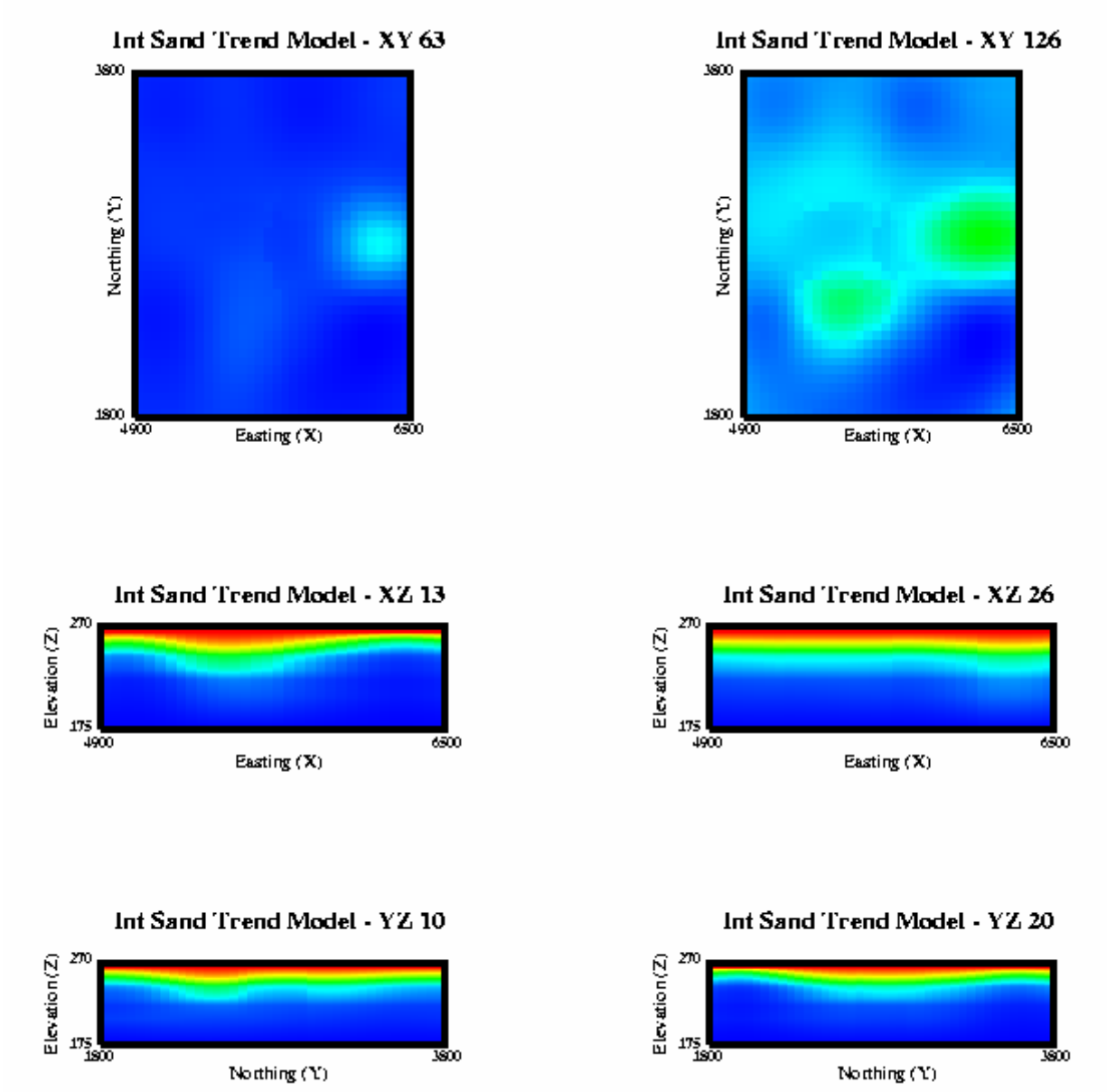

Figure 6.7 – Interbedded Sand Trend Model. Two *XY*, *XZ* and *YZ* sections through the trend model of proportions for the interbedded sand facies. The same proportion color scheme shown in Figure 6.4 is used in this figure.

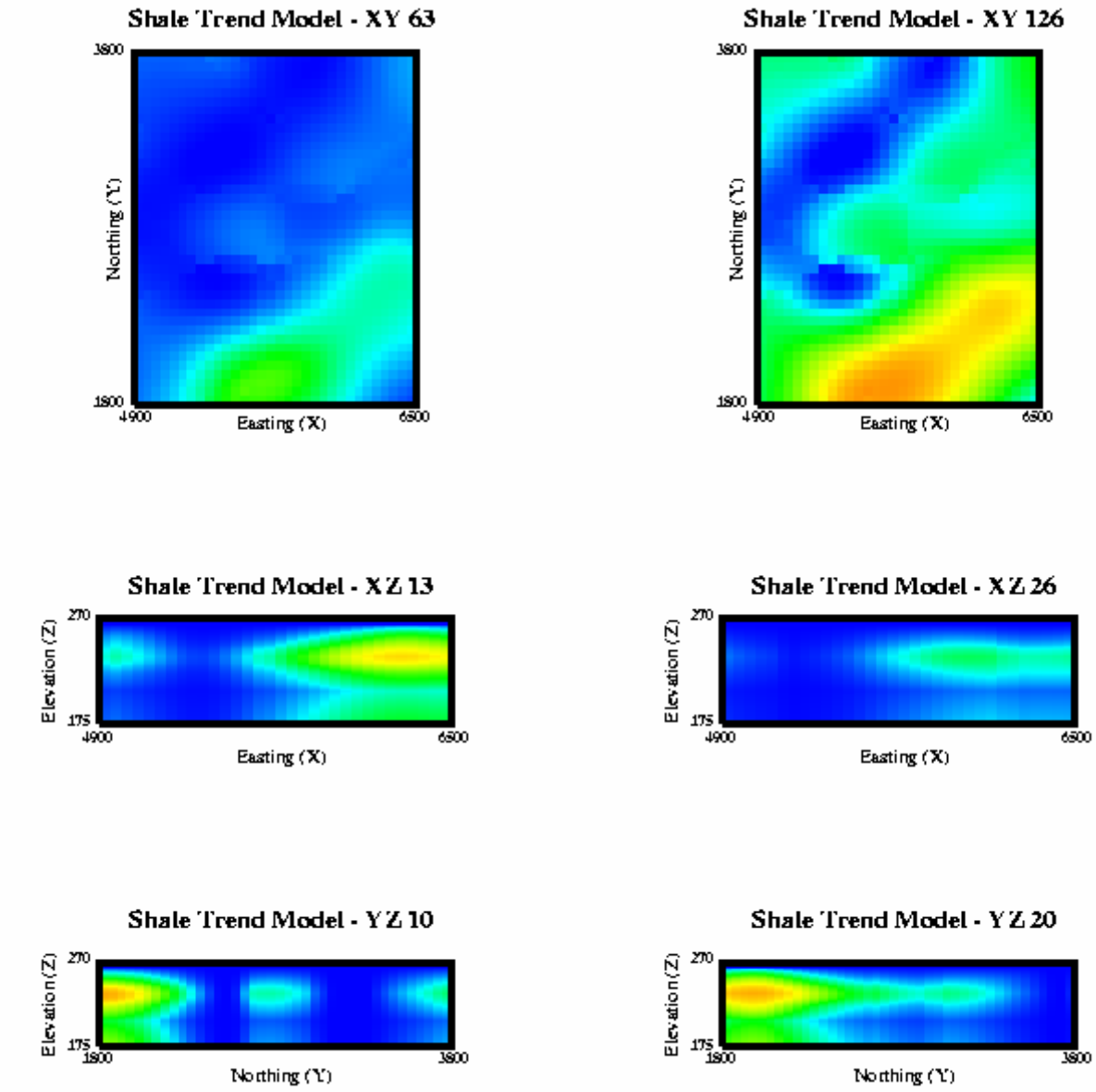

Figure 6.8 – Shale Trend Model. Two *XY*, *XZ* and *YZ* sections through the trend model of proportions for the shale facies. The same proportion color scheme shown in Figure 6.4 is used in this figure.

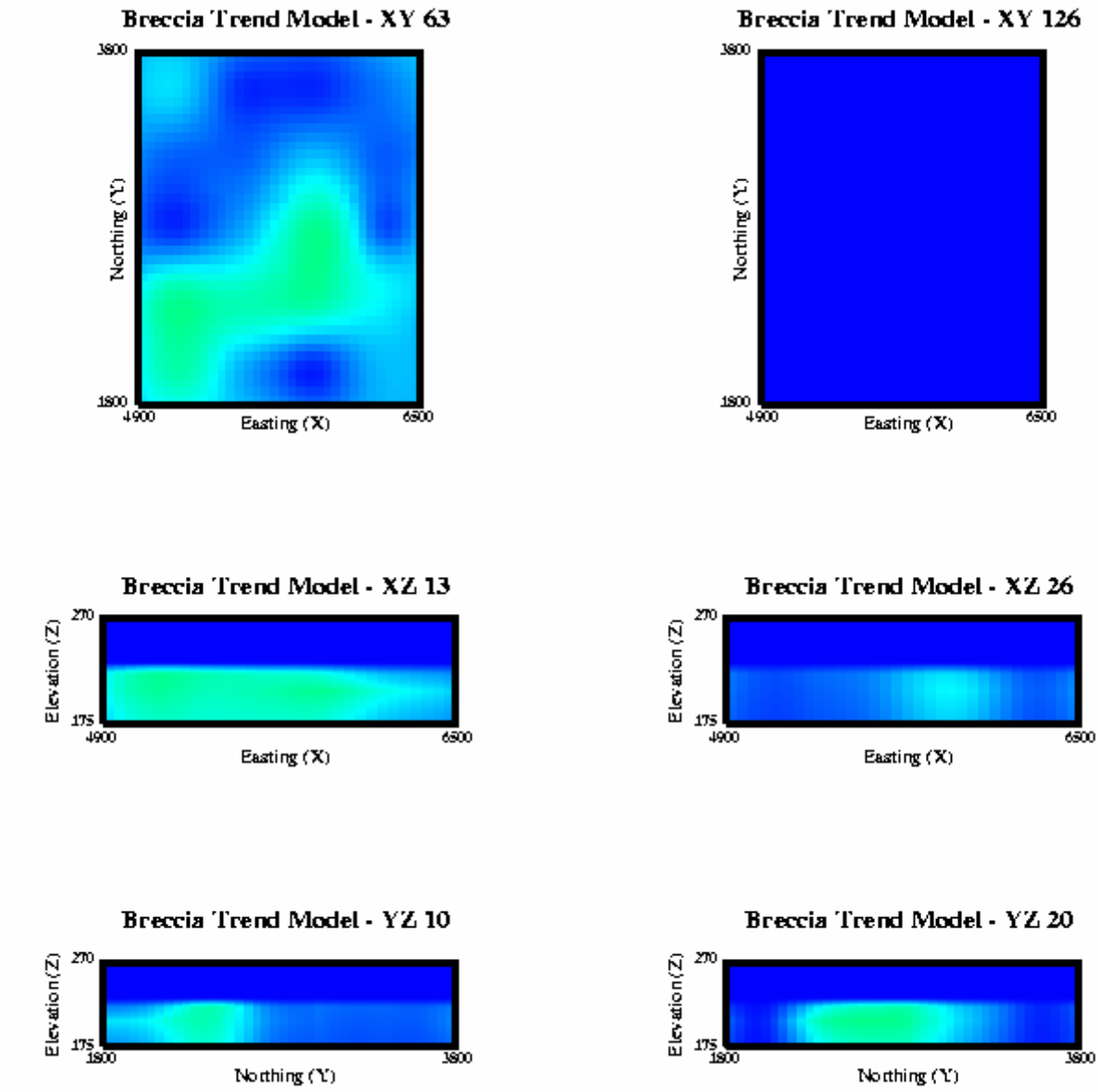

Figure 6.9 – Breccia Trend Model. Two *XY*, *XZ* and *YZ* sections through the trend model of proportions for the breccia facies. The same proportion color scheme shown in Figure 6.4 is used in this figure.

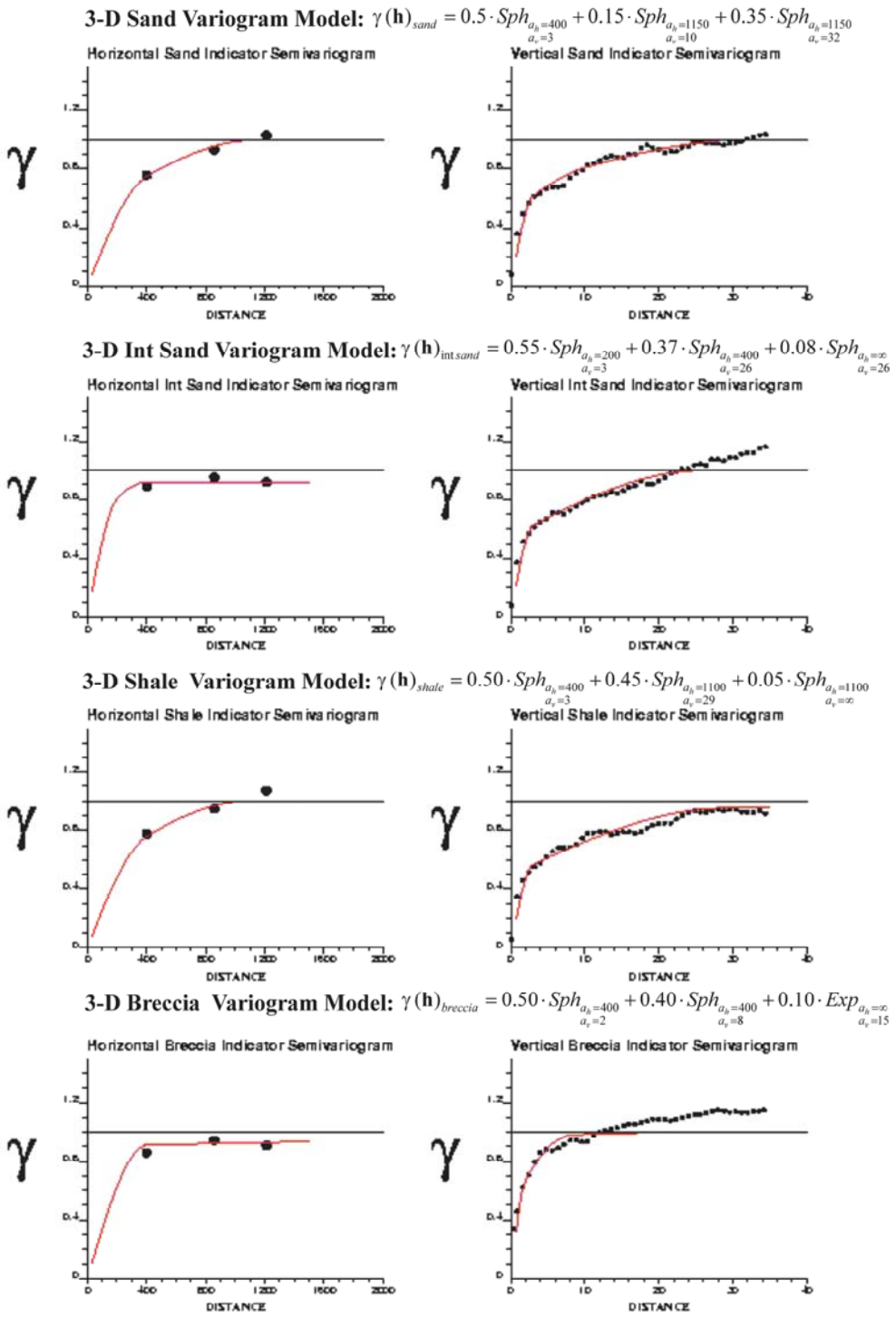

Figure 6.10 – Facies Variograms. An illustration of the calculated horizontal and vertical facies indicator variograms. The experimental points are shown as black dots and the models are shown as red lines. The equation of each 3-D facies variogram model is also shown.

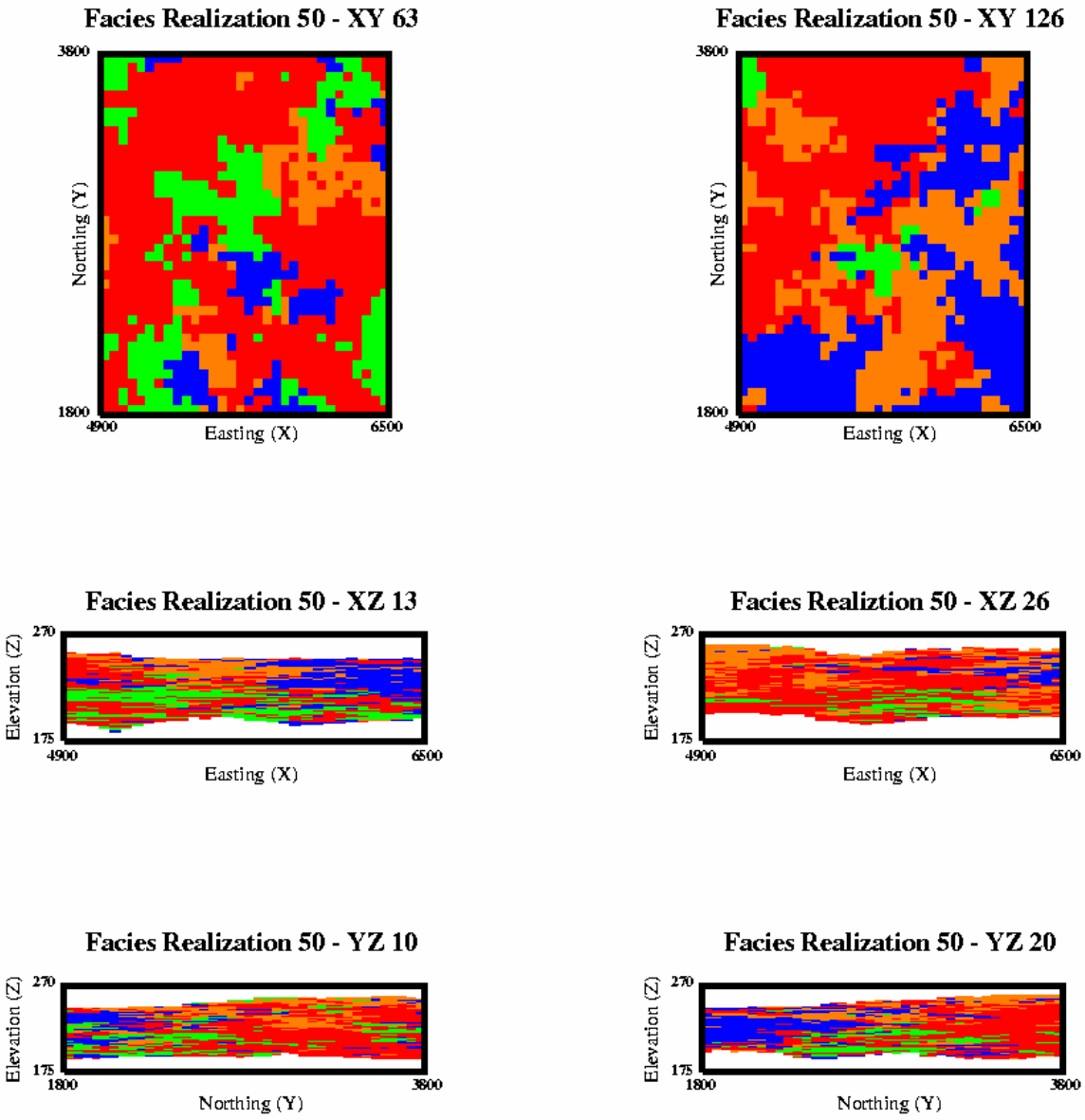

Figure 6.11 – Facies Simulation. An illustration of the 50th lithofacies realization. The same categorical color scheme used in Figure 6.1 is used in this figure. The vertical scale has been exaggerated by five times. The white space contains those cells that were clipped by the previously created structure models.

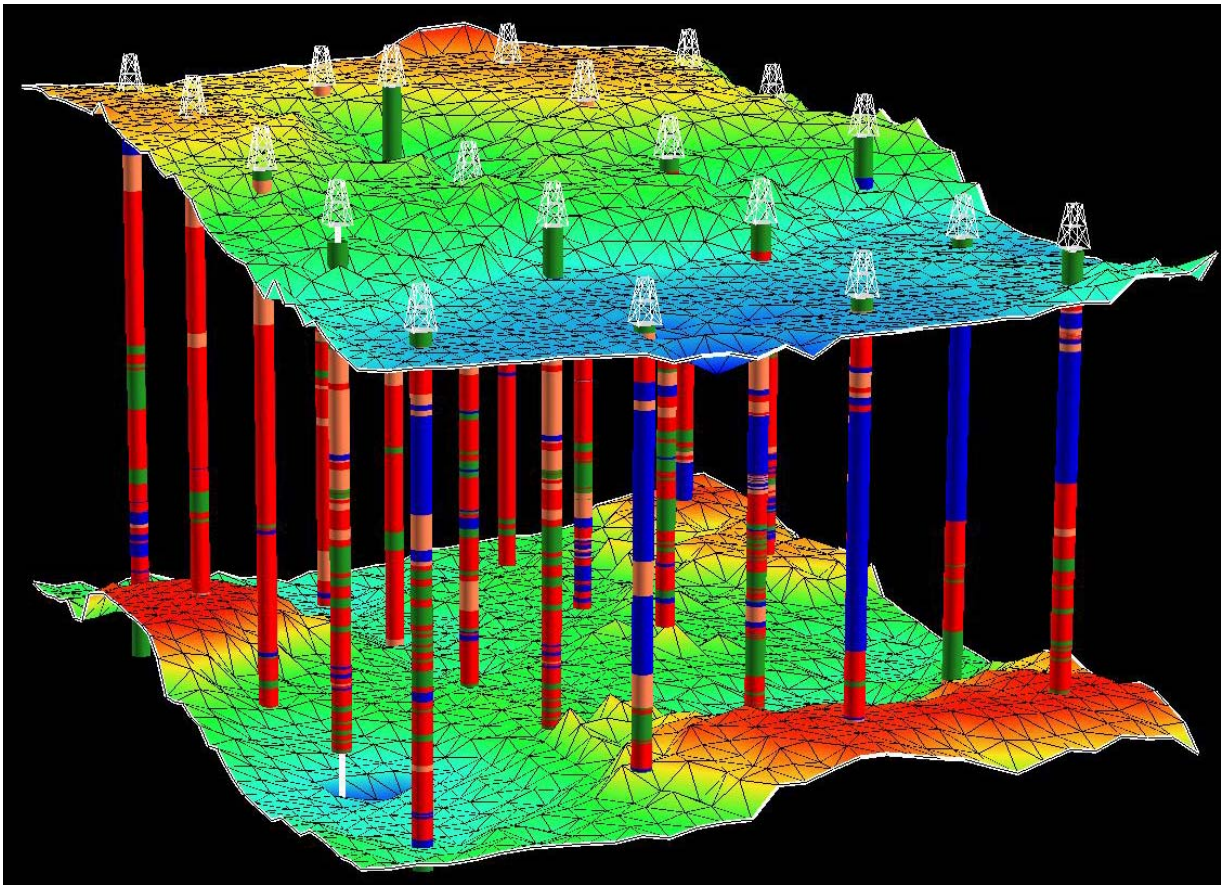

Figure 6.12 – Facies Conditioning Data. An illustration of facies conditioning data within the 10th structure realization. The color scheme is the same as shown in Figure 6.1.

a)

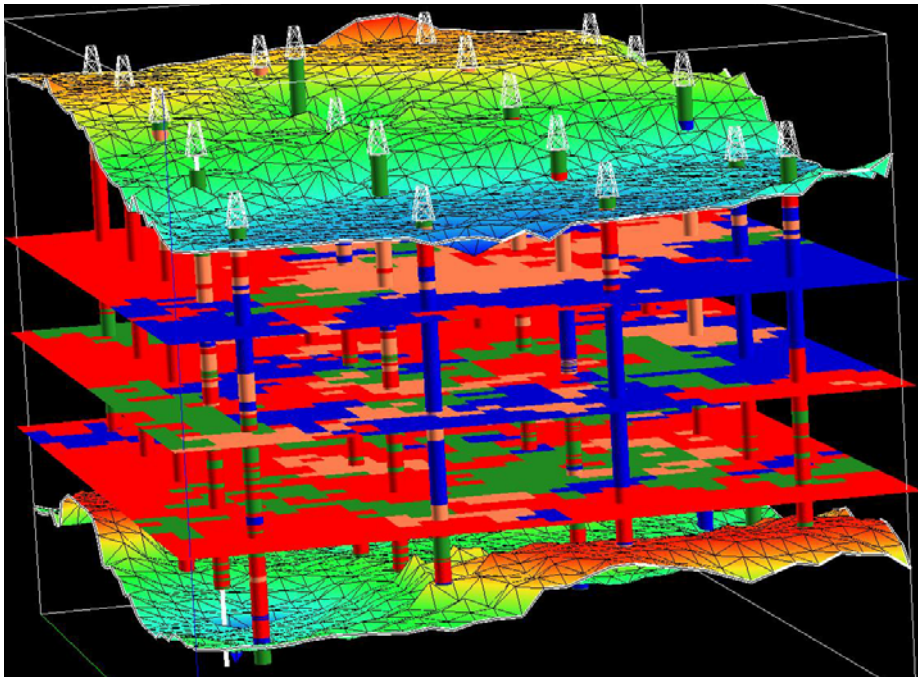

b)

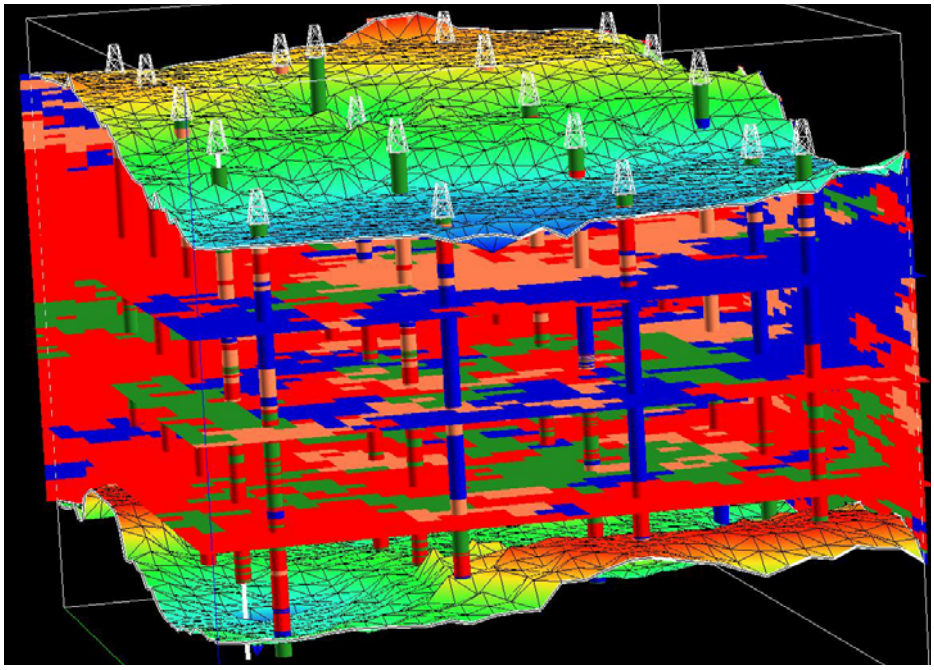

Figure 6.13 – Facies Realization 10. An illustration of 10th facies realization and the facies core hole conditioning data within the 10th structure realization. Part a) of the figure shows elevation slices 60, 90, and 120 (out of 190 in total). Part b) shows, in addition to these three elevation slices, the last Easting and Northing slice.

7 PETROPHYSICAL PROPERTIES MODELING

Continuous properties such as porosity, permeability, impedance and oil, water and gas saturation each constitute a petrophysical property, hereafter referred to simply as properties. Their behavior is often controlled by lithofacies. The distribution of properties within each facies alters flow and, therefore, affects production performance. This section describes the process used to create multiple geostatistical realizations of the properties within each facies.

The only petrophysical property modeled is porosity, although, in practice, additional property models such as permeability would be required for flow simulation. Aside from what will be presented towards geostatistical porosity modeling in this section, there are a number of additional steps and details that need to be dealt with in modeling the other properties, especially permeability, see Deutsch (1999).

Geostatistically modeling porosity is similar to modeling facies in that a 3-D trend and spatial correlation model is needed prior to simulation. The main steps are (1) gather the relevant porosity conditioning data (2) establish the 3-D trend or locally varying mean porosity model, (3) assemble a licit 3-D model of spatial correlation, (4) stochastically construct multiple porosity realizations and (5) validation.

Porosity is a continuous variable modeled within each facies, see Figure 5.3. In addition to differences in basic statistics, porosities' locally varying mean or trend model and model of spatial correlation is also different within each lithofacies. For each simulated realization, porosity is independently simulated assuming a single facies type; the results are then merged using the facies model. This "cookie-cutter" approach is standard.

The final numerical model of porosity will contain a value of 0 if it is located in the non-net shale facies. This is standard based on the histogram of porosity within the shale facies shown in Figure 5.3. Over 75% of the values within shale are 0% porosity or near 0% porosity. Therefore, trend and variogram models are not created within the shale facies.

7.1 THE POROSITY CONDITIONING DATA

Porosity is the volumetric concentration of pore space, derived from core assays. These methods may be used preferentially in some areas of the reservoir and often result in porosity measurements at different scales. In such cases, additional debiasing or declustering, and scaling procedures may be needed.

There is no need for declustering or scaling in our example since the porosity are form the same data source and are uniformly spaced. The global histogram of porosity and the histogram of porosity inside each of the four facies types are shown in Figure 5.2 and 5.3, respectively. Porosity profiles are available at 10cm increments along each of the 20

exploratory core holes. Figure 7.1 depicts the profile of porosity along the vertical span of core hole 9. The porosity color scale that will be used for subsequent illustrations is also shown in this Figure.

The entire set of porosity values are now divided into three separate files, one for each net facies type, that is sand, interbedded sand and breccia. This will simplify the mechanics of modeling porosity. In anticipation of using a Gaussian based simulation algorithm, the normal score porosities are calculated and appended as an extra column in each of these 3 files.

7.2 POROSITY TREND MODEL

Most depositional settings exhibit petrophysical property trends within the facies. For example, the vertical profile of porosity may show a continual “fining upward” or “coarsening upward” behavior. These large-scale variations, locally varying means or non-stationarities should be reproduced in the final numerical model.

The methodology for creating a 3-D porosity trend within each net facies consists of merging a 1-D vertical and 2-D aerial trend into a final 3-D trend model. The result is a 3-D model of locally varying porosity means within the sand, interbedded sand and breccia facies.

The 1-D vertical porosity trends are constructed. The average porosity within 1m vertical bins (10 samples per bin) is calculated. The center of each bin is then plotted against the corresponding average porosity values to visualize the general form of the trend. This process is implemented for all three net facies types. To infer the trend for all 175m to 270m elevations, multiple control points are established on these plots and linear interpolation is implemented. The process and the resulting 1-D vertical porosity trend within each facies are shown in Figure 7.2.

A kriging algorithm is used to construct the aerial porosity trends. There are 3 sets of conditioning data – one set for each lithofacies. Each conditioning data value is the average porosity taken over the vertical domain of one of the three net facies within that particular core hole location. Variography is first performed with these conditioning data. The output cells measure 50m a side. No significant aerial trends within the breccia facies were found. The resulting aerial trend map and corresponding variogram model for the sand and interbedded sand facies is shown in Figure 7.3.

The same scaling procedure that was used to combine the vertical and horizontal facies proportion maps is now used to combine the vertical and horizontal porosity trend maps. That is, the 3-D porosity trend model within the three net facies is calculated to be the aerial mean porosity value multiplied by the vertical mean porosity value divided by the average porosity in that particular facies:

$$porosity(X,Y,Z) = \frac{areal\_porosity(X,Y) \bullet vertical\_porosity(Z)}{global\_porosity}$$

These 3-D porosity trend models are used as conditioning information in subsequent porosity simulation; the final numerical model of porosity should reproduce the general form of these trends within each facies.

To visualize the 3-D porosity trend model within each facies, the same sections used to investigate the 3-D facies proportion maps are used, see Figure 6.5. Two *XY*, *XZ* and *YZ* sections are shown through the porosity trend within the sand, interbedded sand and breccia facies in Figures 7.4 to 7.6, respectively. The scaling procedure can be observed in these figures. The vertical scale is exaggerated by five times.

7.3 POROSITY VARIOGRAPHY

Petrophysical properties within different facies are often significantly different. This is why locally varying property averages are modeled within the separate facies types to condition all locations to be simulated. The properties will also often exhibit different anisotropy depending on which facies they are in. This is accounted for in simulation by creating a separate 3-D variogram model for each lithofacies.

We now calculate and model 3-D variograms of normal-score porosity within each facies. Normal-score variograms are convenient for Gaussian-based simulation. The same challenges present in calculating the horizontal indicator facies variogram exist here: the horizontal exploratory core hole spacing allows for only 3 experimental horizontal variogram points. Although we followed conventional modeling practice, various techniques could be applied in practice to model horizontal variogram models such as seismic calibrations, anisotropy ratios and expert judgment. The experimental vertical porosity variogram is well informed and easier to model due to the 10cm vertical porosity data spacing. The resulting calculated and modeled normal-score horizontal and vertical porosity variograms within each net facies is shown in Figure 7.7. The 3-D variogram model used in simulation within each net facies is also shown in mathematical equation form in this figure.

7.4 POROSITY SIMULATION

All of the information needed to condition multiple geostatistical realizations of porosity within each of the lithofacies is available. The same grid specification used for structure and facies modeling is used for porosity modeling. The same cells populated with simulated facies codes, are populated with simulated porosity values so that each 3-D cell that has not been clipped by the top and bottom structure will contain a simulated facies type and porosity value. *sgsim* (sequential Gaussian simulation) from the GSLIB package is now used with the original conditioning data and the established by-facies porosity trend and variogram model to create 100 3-D geostatistical realizations of the porosity variable.

It was previously mentioned that a “cookie cutter” approach is used in simulating porosity in the SAGD example. The details should be mentioned. Three complete 3-D models of porosity are simulated; one for each lithofacies, assuming the entire 3-D reservoir is one facies type at a time. These simulations amount to using each of the four previously created by-facies porosity data files, trend and variogram models as conditioning data. These three by-facies porosity models are then merged into a final porosity model using the previously created facies models, that is, the final porosity model values are taken from the appropriate facies-dependant model. In this way, locations that are simulated within any of the by-facies models using limited conditioning data – this happens often since the conditioning data for each by-facies model is located within only one facies – will not be merged into the final model. If the facies is shale, porosity is automatically assigned a value of 0 at that location. This is repeated for each geostatistical realization.

Figure 7.8 shows the 50^{th} of the 100 equal-probable porosity realizations. The general forms of the vertical and horizontal porosity trends are reproduced. The same section locations used to visualize the 3-D porosity trend models are used to visualize the 50^{th} porosity realization in this figure.

Figures 7.9 and 7.10 aid in visualizing the porosity conditioning data and the simulation results, in particular, the 10^{th} porosity realization. The conditioning porosity core hole data in Figure 7.9 shows higher porosity within the Northern part of the reservoir where it is thickest and lower porosity within the Southern part of the reservoir where it is thinnest. The cross sections shown in Figure 7.9 show that the simulated facies data honor the conditioning core hole data.

7.5 VALIDATION

Before continuing, it is necessary to validate the multiple realizations of porosity. In validating these realizations, we check to make sure the conditioning data are honored, the global average is reproduced and the form of the 3-D trend and variogram model is reproduced. The simulated porosity values are compared to the collocated porosity conditioning data values; the global average of the simulated porosity values within each net facies is compared to those of the conditioning data (Figure 5.3); the vertical and horizontal porosity averages are re-calculated within each net facies and compared with the conditioning by-facies porosity trends (Figure 7.2 and 7.3); and the horizontal and vertical variograms are re-calculated within each net facies and compared to the originals (Figure 7.7). These checks are performed on each realization, then averaged and compared to the original conditioning information. The original conditioning data are honored and within each net facies, the global porosity averages are reproduced, the general form of the vertical and horizontal trend is reproduced and the 3-D variogram model is reproduced.

7.6 POROSITY UNCERTAINTY

One of the goals of using geostatistics to characterize a potential SAGD reservoir is to establish geological uncertainty and then transform that geological uncertainty into production, that is, cumulative SOR and oil production rate, uncertainty. We now have all of the resources needed to define the geological uncertainty.

The uncertainty in porosity, that is the fluctuation from porosity realization to realization, makes the last contribution to geological uncertainty. Recall that each model of the geology consists of a single realization of each parameter, therefore, only one porosity realization is associated to one facies realization, which is associated to only one top and bottom realization. A single geological realization is defined by a single realization of each of the modeled reservoir variables or parameters. For instance, in our SAGD example, a geological realization is defined by a single realization of thickness, lithofacies and porosity (in practice, other petrophysical properties would need to be modeled). Each geological realization has an attached uncertainty, which is defined by the uncertainty in each of the parameter realizations. The final geological uncertainty is the fluctuation from geological realization to realization.

In the SAGD example, geological uncertainty will be transformed into production uncertainty via a transfer function. In our case, this transfer function is flow simulation. Each realization of the geology is passed into the flow simulator to get a realization of the production performance. The fluctuation of cumulative SOR and oil production rate is the production uncertainty.

7.7 FIGURES

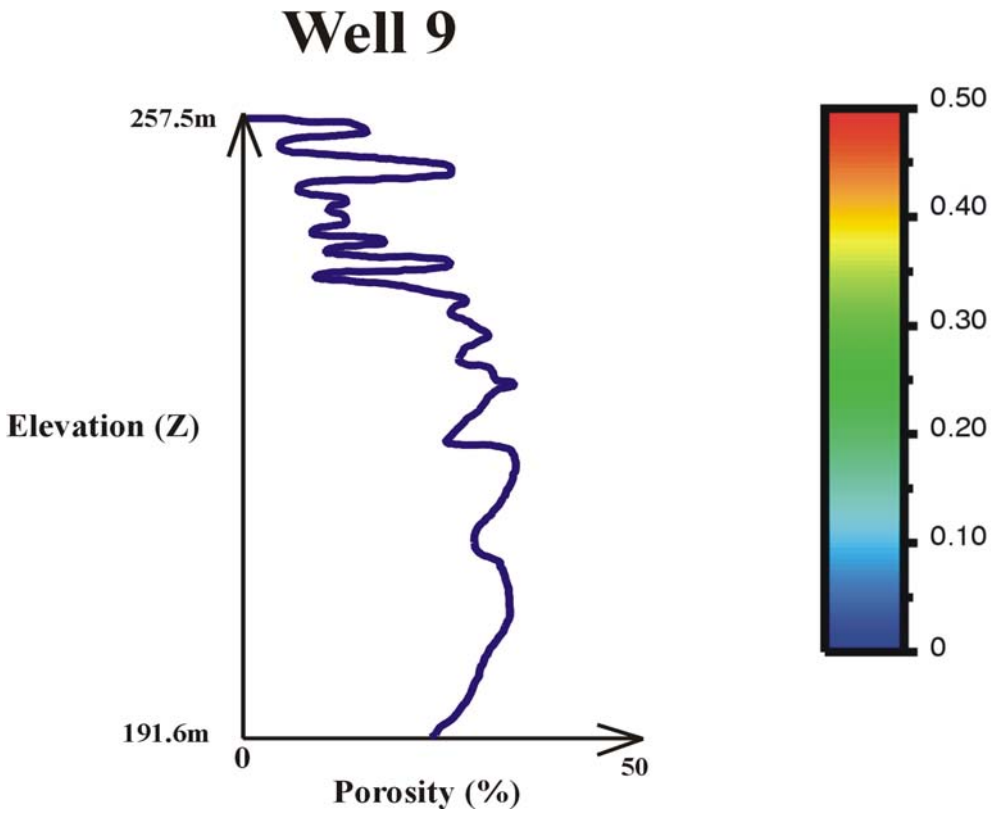

Figure 7.1 – Porosity Conditioning Data. An illustration of the porosity conditioning data available at each of the 20 exploratory core holes. The porosity profile for well 9 is shown on the left. The color scale on the right will be used in subsequent porosity illustrations.

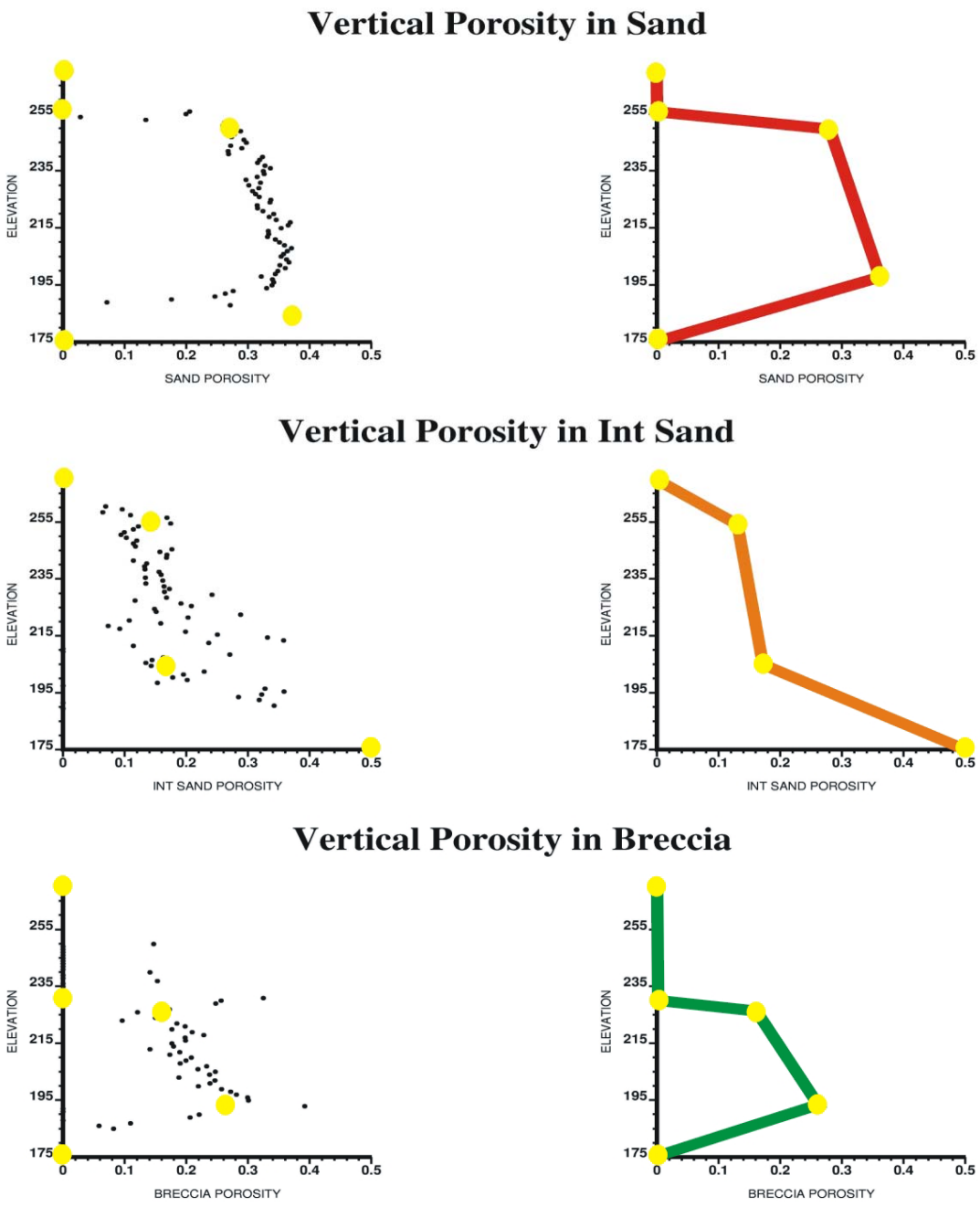

Figure 7.2 – Vertical Porosity Trends. An illustration of the cross-plots and the control points used to infer the vertical porosity trend within each facies. The cross-plots on the left show the center of each elevation bin vs. the corresponding calculated porosity average. The control points are shown on these cross-plots in yellow. Linearly interpolating between these control points allows us to create the final 1-D vertical porosity trend models shown on the right.

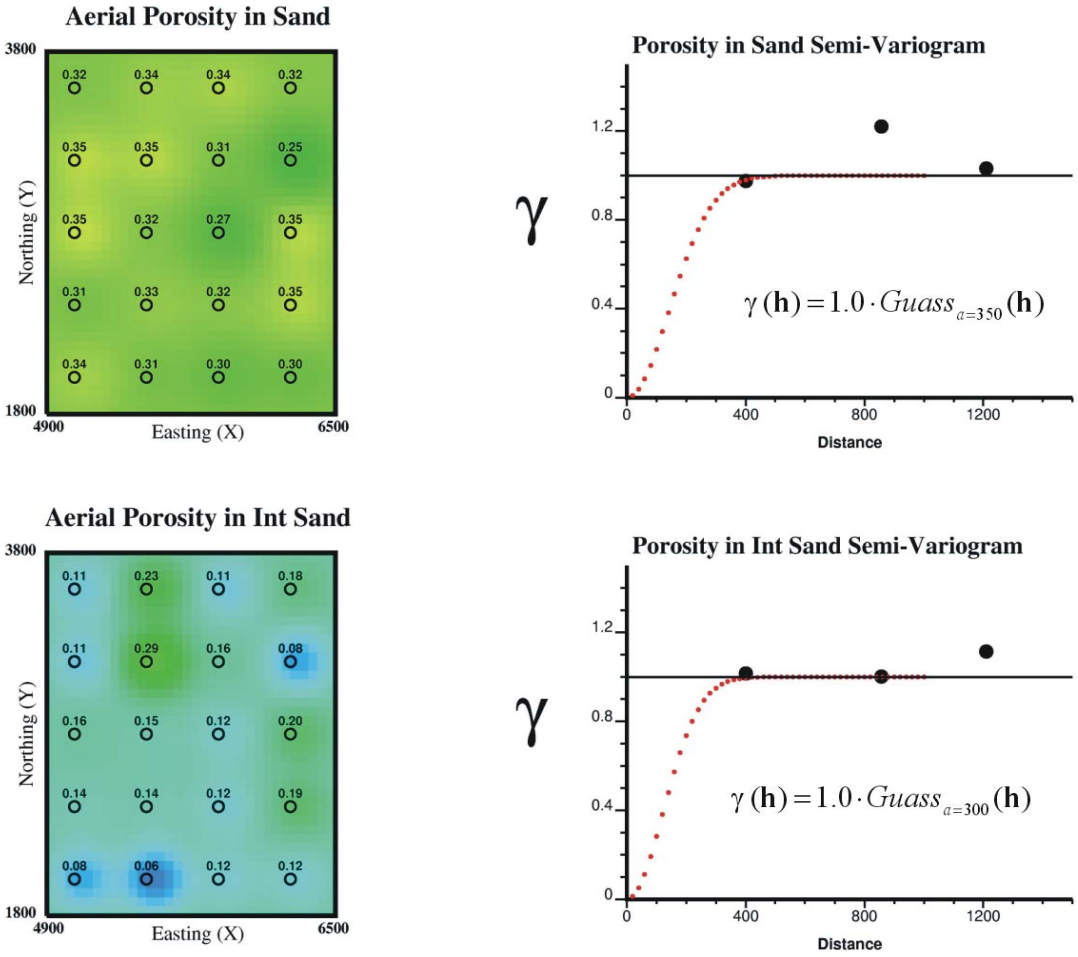

Figure 7.3 – Horizontal Porosity Trends. An illustration of the smoothly kriged aerial porosity trend maps within the sand and interbedded sand facies. The conditioning data are superimposed on top of the aerial proportion maps on the left. Both the conditioning data and the kriged values follow the porosity color scale shown in Figure 7.1. The right side of the figure shows the variogram (in graphical and equation form) used to create the corresponding aerial porosity trend maps.

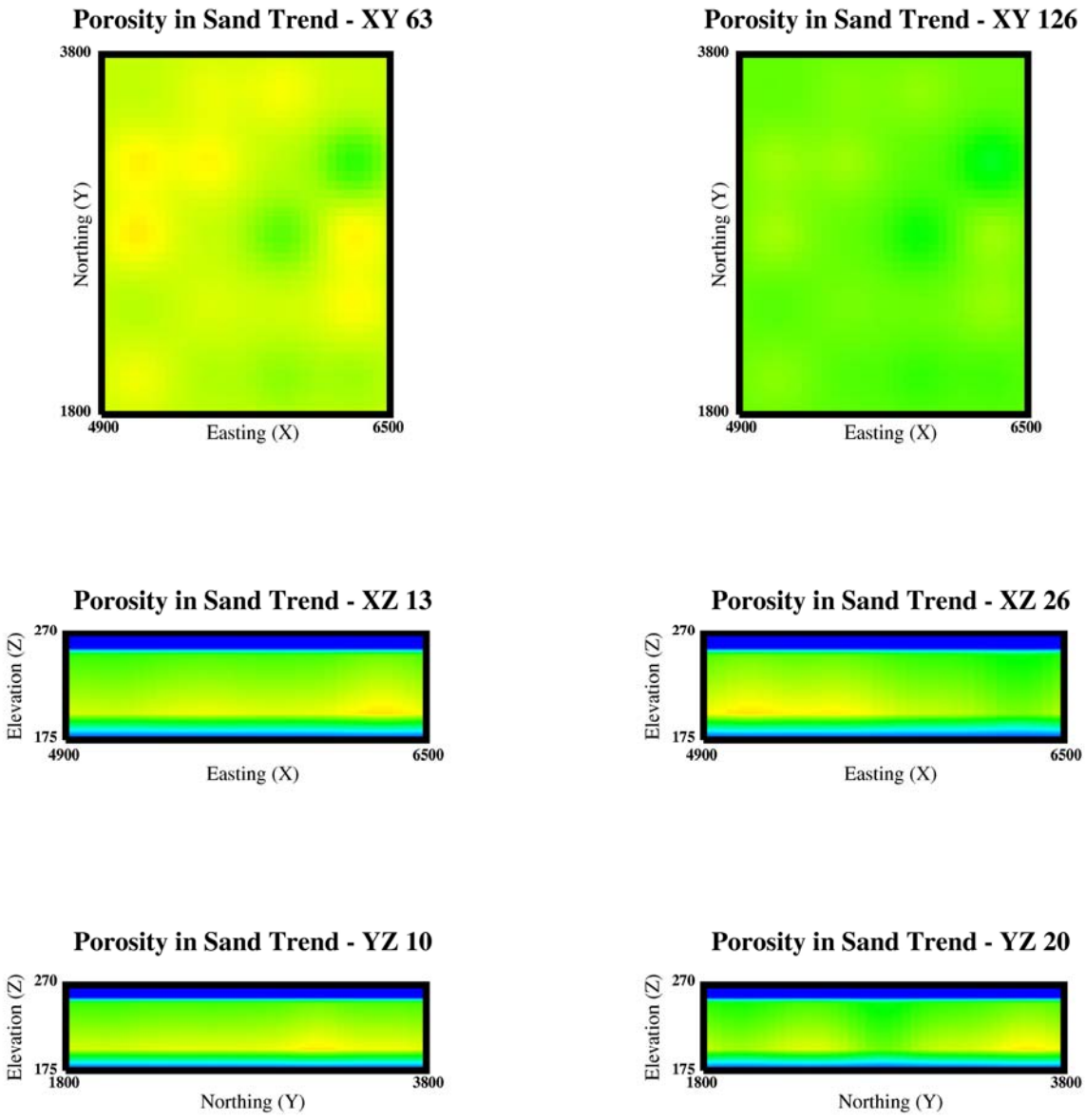

Figure 7.4 – Porosity Trend Model in Sand. Two *XY*, *XZ* and *YZ* sections through the trend model of porosity for the sand facies. The same porosity color scale shown in Figure 7.1 is used in this figure.

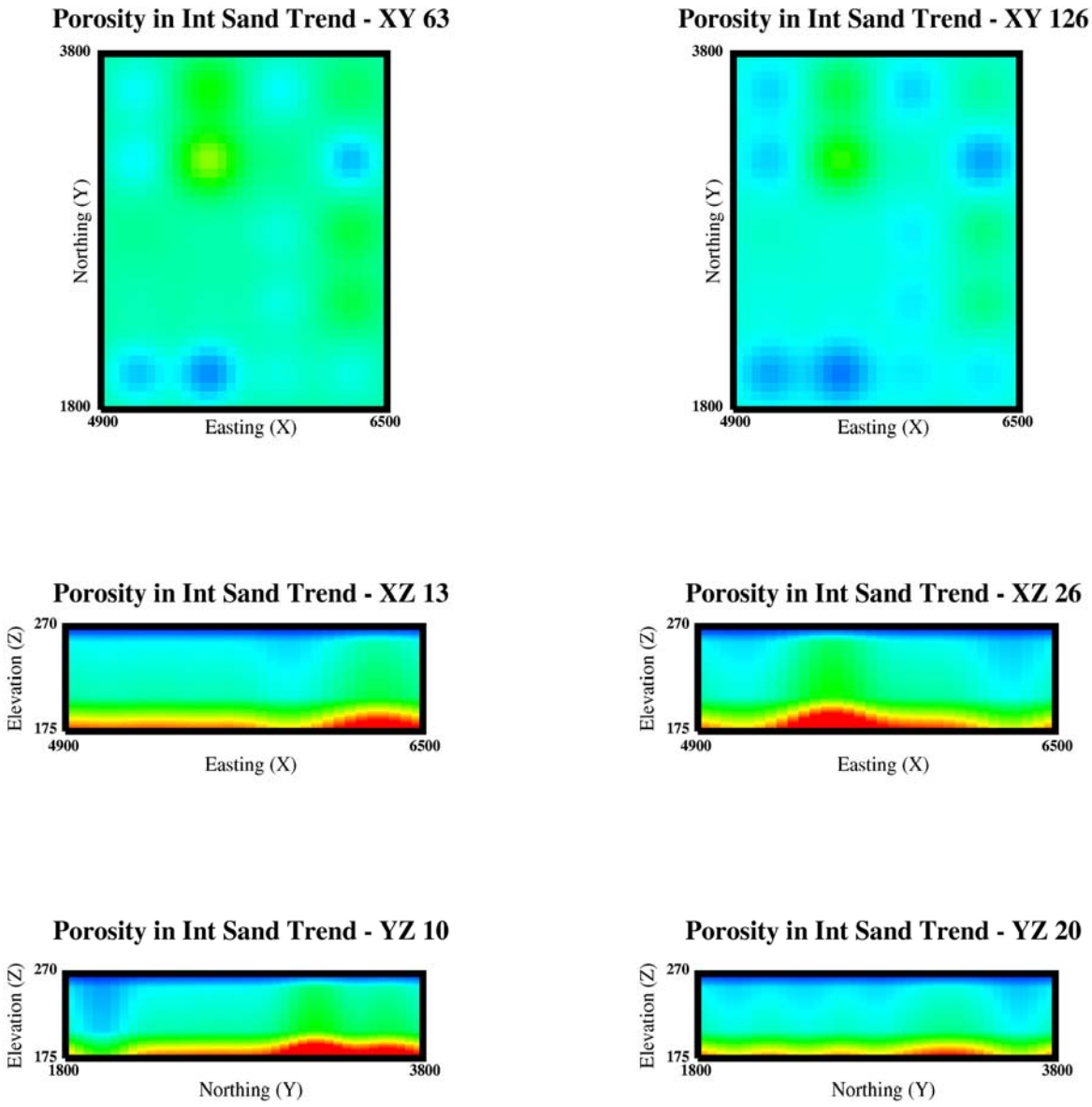

Figure 7.5 – Porosity Trend Model in Interbedded Sand. Two *XY*, *XZ* and *YZ* sections through the trend model of porosity for the interbedded sand facies. The same porosity color scale shown in Figure 7.1 is used in this figure.

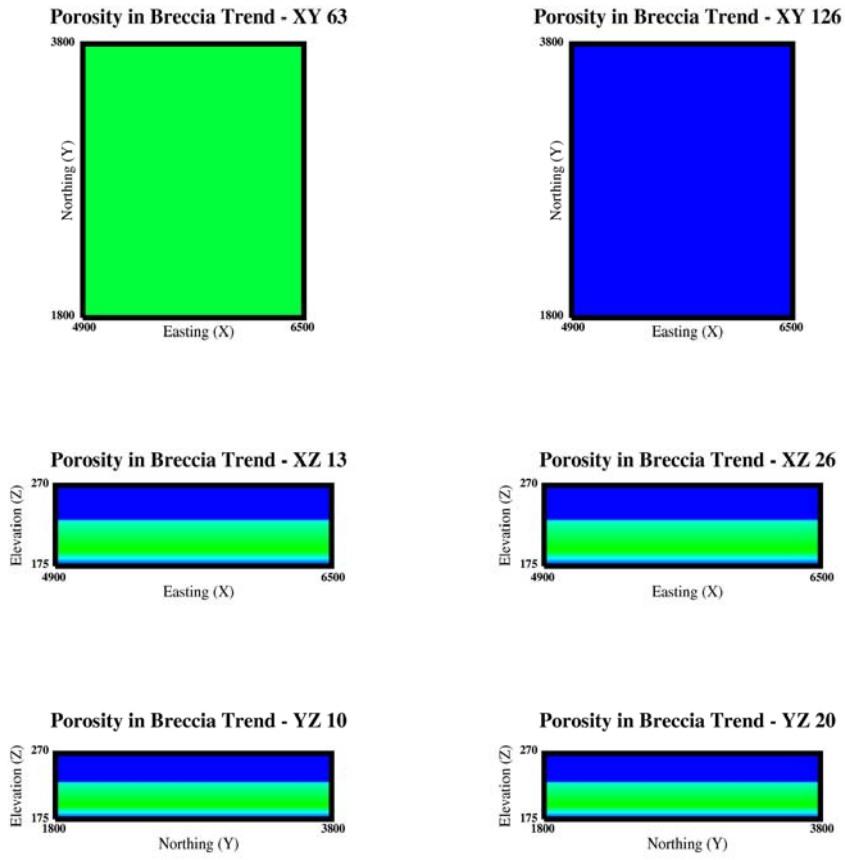

Figure 7.6 – Porosity Trend Model in Breccia. Two *XY*, *XZ* and *YZ* sections through the trend model of porosity for the breccia facies. The same porosity color scale shown in Figure 7.1 is used in this figure.

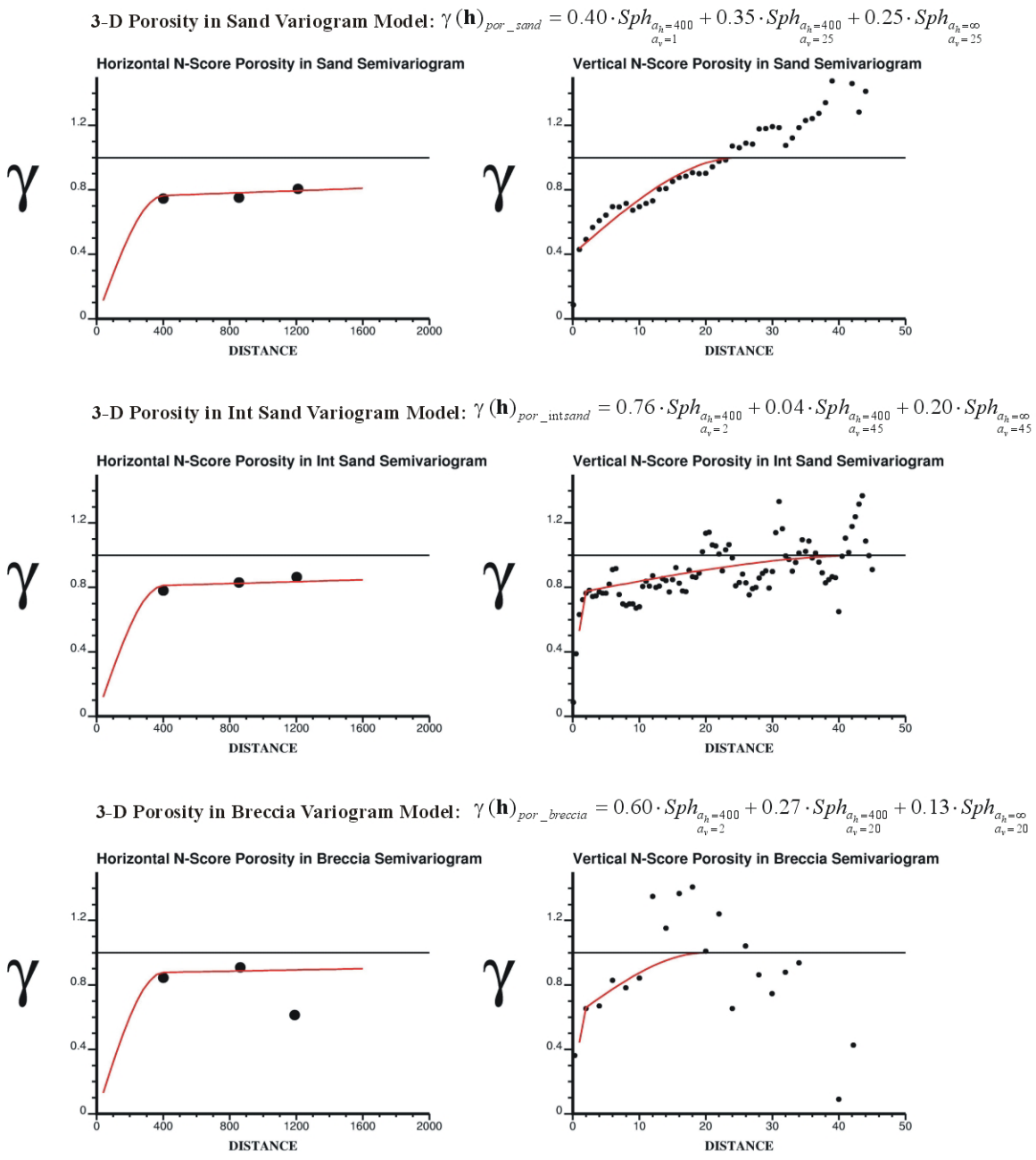

Figure 7.7 – Porosity Variograms. An illustration of the calculated horizontal and vertical porosity variograms within each net facies. The experimental points are shown as black dots and the models are shown as red lines. The equation of each 3-D porosity variogram model is also shown.

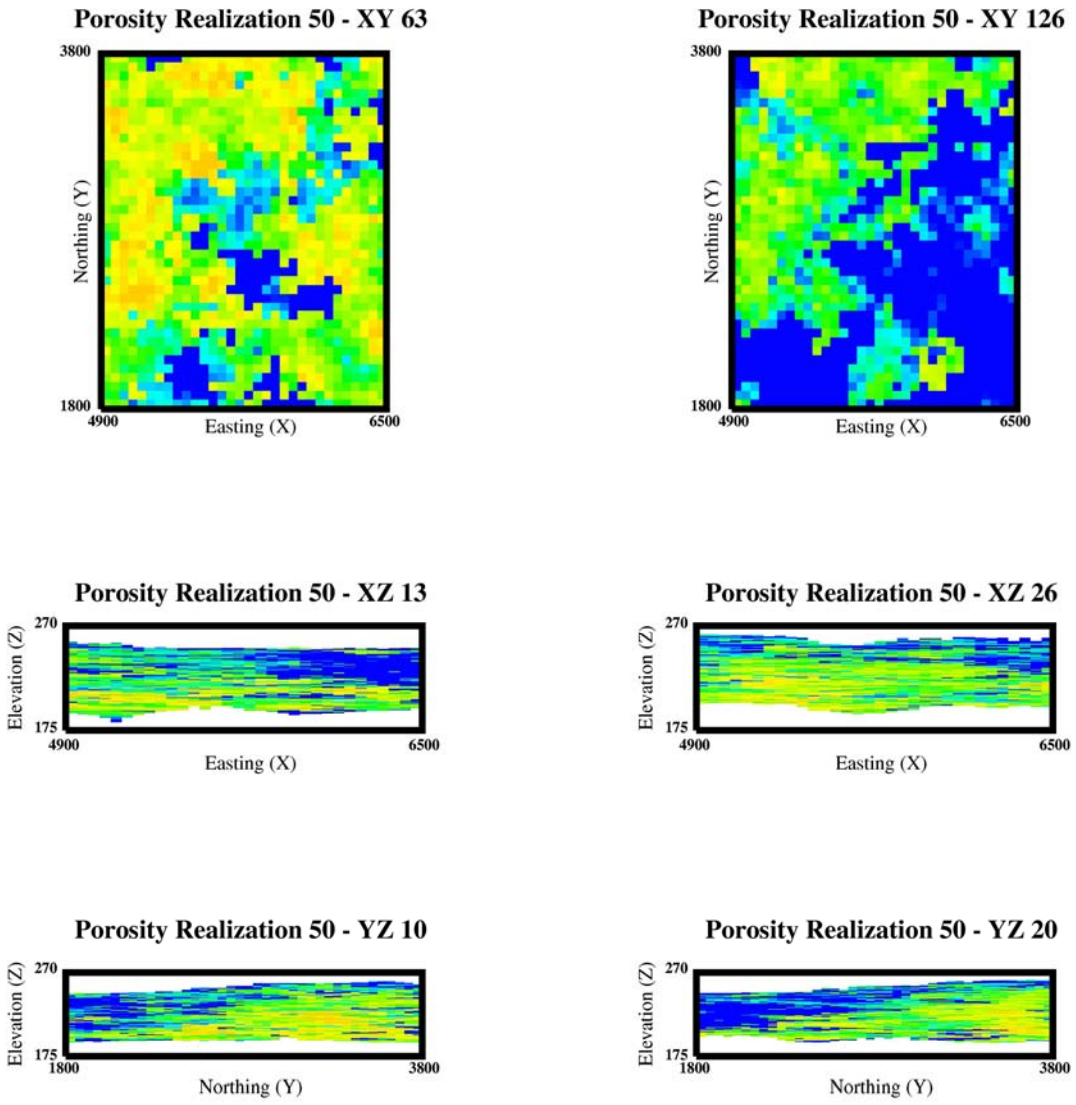

Figure 7.8 – Porosity Simulation. An illustration of the 50th porosity realization. The same color scale used in Figure 7.1 is used in this figure. The vertical scale has been exaggerated by five times. The white space contains those cells that were clipped by the previously created structure models.

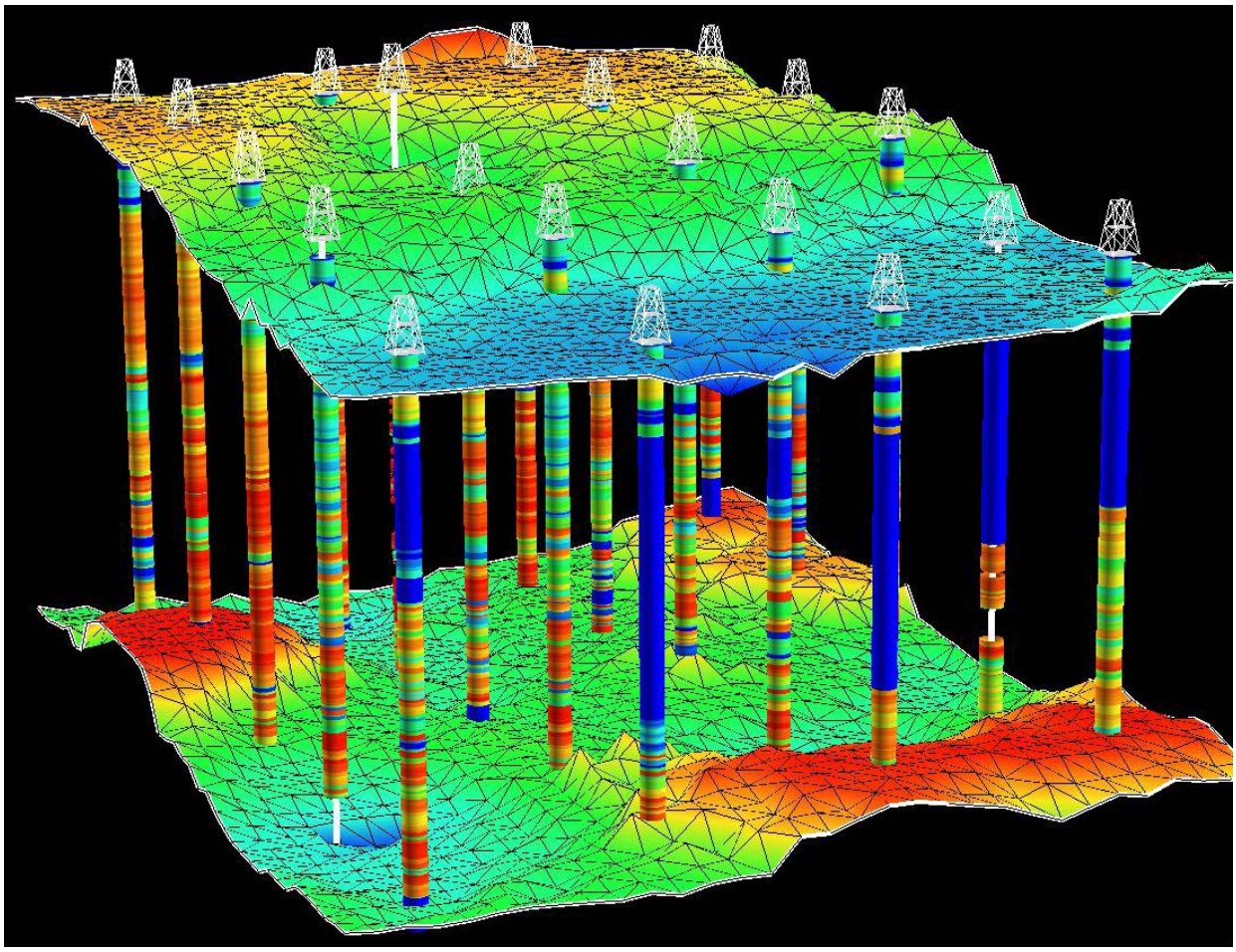

Figure 7.8 – Porosity Conditioning Data. An illustration of porosity conditioning data within the 10th structure realization. The color scheme is the same as shown in Figure 7.1.

a)

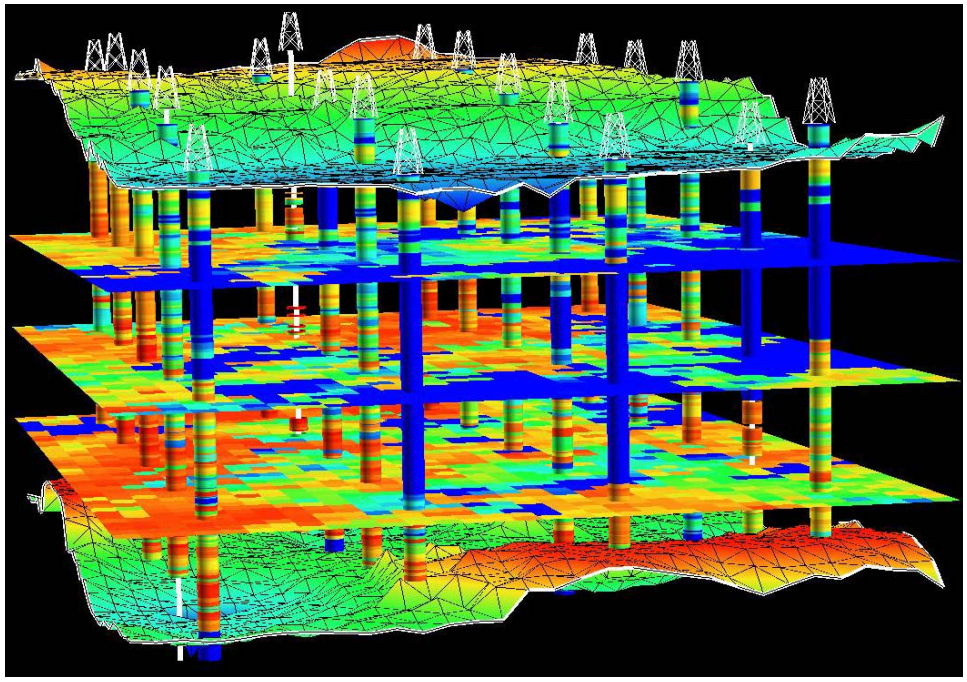

b)

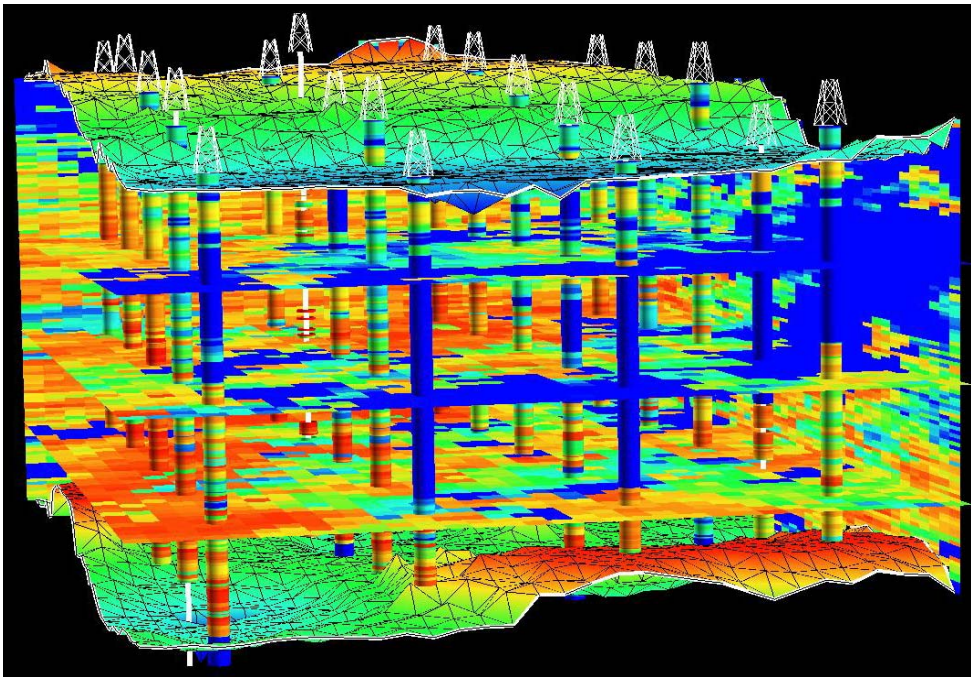

Figure 6.13 – Porosity Realization 10. An illustration of 10th porosity realization and the porosity core hole conditioning data within the 10th structure realization. Part a) of the figure shows elevation slices 60, 90, and 120 (out of 190 in total). Part b) shows, in addition to these three elevation slices, the last Easting and Northing slice.

8 POST-PROCESSING, CONNECTIVITY AND WELL PLACEMENT

Modeling structure, facies and petrophysical properties are preliminary procedures needed for reservoir characterization and flow simulation; reservoir characterization is discussed in this section. For each geological realization, engineering parameters such as rates and pressures are calculated with a formula or solution to discretized conservation equations. For example, to calculate contained bitumen, we could sum the product of the cell volume and cell porosity over all cells. Such formulas are referred to as “transfer functions”, that is, multiple realizations of geological parameters are transferred into engineering parameter realizations. Using these transfer functions, the expected value and uncertainty in each engineering parameter can be calculated and visualized in order to characterize the reservoir.

SAGD reservoir characterization includes a general resource assessment as well as a “connected” resource assessment. For a SAGD reservoir, we want to know where and how much bitumen will be heated and potentially recovered by the SAGD process; a connected resource assessment is performed to quantify the reservoir’s potential for this. A connectivity program is the main transfer function considered here. The details of thermal flow simulation are beyond the scope of this handbook.

In the SAGD example of this report, 100 sets of reservoir parameter realizations (geological realizations) have been constructed, that is, 100 sets of structure, lithofacies and porosity parameter realizations exist. In this section, we describe the implementation details involved in characterizing the SAGD potential of the reservoir using this geological model. Both a general resource assessment and a connected resource assessment are discussed and implemented. The same engineering parameters calculated for the general resource assessment, are re-calculated for the connected resource assessment taking into account a calculated net connectivity indicator.

The final connected resource assessment that identifies the net reservoir that can be potentially heated and recovered by the SAGD process, can be used to infer areas of high SAGD potential. This information assists well placement decisions. In the SAGD example, we choose the SAGD well pair location with the highest recovery potential.

Although we have only modeled porosity, there are additional engineering parameters that can be calculated to characterize the potential of the reservoir in our example for the SAGD recovery process. Various others include permeability or oil/water saturation are modeled.

8.1 GENERAL RESOURCE ASSESSMENT

Using our geostatistically created models of structure (2-D top and bottom surface elevations), facies type (sand, interbedded sand, shale or breccia) and porosity, there are a

number of general engineering parameters that we can calculate in order to characterize the reservoir. The contained bitumen in m^3 or barrels, sand thickness in m, average net porosity in % and net bitumen thickness in m are the simplest summaries we chose to calculate for the SAGD example. The proven-probable-possible reserves could be calculated on the basis of various approaches using the uncertainty we have modeled.

For each of the 100 geological realizations, the resource is calculated for the entire reservoir and the sand thickness, average net porosity and net bitumen thickness is calculated at each *X*-*Y* location. The distribution of the resource or contained value is visualized in the form of a histogram and probability plot. The distribution of the sand thickness, average net porosity and net bitumen thickness at each *X*-*Y* location is used to calculate various statistics, namely, the expected value, the value where the probability of exceeding is 90% and 10% and the difference between these two values. The values where the probability of exceeding is 90% and 10% are referred to as the 0.10 quantile and 0.90 quantile values or p-10 and p-90 values, respectively. The difference between these quantile values is a measure of uncertainty, that is, the larger the difference between the 0.90 and 0.10 quantile, the larger the uncertainty. These calculated statistics are then plotted on 2-D maps for visualization and general reservoir characterization.

The map of the difference between the 0.90 and 0.10 quantiles (never less than 0) is referred to as a map of spatial uncertainty. Since the geostatistical models honor the original conditioning data, the distribution of engineering parameters at the data locations are single valued spikes centered at the transfer function output using the original conditioning data. Therefore, there is 0 uncertainty in the calculated engineering parameters at the original data locations; uncertainty generally is highest at locations furthest away from the original conditioning data. Although not done, we could divide this difference by the expected value to get a relative uncertainty.

Based on these summaries, some general well placement engineering decisions can be made. Locations with high sand thickness, average net porosity and net bitumen thickness and low uncertainty are preferred for optimal well placement.

8.1.1 CONTAINED BITUMEN

The contained bitumen is the net amount of bitumen contained within the reservoir structure. This parameter is vital for many engineering concerns such as economic forecasting and feasibility studies. Using our geological realizations, we can create 100 realizations of the contained bitumen via a transfer function. Uncertainty in the contained bitumen is the fluctuation of the resulting 100 contained bitumen values.

Within the reservoir structure, on a cell-by-cell basis, the contained bitumen is either set to 0 or calculated as the product of the cell volume, cell porosity and the difference between 1 and the water saturation, depending on the facies type and porosity value present. If the cell is non-net, that is, the facies type is shale *or* the porosity value is less than a predefined porosity threshold, the contained bitumen is set to 0. The sum of all the resulting cell-by-cell contained bitumen values is the contained bitumen within the

structure of the reservoir. This process is repeated 100 times, once for each geological realization. The contained bitumen transfer function can be summarized by the following formula:

$$Q^{(l)} = \sum_{all\ cells} V_{(X,Y,Z)} \cdot \phi^{(l)}_{(X,Y,Z)} \cdot (1 - S_{(X,Y,Z)}) \cdot i^{(l)}_{net\_bit\,(X,Y,Z)} \qquad for\ l = 1,...,100$$

where

$Q^{(l)}$ is the contained bitumen value for realization l;
X, Y, Z are the Easting, Northing and Elevation coordinates, respectively;
$V_{(X,Y,Z)}$ is the volume in each cell;
$\phi^{(l)}_{(X,Y,Z)}$ is the porosity value in each cell for realization l;
$S_{(X,Y,Z)}$ is the water saturation in each cell;
and $i^{(l)}_{net\_bit\,(X,Y,Z)}$ is a net bitumen indicator variable taking the following form:

$$i^{(l)}_{net\_bit\,(X,Y,Z)} = \begin{cases} 0, & if\ \ fcs^{(l)}{}_{(X,Y,Z)} = 3\,(shale),\ or\ \phi^{(l)}{}_{(X,Y,Z)} < \phi_{thresh} \\ 1, & otherwise \end{cases}$$

where

$fcs^{(l)}{}_{(X,Y,Z)}$ is the binary facies type code in each cell for realization l;
ϕ_{thresh} is the porosity threshold;

This transfer function is now implemented using $V_{(X,Y,Z)} = 50m \cdot 50m \cdot 0.5m = 1250m^3$, assuming $S_{(X,Y,Z)}$ to be 0.15 and setting ϕ_{thresh} equal to 0.09. The result is 100 realizations of the contained bitumen. The distribution of the resulting contained bitumen values in m^3 and barrels are visualized in the form of a histogram and probability plot. The mean and variance or expected value and uncertainty, respectively, can be derived from the histograms while the value where a fixed conditional cumulative distribution function (ccdf) value p is reached, that is, the conditional p-quantile value, can be derived from the probability plots.

The final results of the contained bitumen transfer function are shown in the form of a histogram and probability plot in Figure 8.1. The mean and standard deviation of the contained bitumen is 32.7 x 10^6 and 0.5 x 10^6 m^3, respectively, or 205.8 x 10^6 and 3.0 x 10^6 barrels, respectively. The p-90 contained bitumen value (where the probability of exceeding is 10%) and p-10 contained bitumen value (where the probability of exceeding is 90%) are 33.3 x 10^6 and 32.1 x 10^6 m^3, respectively, or 209.6 x 10^6 and 201.8 x 10^6 barrels, respectively.

The global uncertainty in contained bitumen, as prescribed by the difference between the p-90 and p-10 values is quite low; however, uncertainty at smaller volumes such as a nominal SAGD drainage volume may be higher. Further investigation into local contained bitumen uncertainty may be required in practice.

8.1.2 SAND THICKNESS

Sand thickness is simply the thickness of sand at each *X*-*Y* location in the model. Sand thickness is a good indicator of the spatial quality of the reservoir in plan view and can be used to infer locations where accumulations of bitumen will likely exist. From our 100 geological realizations, we can create a distribution of 100 realizations of the sand thickness at each *X*-*Y* location.

The *X*-*Y* sand thickness values are calculated as the product of the number of sand cells found while looping over the *Z* locations within the reservoir structure for each *X*-*Y* location and the thickness of the cells. This sand thickness transfer function takes the following form:

$$T_{sand\,(X,Y)}{}^{(l)} = \sum\nolimits_{Z} T_{(X,Y,Z)} \cdot i^{(l)}_{sand\_fcs} \qquad for\ l = 1,...,100$$

where

$T_{sand\,(X,Y)}{}^{(l)}$ is the sand thickness at each *X*-*Y* location for realization *l*;
$T_{(X,Y,Z)}$ is the thickness of each cell;
and $i^{(l)}_{sand\_fcs}$ is an indicator variable taking the following form:

$$i^{(l)}_{sand\_fcs} = \begin{cases} 1, & if\ \ fcs^{(l)}{}_{(X,Y,Z)} = 1\,(sand) \\ 0, & otherwise \end{cases}$$

Using $T_{(X,Y,Z)}$ = 0.5m, the sand thickness transfer function is now implemented. At each *X*-*Y* location in the model, there is now a distribution of 100 possible sand thickness values. For each local distribution, the expected value, the p-90 and p-10 values and the difference between the p-90 and p-10 values are calculated. Figure 8.2 shows the 2-D maps of these calculated statistics. The map of expected sand thickness values shows an accumulation of sand in the Northern area of the reservoir and a deficit of sand in the Southern area of the reservoir. Notice, there is 0 uncertainty at the original data locations; locations farther away from the original data locations, e.g. along the border of the reservoir and between conditioning data, host larger uncertainties.

8.1.3 AVERAGE NET POROSITY

The average net porosity is the average cell-by-cell porosity taken over a specified area of the reservoir. For each geological realization, we chose to calculate an average net porosity value for each *X*-*Y* column, that is, the average is taken over all the *Z* locations for each *X*-*Y* column. Average net porosity allows us to infer areas in the reservoir where oil accumulation will likely be. At each *X*-*Y* location, 100 realizations of the average net porosity can be created corresponding to the 100 geological realizations.

While summing the porosity over all of the *Z* locations for a particular *X*-*Y* column location, certain cells are flagged depending on the facies type and porosity value present. The dependence on facies type and porosity value is the same as in the contained bitumen transfer function in section 8.1.1. The number of cells flagged in the sum then divides the porosity sum. The average net porosity transfer function takes the following form:

$$\overline{\phi}_{net(X,Y)}^{(l)} = \frac{\sum_Z \phi_{(X,Y,Z)}^{(l)} \cdot i^{(l)}{}_{(X,Y,Z)}}{\sum_Z i^{(l)}{}_{(X,Y,Z)}} \qquad for\ l = 1,...,100$$

where

$\overline{\phi}_{net(X,Y)}^{(l)}$ is the average net porosity at each *X*-*Y* column location for realization *l*, and the rest of the components are the same as in the contained bitumen transfer function in Section 8.1.1.

The average net porosity transfer function is now implemented using ϕ_{thresh} = 0.09. At each *X*-*Y* column location there is now a distribution of 100 equally probable realizations of the average net porosity value, from which we calculate the expected value, the p-90 and p-10 values and the difference between the p-90 and p-10 values. Figure 8.3 illustrates these calculated statistics in 2-D maps. Consistent with the sand thickness results, this figure shows bitumen accumulation and deficit in the Northern and Southern areas of the reservoir, respectively.

8.1.4 NET BITUMEN THICKNESS

The net bitumen thickness is the thickness of the bitumen column at each *X*-*Y* location. Net bitumen thickness is indicative of areas of bitumen accumulation and deficit and is useful for reservoir forecasting. For example, to cover initial capital expenditures for a project, a production well may be placed in an area of the reservoir where the net bitumen thickness is largest. At each *X*-*Y* location, we can create 100 realizations of the net bitumen thickness.

At each cell, the bitumen thickness is calculated as the product of cell thickness, cell porosity and the difference between 100% and the water saturation or is set to 0,

depending on the facies type and porosity value present. The dependence on facies type and porosity value is the same as in the contained bitumen transfer function in Section 8.1.1. The net bitumen thickness transfer function takes the following form:

$$T_{bit(X,Y)}^{(l)} = \sum_Z T_{(X,Y,Z)} \cdot \phi_{(X,Y,Z)}^{(l)} \cdot (1 - S_{(X,Y,Z)}) \cdot i^{(l)}{}_{(X,Y,Z)} \qquad for\ l = 1,...,100$$

where

$T_{bit(X,Y)}^{(l)}$ is the net bitumen thickness at each *X*-*Y* location for realization *l* and the rest of the components are the same as in the contained bitumen and sand thickness transfer function.

Using $T_{(X,Y,Z)}$ = 0.5m, $S_{(X,Y,Z)}$ = 0.15 and ϕ_{thresh} = 0.09, the net bitumen thickness transfer function is now implemented. At each location, there is a distribution of 100 possible net bitumen thickness values. For each distribution, the expected value, p-90 and p-10 values and the difference between the p-90 and p-10 values is calculated. Figure 8.2 shows the 2-D maps of these calculated statistics. These maps show an accumulation of bitumen in the Northern area of the reservoir and a deficit of bitumen in the Southern area of the reservoir.

8.1.5 GENERAL WELL PLACEMENT

Well placement is a significant decision that petroleum engineers and geologists often struggle with. In the SAGD example, we are now in a position to make some general well placement conclusions. Preference to the Northern area of the reservoir (where the sand thickness, average net porosity and net bitumen thickness are highest and the uncertainty (p90 – p10) is low) is given.

Connected resource summaries will help place horizontal SAGD wells. The SAGD process described in Section 1.2 depends on where and how much of the reservoir is connected. The effectiveness of the steam chamber depends on the amount of net bitumen, and on the amount of *connected* net bitumen. A connected resource assessment will be useful to assess SAGD recovery.

8.2 CONNECTED RESOURCE ASSESSMENT

Figure 8.5 illustrates the importance of a connected resource assessment for the SAGD recovery process. Three horizontal SAGD well pair locations and the assumed cumulative steam chamber area of influence for each are superimposed on a schematic cross section through a geological reservoir model. The net/non-net facies model and connected/unconnected reservoir within the steam chamber area of influence are shown. The SAGD well pair on the left can potentially produce all of the net bitumen contained within the steam chamber area of influence since this area is all connected. Even though a shale lens partially blocks this steam chamber, steam will likely distribute through and

around the shale lens eventually heating the net bitumen on top of the lens. The situation is different for the other two well pairs, however. There, the net bitumen above the steam chamber cannot flow through the impermeable non-net shale facies; the unconnected bitumen cannot be recovered. Engineering and production decisions based on a SAGD recovery process, especially horizontal well pair placement, must account for the connected net bitumen.

In the context of this report, spatial connectivity is defined as whether or not the steam chamber is able to heat and recover net bitumen at a particular location. The cumulative steam chamber area of influence and the distribution of shale facies are interdependent factors that affect spatial connectivity.

A connected resource assessment is now performed for our example. A connectivity indicator is calculated at each location for each of the 100 geological realizations previously created; the details of the custom-built local connectivity program are first discussed. The immediate connectivity results are then presented. The general resource assessment parameters calculated in Section 8.1 will then be re-calculated while considering the spatial connectivity indicator. Also, additional engineering parameters are explored to more fully characterize the SAGD potential of the example reservoir. The resulting connected resource assessment is then used to make some engineering decisions such as optimal horizontal SAGD well placement.

8.2.1 THE CONNECTIVITY PROGRAM

Conventional connectivity programs are not immediately applicable to SAGD reservoirs since the output only discerns whether or not the entire net reservoir is connected or not. In these cases, the connected path may be unrealistically far away from the steam chamber. We should only include connected bitumen within some realistic limited aerial extent. A program to calculate local or spatial connectivity is, therefore, described for the subsequent connected resource assessment.

8.2.1.1 OVERVIEW

The local connectivity program, calculates a connectivity indicator (1 if connected, 0 if unconnected) within “windows” centered on each *X*-*Y* stack of cells within the reservoir structure. The connectivity for a particular *X*-*Y* stack only includes those cells in the same stack – even if they are connected through other cells. The windows span from the *X*-*Y* cell stacks to a user specified radius or number of cells in the *X* and *Y* direction. A particular cell in an *X*-*Y* stack surrounded by a specified window span is deemed connected when a path from the bottom to the top of the stack exists there, meaning, there is no impermeable shale facies covering the entire window span at that cell’s particular *Z* location.

Figure 8.6 shows the implementation of the local connectivity program on a simplified reservoir facies model. The connectivity for two different *X*-*Y* stacks of cells is calculated within the same window span of 1 cell. For the first stack shown at the top, the first four

cells are connected. All subsequent cells in that stack are not connected because an impermeable shale layer completely covers the span of the calculation window; a path from the bottom to the top of the stack does not exist through these top three cells. For the second stack at the bottom, the shale layer does not completely cover the span of the window size. Here, the first four, as well as the last three cells, visited are connected because there is a path (black arrow) from the bottom to the top of the stack uninterrupted by an overriding shale facies covering the entire window span.

The difference between global and local connectivity for the SAGD recovery process is important. Using the horizontal SAGD well pair location in the left illustration of Figure 8.6, local connectivity calculations would yield a portion of the net reservoir (mostly the area underneath the shale facies) as connected. A conventional global connectivity program, however, would likely yield the entire net reservoir as connected and include all of these net reservoir cells in the resource assessment, significantly overestimating the recoverable reservoir.

In practice, there will be multiple connected zones within a given *X*-*Y* stack of cells; however, a SAGD well pair could produce only one. That is, for a fixed aerial *X*-*Y* position, only one production SAGD well placement is implemented. The local connectivity program is constructed to find the elevation of the lowest cell within the "lowest thickest" connected zone for each *X*-*Y* stack. To infer the lowest thickest connected zone, the thickness of the multiple connected zones is weighted according to the elevation of the lowest cell in each connected unit. Lower elevations are given higher weights. For example, between two connected units with the same thickness at the top and bottom of the reservoir, the unit at the bottom will be given the higher weighted thickness; and the elevation of the lowest cell in the lower connected unit would be the elevation of the bottom of the connected reservoir and the *Z* location where the SAGD production well were to be placed given that particular *X*-*Y* location.

8.2.1.2 INPUTS/OUTPUTS

The local connectivity program requires a number of inputs; most important, the multiple realizations of lithofacies. To define the net reserve, the user must then indicate which facies types in the lithofacies model are net facies, e.g. sand, and which are non-net, e.g. shale. A porosity and permeability threshold can also be used, in which case these 3-D models are required. The window size is user-established by the calculation window. Finally, the grid details and name of the output file must be specified.

Other than a 1 or 0 indicating whether or not a particular cell is connected and the elevations of the bottom of the connected reservoir, the local connectivity program outputs a number of other interesting engineering parameters specific to characterizing potential SAGD reservoirs. The facies type of the connected cells and the number of adjacent cells are calculated for each 3-D cell in the reservoir structure. The connected net thickness, gross net thickness and ratio of connected net thickness to gross net thickness, in addition to the elevation of the lowest cell in the lowest thickest connected

zone, are calculated for each 2-D *X-Y* location. The program also outputs the number of net reservoir cells that are connected within the reservoir structure.

8.2.1.3 IMPLEMENTATION ON THE SAGD EXAMPLE

We now use our multiple geological realizations to create multiple connectivity realizations. If the local connectivity program deems a particular cell as connected, it is assigned the binary code 1; otherwise the cell is assigned a 0. This connectivity indicator transform takes the following form:

$$i^{(l)}_{conn(X,Y,Z)} = \begin{cases} 1, & \text{if connected} \\ 0, & \text{otherwise} \end{cases}$$

A window size of 1 cell is used. The structure, lithofacies and porosity models are all inputs. The sand, interbedded sand and breccia facies (binary facies codes of 1, 2 and 4, respectively) are input as the net facies. A porosity threshold of 0.09 is also used to define the net cells. At each location in the reservoir structure, we now have 100 realizations of the connectivity indicator.

In Figure 8.7, a histogram of the ratio in percent of the number of connected cells to the number of net cells is shown. The average connected-to-net ratio is 84.9%. The difference between 100% and these ratios in percent is the proportion of cells that are used for the general resource assessment but not used for the connected resource assessment. At these cells the net bitumen indicator, $i^{(l)}_{net\_bit(X,Y,Z)}$, is equal to 1 and the connectivity indicator, $i^{(l)}_{conn(X,Y,Z)}$, is equal to 0.

The 50th of the 100 equally probable connectivity realizations is shown in Figure 8.8. The same sections used throughout this report to visualize 3-D models (see Figure 6.5) are shown through this 3-D connectivity realization. Compare this Figure with Figure 6.11, the 50th facies realization at the same locations. Notice in the elevation cross sections, the effect predominant impermeable shale facies has on connectivity. In the *XZ*-13 section, for example, the shale facies in the top Eastern part of the section yields all of the cells directly above the unit unconnected, that is, the SAGD steam chamber will not be able to reach and recover bitumen from this concentrated unit of unconnected cells.

Perhaps the best summary of the multiple connectivity indicator realizations is the "probability of connection". 100 realizations of the connectivity indicator are present at each *X-Y-Z* location in the reservoir model; the proportion of 1's at each cell location in the reservoir model is calculated to obtain a 3-D model of the probability of connection. The results are shown in Figure 8.9. By comparison with Figure 6.5, notice the low probability of connection values at locations above the shale facies and the correlation between the density of simulated shale and probability of connection. Probability of connection can be used as a tool in making various production engineering decisions such as SAGD well placement.

8.2.2 RE-CALCULATION OF GENERAL ENGINEERING PARAMETERS

A connected resource assessment is now performed with a modified version of the general resource assessment transfer functions presented in Section 8.1. Connectivity is incorporated as an additional condition. For each transfer function, the connectivity indicator, $i^{(l)}_{conn(X,Y,Z)}$, is placed inside the sum as an additional multiplier. Even if the net bitumen indicator, $i^{(l)}_{net\_bit(X,Y,Z)}$ is 1, the engineering parameter being inferred can still be set to 0 if $i^{(l)}_{conn(X,Y,Z)}$ is 0, that is, if the cell is net but not connected. Both the net bitumen indicator and the connectivity indicator must equal 1 for the engineering parameter to be calculated. This way, not the net reservoir, but the net "connected" reservoir is accounted for in the final SAGD resource assessment.

For each of the 100 geological realizations, the connected contained bitumen is calculated for the entire reservoir and the connected sand thickness, connected average net porosity and the connected net bitumen thickness is calculated at each *X-Y* location. Similar to the general resource assessment, a histogram and probability plot are calculated to visualize the connected contained bitumen results and 2-D maps of the expected value, the p-90 and p-10 quantiles and the difference between the p-90 and p-10 quantiles are created to visualize the results.

The additional connectivity uncertainty due to the fluctuation of connectivity realization to connectivity realization (see Figure 8.7) can be seen by comparing the 2-D spatial uncertainty maps in Figures 8.2 to 8.4 to Figures 8.11 to 8.13, respectively. The uncertainty at the data locations is no longer 0 since we now account for connectivity conditioning data; the uncertainty at data locations is entirely made up of "connectivity" uncertainty.

8.2.2.1 CONNECTED CONTAINED BITUMEN

At each *X-Y-Z* cell location for each realization, connected contained bitumen, $Q^{(l)}_{conn}$, is either set to 0 or calculated as the product of the cell volume, cell porosity and the difference between 1 and the water saturation as a decimal, depending on the net bitumen and connectivity indicators. The connected contained bitumen transfer function takes the following form:

$$Q^{(l)}_{conn} = \sum_{all\ cells} V_{(X,Y,Z)} \cdot \phi^{(l)}_{(X,Y,Z)} \cdot (1 - S_{(X,Y,Z)}) \cdot i^{(l)}_{net\_bit(X,Y,Z)} \cdot i^{(l)}_{conn(X,Y,Z)} \qquad for\ l = 1,...,100$$

This transfer function is now implemented using $V_{(X,Y,Z)} = 50m \cdot 50m \cdot 0.5m = 1250m^3$, assuming $S_{(X,Y,Z)}$ to be 0.15 and ϕ_{thresh} to be 0.09. The final connected contained bitumen results are shown in the form of a histogram and probability plot in Figure 8.10. The

mean and standard deviation of the connected contained bitumen is 29.6 x 10^6 and 0.6 x 10^6 m^3, respectively, or 186.3 x 10^6 and 3.9 x 10^6 barrels, respectively. The p-90 and p-10 contained bitumen values are 30.4 x 10^6 and 28.8 x 10^6 m^3, respectively, or 191.2 x 10^6 and 181.0 x 10^6 barrels, respectively.

The connected net reservoir encompasses fewer cells than the net reservoir. Some of the cells used in the general resource assessment are not included in the connected resource assessment; this situation is true for the cells with $i^{(l)}_{net\_bit(X,Y,Z)} = 1$ and $i^{(l)}_{conn(X,Y,Z)} = 0$. Comparing the results of Figure 8.10 with Figure 8.1, the connected contained bitumen transfer function consistently calculates a lower but more realistic reservoir bitumen reserve.

8.2.2.2 CONNECTED SAND THICKNESS

At each *X*-*Y* cell location for each realization, connected sand thickness, $T^{(l)}_{conn\_sand(X,Y)}$, is either set to 0 or calculated as the product of the number of connected sand (binary facies code 1) cells found while looping over that particular *X*-*Y* stack of cells and the thickness of the cells. The connected sand thickness transfer function takes the following form:

$$T^{(l)}_{conn\_sand(X,Y)} = \sum_Z T_{(X,Y,Z)} \cdot i^{(l)}_{sand\_fcs} \cdot i^{(l)}_{conn(X,Y,Z)} \qquad for\ l = 1,...,100$$

Using $T_{(X,Y,Z)}$ = 0.5m, the sand thickness transfer function is now implemented on the SAGD example. The 2-D maps of expected value, the p-90 and p-10 quantile values and the difference between the p-90 and p-10 quantile values are shown in Figure 8.11. Notice, the connected sand thickness is consistently less than the sand thickness values calculated in Figure 8.2.

8.2.2.3 CONNECTED AVERAGE NET POROSITY

At each *X*-*Y* cell location for each realization, connected average net porosity, $\overline{\phi}^{(l)}_{conn\_net(X,Y)}$, is either set to 0 or calculated as the sum of porosity over all the *Z* locations in a particular *X*-*Y* stack of cells that satisfy the net bitumen and connectivity conditions divided by the number of chosen cells. The connected average net porosity transfer function takes the following form:

$$\overline{\phi}^{(l)}_{conn\_net(X,Y)} = \frac{\sum_Z \phi^{(l)}_{(X,Y,Z)} \cdot i^{(l)}_{net\_bit(X,Y,Z)} \cdot i^{(l)}_{conn(X,Y,Z)}}{\sum_Z \cdot i^{(l)}_{net\_bit(X,Y,Z)} \cdot i^{(l)}_{conn(X,Y,Z)}} \qquad for\ l = 1,...,100$$

The connected average net porosity transfer function is now implemented. ϕ_{thresh} is set to 0.09. The 2-D maps of statistical summaries are shown in Figure 8.12. Comparing

these results with Figure 8.3, connectivity seems to have substantial control on average net porosity as the connected average net porosity values are much lower.

8.2.2.4 CONNECTED NET BITUMEN THICKNESS

At each *X*-*Y* cell location for each realization, connected net bitumen thickness is either set to 0 or calculated as the product of cell thickness, cell porosity and the difference between 100% and the water saturation in percent, depending on the net bitumen and connectivity indicator values. The connected net bitumen thickness transfer function takes the following form:

$$T^{(l)}_{conn\_bit\,(X,Y)} = \sum_Z T_{(X,Y,Z)} \cdot \phi^{(l)}_{(X,Y,Z)} \cdot (1 - S_{(X,Y,Z)}) \cdot i^{(l)}_{net\_bit\,(X,Y,Z)} \cdot i^{(l)}_{conn\,(X,Y,Z)} \qquad for\ l = 1,...,100$$

Using $T_{(X,Y,Z)}$ = 0.5m, $S_{(X,Y,Z)}$ = 0.15 and ϕ_{thresh} = 0.09, the net bitumen thickness transfer function is now implemented. The results are shown in Figure 8.13. Notice, the connected net bitumen thickness is less than the net bitumen thickness calculated in the general resource assessment in Figure 8.4.

8.2.3 OTHER CONNECTED RESOURCE ASSESSMENT ENGINEERING PARAMETERS

So far, the connected resource assessment has only used the binary connectivity indicator output of the local connectivity program. However, there are a number of other interesting outputs available to characterize the reservoir. These additional summaries include connected facies types and number of adjacent cells connected in 3-D as well as connected net thickness, gross net thickness, the connected-to-gross net thickness ratio and the base of the connected reservoir in 2-D. The connected net thickness versus gross net thickness and the base of the connected reservoir are explored in the SAGD example.

8.2.3.1 CONNECTED NET THICKNESS VERSUS GROSS NET THICKNESS

The connected net thickness is an important engineering parameter – it can be used to identify optimal aerial SAGD potential locations. At each *X*-*Y* location for each realization, connected net thickness is the sum of the product of the number of connected net cells in that particular *X*-*Y* stack and the cell thickness; gross net thickness is simply the sum of the product of the number net cells in that particular *X*-*Y* stack and the cell thickness. 2-D maps of the expected value of connected net thickness, gross net thickness and the connected-to-gross net thickness ratio are presented in Figure 8.14. These maps suggest optimal SAGD well locations in the Northern area of the reservoir.

8.2.3.2 THE BASE OF THE CONNECTED RESERVOIR

The base of the connected reservoir is also an important SAGD engineering parameter; given particular aerial locations, it can be used to identify the vertical SAGD production well locations. At each *X*-*Y* location for each realization, the base of the connected reservoir is equal to the elevation of the lowest cell within the lowest thickest connected net reservoir unit (determined by the elevation weighted thickness) in that particular *X*-*Y* stack of cells. A 2-D map of the expected value of the base of the connected reservoir is presented in Figure 8.15. Comparing these elevations with the cell average bottom surface elevations in Figure 3.3 reveals that the base of the connected reservoir is often the same or very near the same to the modeled base of the reservoir structure. The map in Figure 8.15 can be referred to as a map of the vertical SAGD production well positions.

8.2.4 SAGD WELL PLACEMENT

The post-processing step includes a general resource assessment and a connected resource assessment. For the SAGD example of this report, we are now in a place to make some SAGD production engineering decisions. Perhaps, the decision with the most impact on recovery efficiency is SAGD well pair placement. That is, even if the SAGD process parameters such as steam injection rate, steam pressure, reservoir pressure, minimization of water intrusion, etc. are implemented as well as they could be, the final cumulative SOR and oil production rate performance could still be poor if the SAGD well pairs are located in un-optimal areas. A connected resource assessment aids the inference of optimal SAGD well pair placement.

There are a number of connected resource summaries that can be used to decide optimal SAGD well pair locations. For instance, SAGD well pairs could be aerially placed so that their subsequent cumulative steam chamber influences areas of high probability of connection, high connected sand thickness, high connected average porosity, high connected net bitumen thickness and high connected net thickness. Our knowledge of the base of the connected reservoir can be used to infer appropriate production well vertical positions, given an established aerial position.

The SAGD well pair locations for a reservoir may be based simply on drilling pad accessibility and producing the entire reservoir. However, for production sequencing, knowledge about the productivity of well pairs is useful. Figure 8.16 illustrates possible aerial positions of well pairs as if the reservoir were being produced in practice.

Flow simulation is used to provide accurate cumulative SOR and oil production rate production parameters needed to characterize the SAGD performance.

We now pick a well pair location for the SAGD example, based on the connected resource assessment results of section 8.2. Figure 8.17 illustrates the chosen SAGD well pair location. The aerial well pair location (green) is from 5200 to 6200m Easting at 3350m Northing. The production and injection wells are located at elevations of 190m

and 195m, respectively. The red outline represents the nominal drainage volume for that chosen well pair location.

8.3 FIGURES

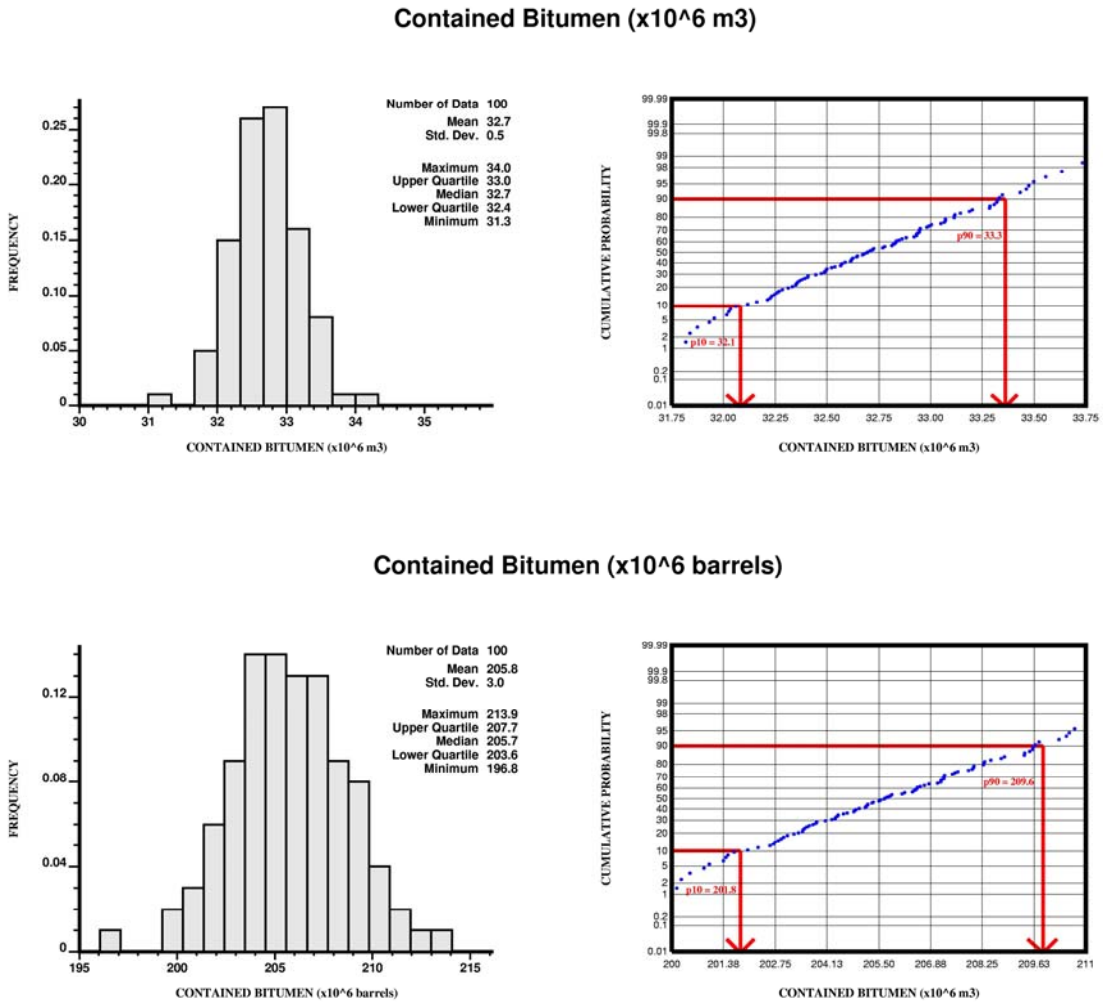

Figure 8.1 – Contained Bitumen. The results of the contained bitumen transfer function. The histograms on the left show the expected value and uncertainty in units of m^3 and barrels. The probability plots on the right reveal the contained bitumen values where the probability of exceeding are 10% (the 0.90 quantile) and 90% (the 0.10 quantile); the red lines and writing show the method to obtain the 0.10 and 0.90 quantile values.

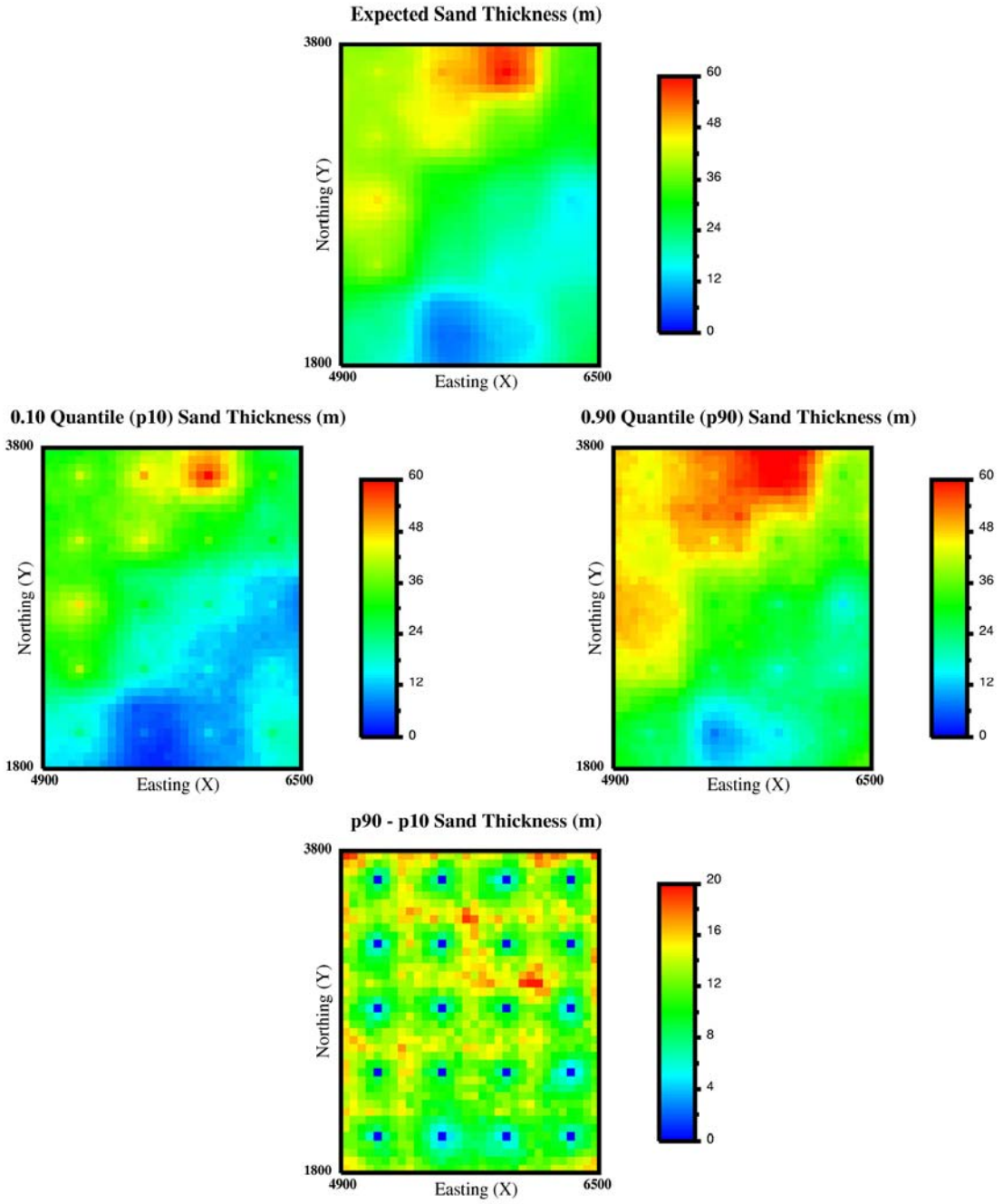

Figure 8.2 – Sand Thickness. The results of the sand thickness transfer function. The expected value, the sand thickness values where the probability of exceeding are 10% (the 0.90 quantile) and 90% (the 0.10 quantile) and the difference between the 0.90 and 0.10 quantile values are shown at each *X*-*Y* location in a 2-D map. The color scale used is shown immediately to the right of each 2-D map.

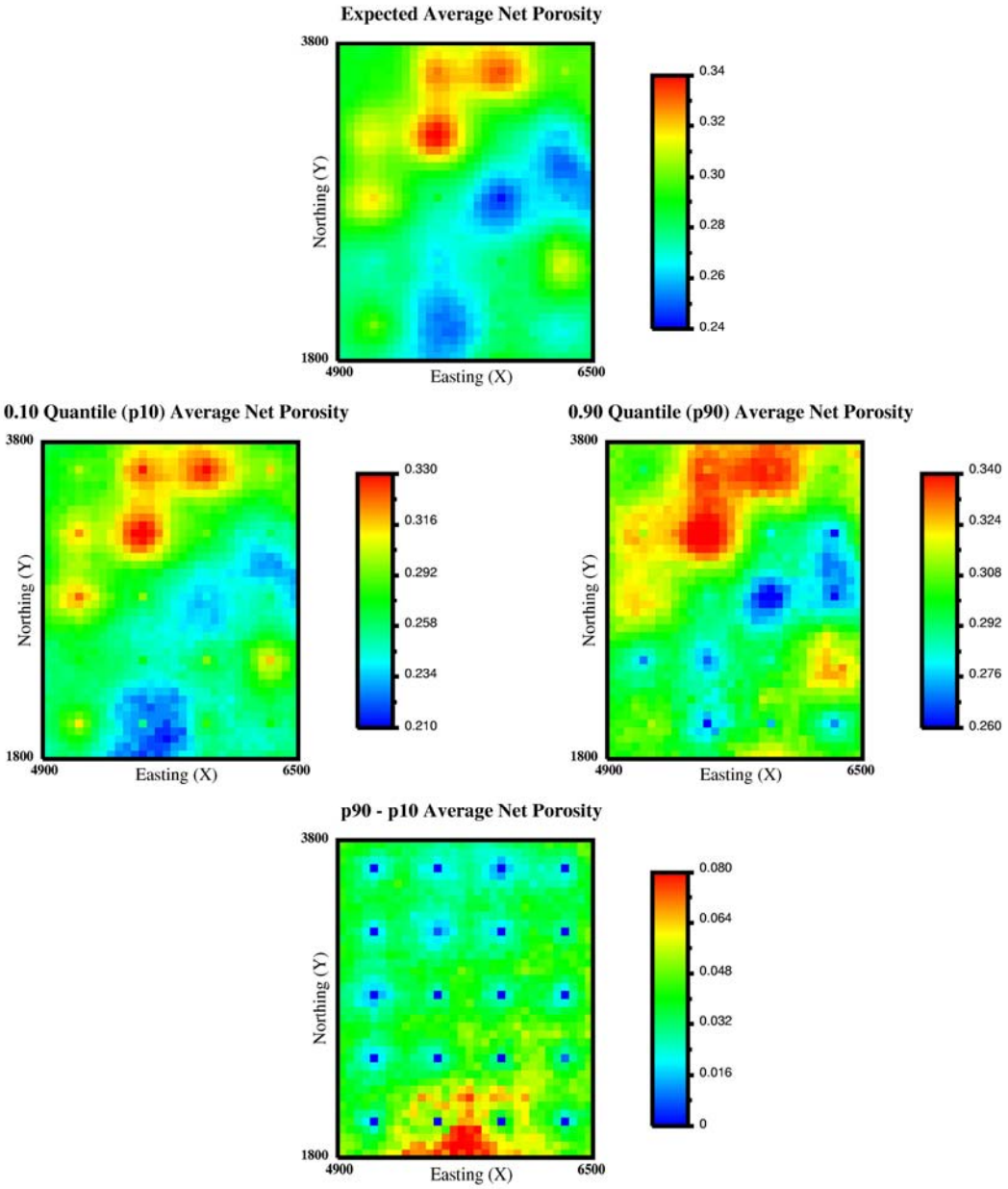

Figure 8.3 – Average Net Porosity. The results of the average net porosity transfer function. The expected value, the average net porosity values where the probability of exceeding are 10% (the 0.90 quantile) and 90% (the 0.10 quantile) and the difference between the 0.90 and 0.10 quantile values are shown at each *X*-*Y* location in a 2-D map. The color scale used is shown immediately to the right of each 2-D map.

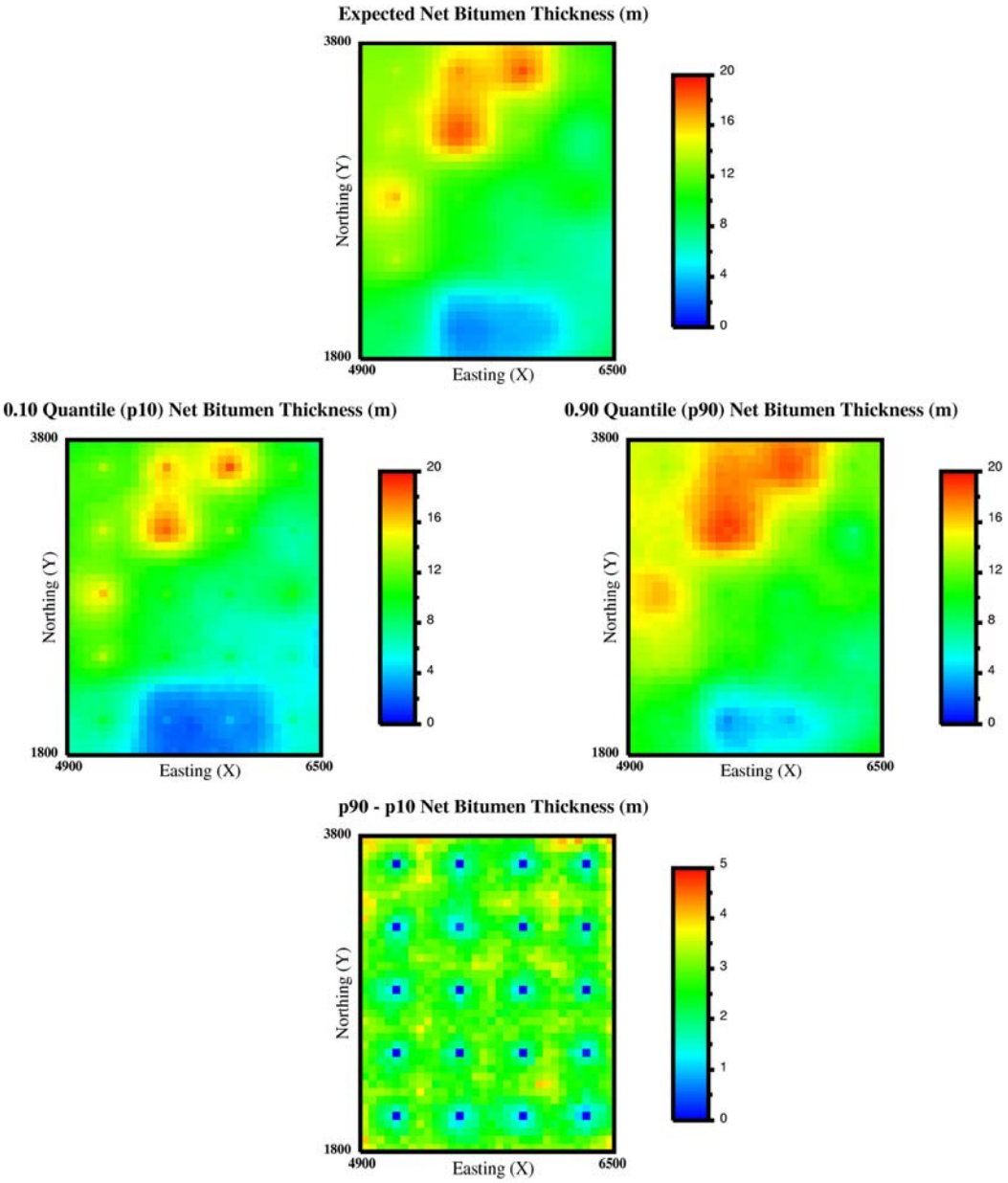

Figure 8.4 – Net Bitumen Thickness. The results of the net bitumen thickness transfer function. The expected value, the net bitumen thickness values where the probability of exceeding are 10% (the 0.90 quantile) and 90% (the 0.10 quantile) and the difference between the 0.90 and 0.10 quantile values are shown at each *X*-*Y* location in a 2-D map. The color scale used is shown immediately to the right of each 2-D map.

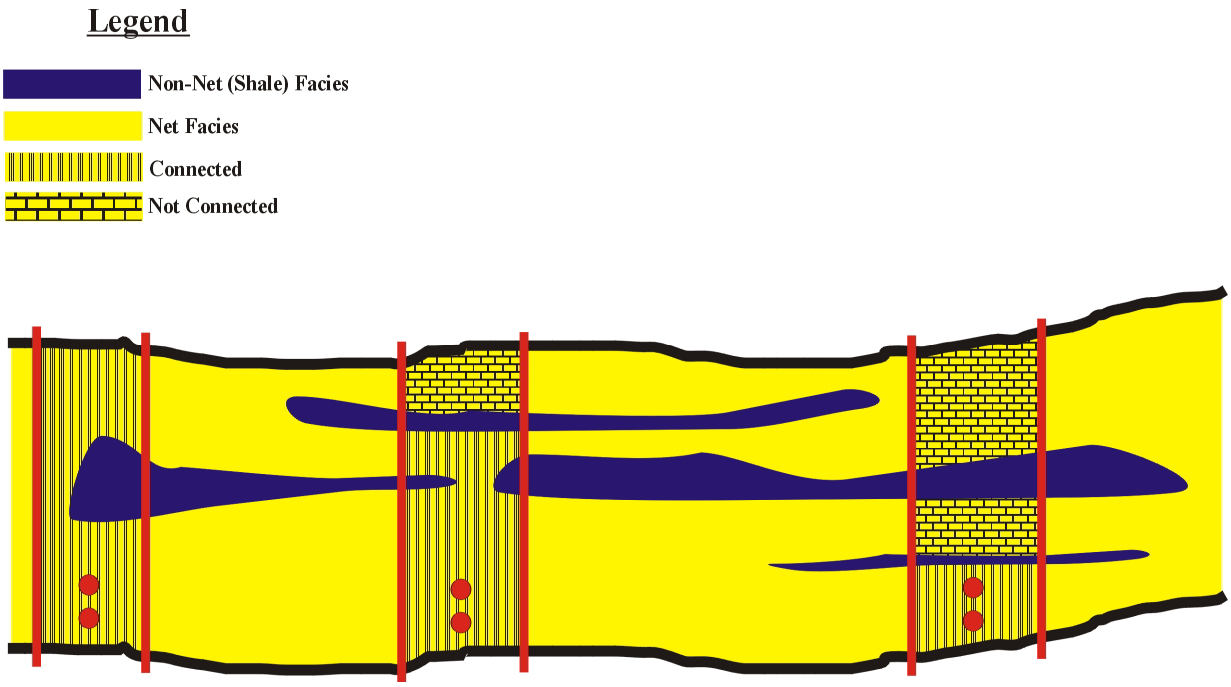

Figure 8.5 – The Need for a Connected Resource Assessment. A geological cross section illustrating the importance of a connected resource assessment for a SAGD recovery process. Three horizontal SAGD well pairs and the cumulative steam chamber area of influence of each are shown in red. The net/non-net facies model and connected/unconnected reservoir area within the steam chamber area of influences can be seen in the legend.

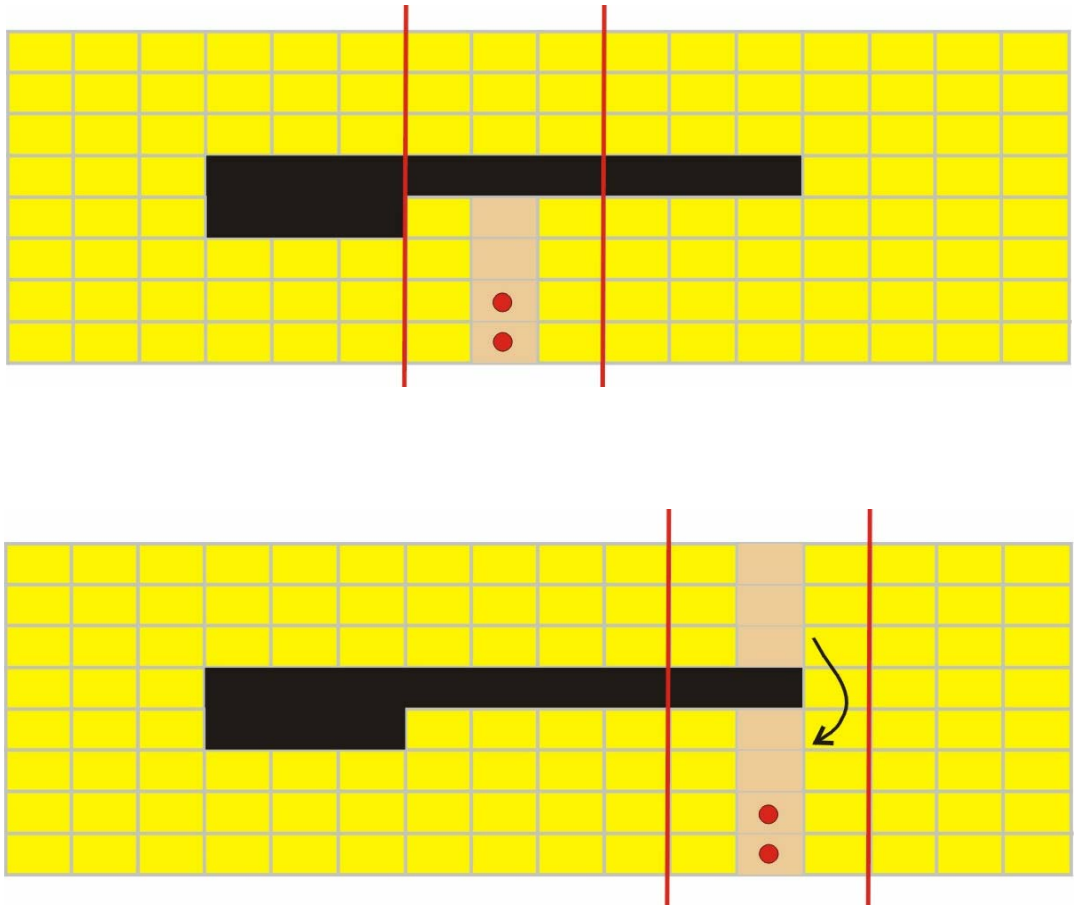

Figure 8.6 – Local Connectivity Program Implementation. Two implementations of the local connectivity program on a simplified reservoir facies model. The red dots represent horizontal SAGD well pairs, the red lines are the window boundaries and the net and non-net (shale) facies are shown in yellow and black, respectively. The connected cells are shown in peach.

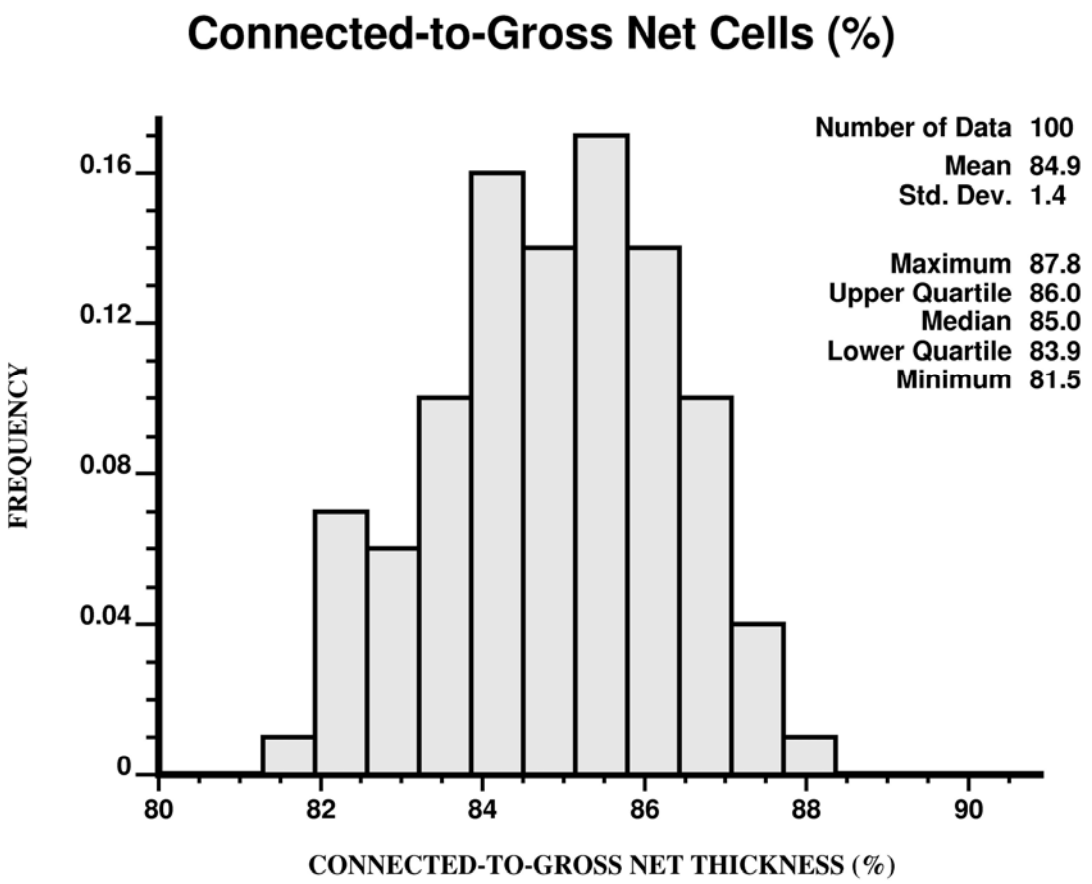

Figure 8.7 – Connected Net Cells vs. Net Cells. A histogram of the ratio in percent of the connected net reservoir cells to the total net reservoir cells. There are 100 values corresponding to the 100 connectivity realizations. This histogram is indicative of the amount of cells included in the general resource assessment, but excluded in the connected resource assessment.

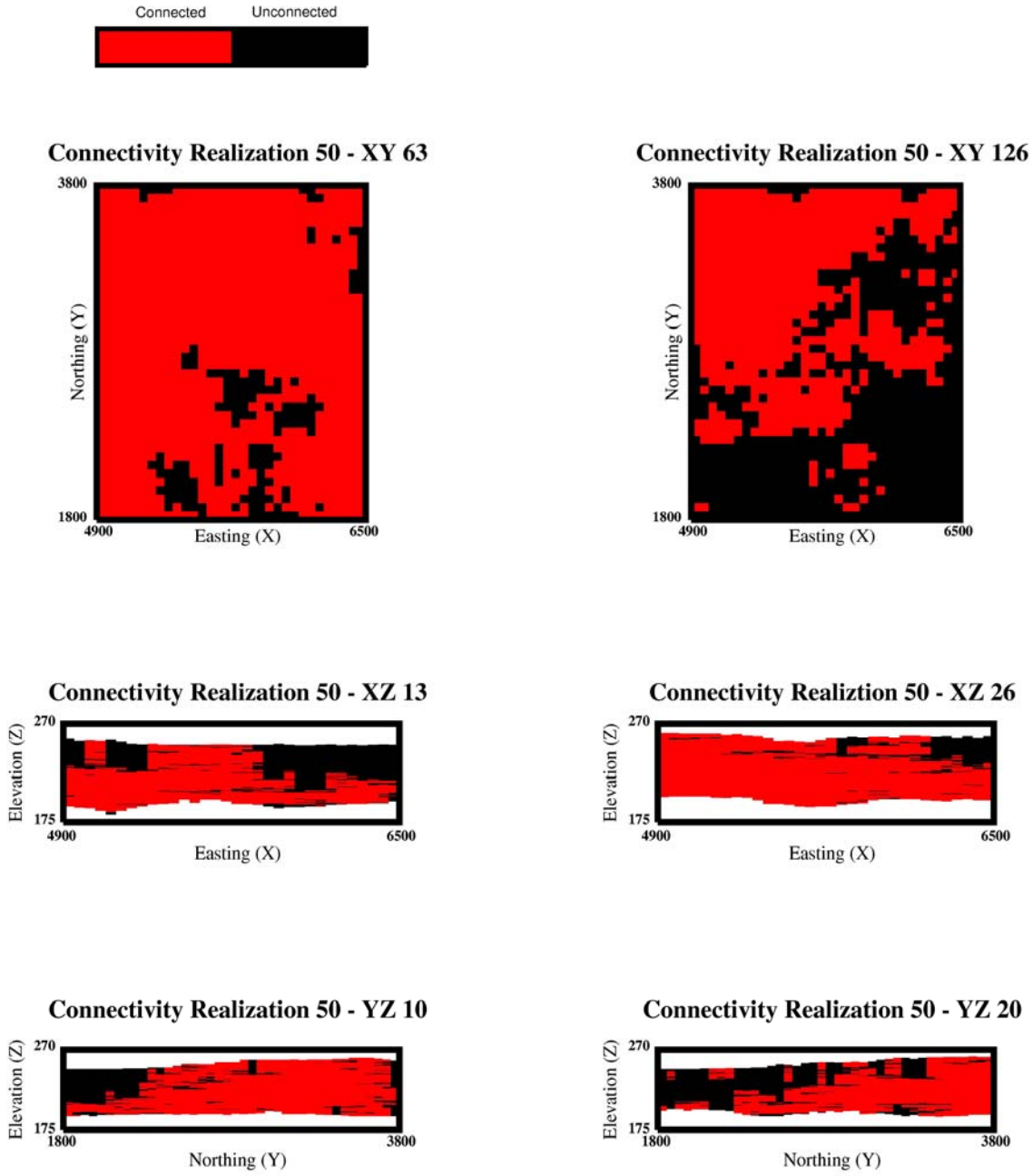

Figure 8.8 – Connectivity Realization. An illustration of the 50th of 100 possible connectivity indicator realizations. The same sections specified in Figure 6.5 are used in this figure. The indicator color scheme shown at the top is the same for each section; the white areas contain cells that were clipped by the bottom and top surface elevation realizations.

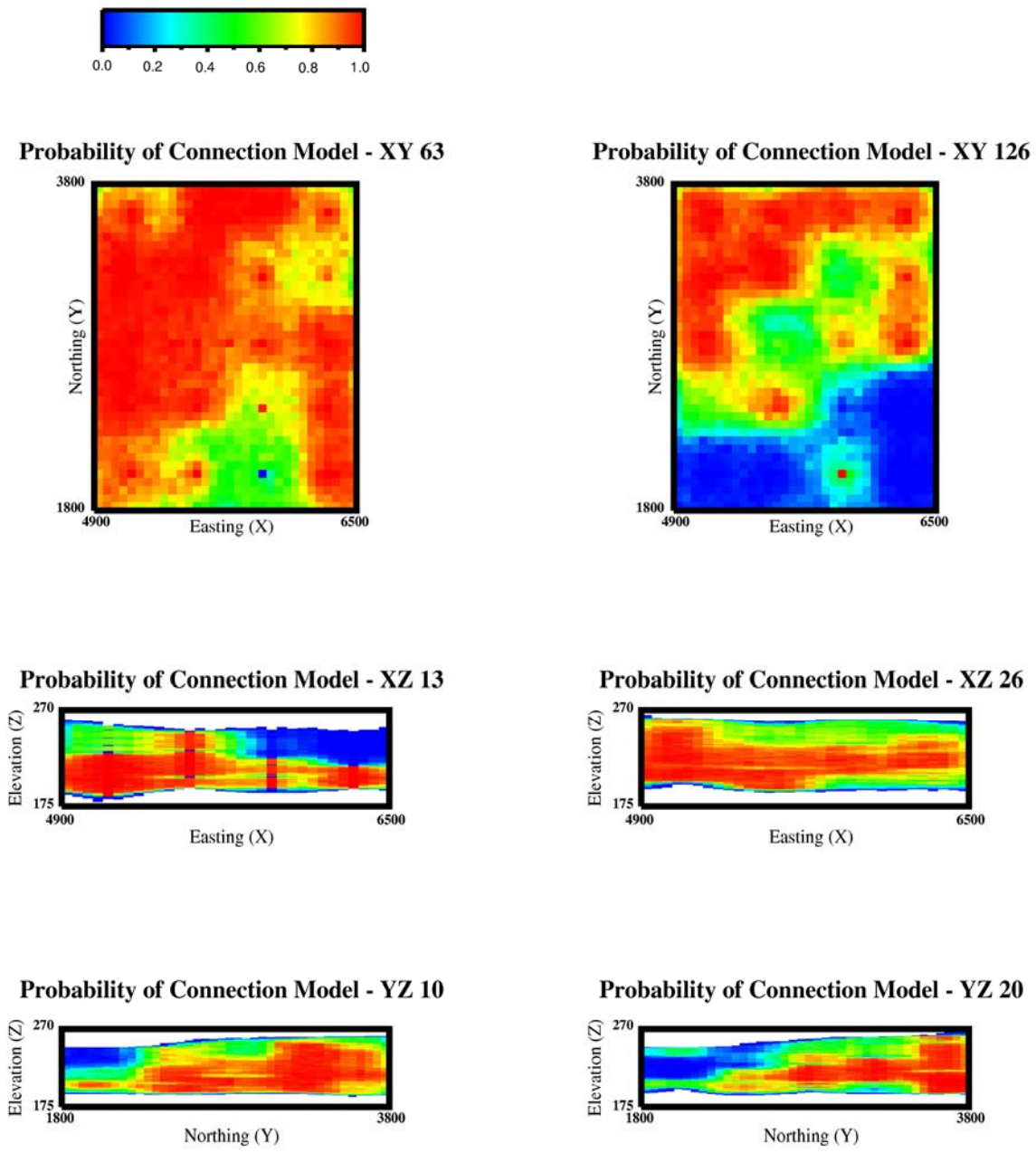

Figure 8.9 – Probability of Connection. An illustration of the probability of connection 3-D model. The same sections specified in Figure 6.5 are used in this figure. The color scheme shown at the top is the same for each section; the white areas contain cells that were clipped by the structure realizations.

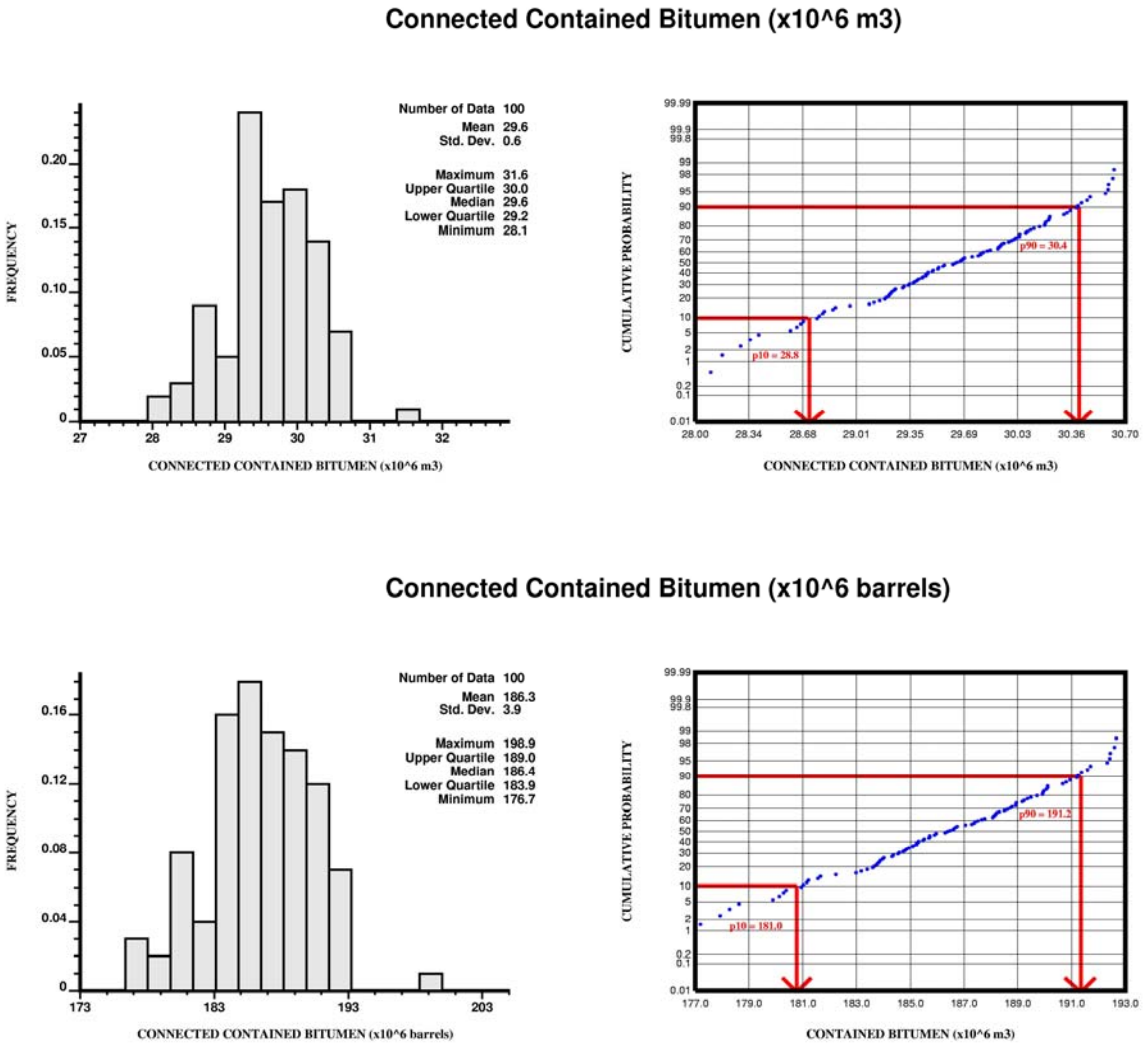

Figure 8.10 – Connected Contained Bitumen. The results of the connected contained bitumen transfer function. The histograms on the left show the expected value and uncertainty in units of m^3 and barrels. The probability plots on the right reveal the contained bitumen values where the probability of exceeding are 10% (the 0.90 quantile) and 90% (the 0.10 quantile); the red lines and writing show the method to obtain these 0.10 and 0.90 quantile values.

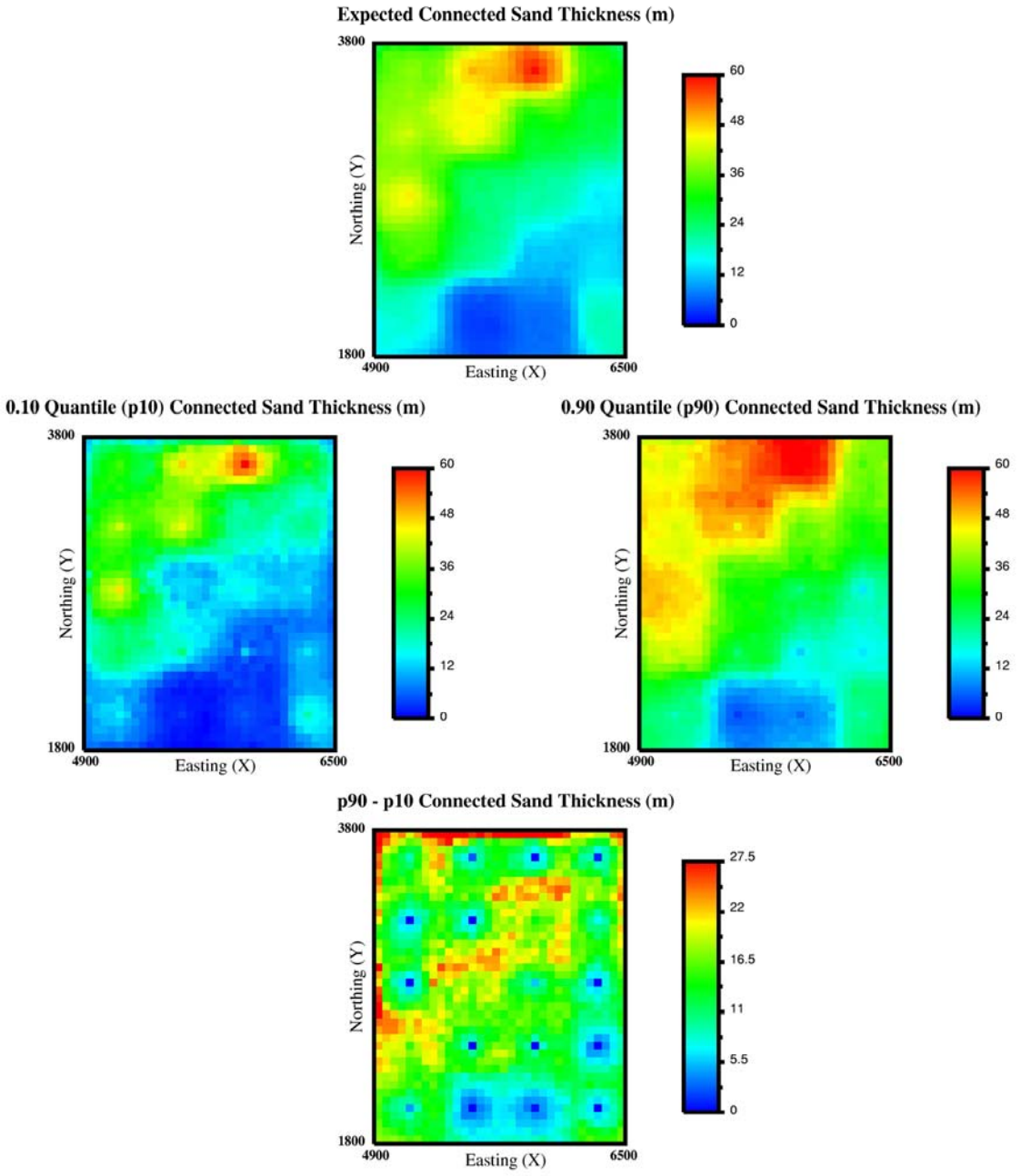

Figure 8.11 – Connected Sand Thickness. The results of the connected sand thickness transfer function. The expected value, the connected sand thickness values where the probability of exceeding are 10% (the 0.90 quantile) and 90% (the 0.10 quantile) and the difference between the 0.90 and 0.10 quantile values are shown at each *X*-*Y* location in a 2-D map. The color scale used is shown immediately to the right of each 2-D map.

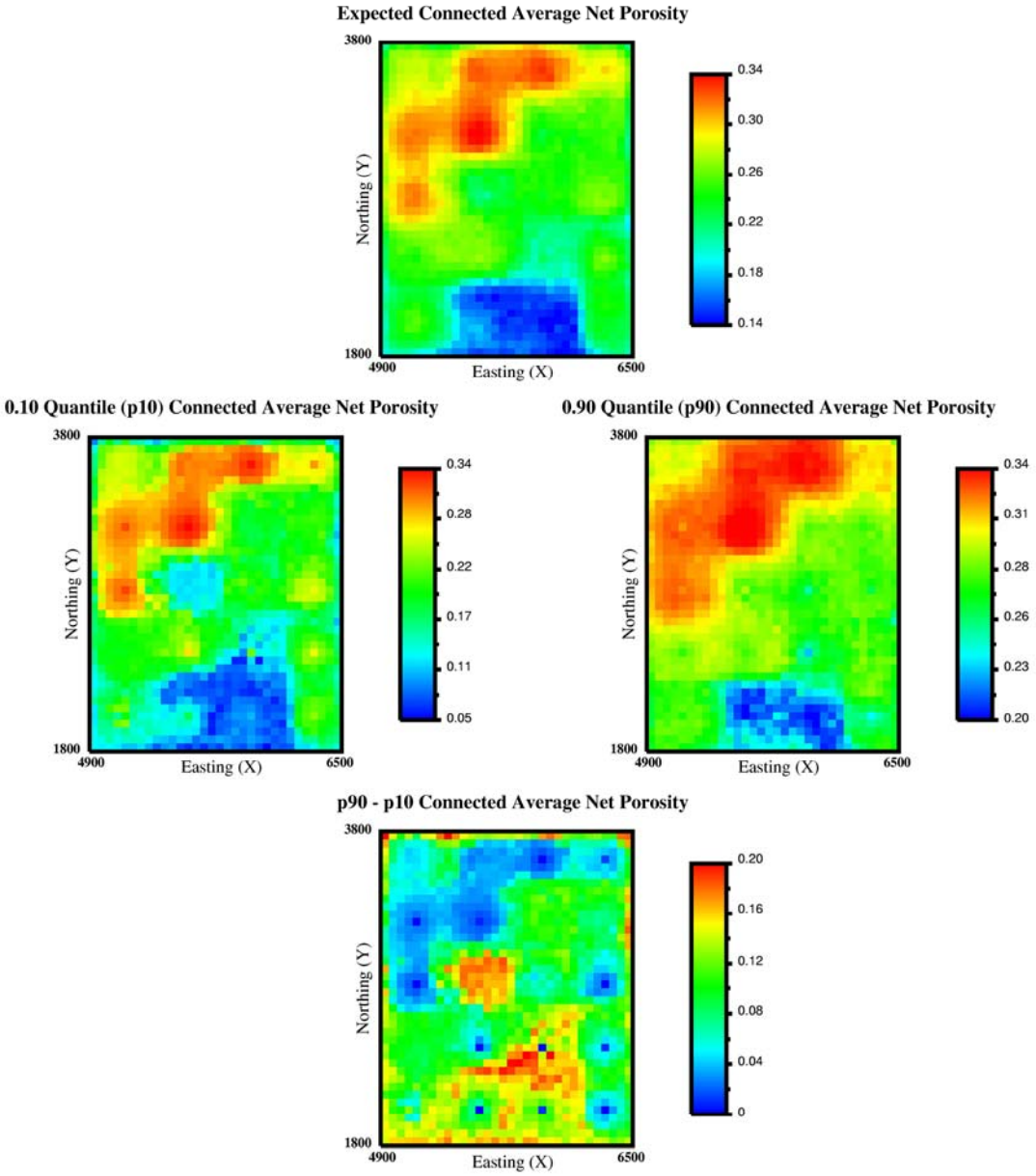

Figure 8.12 – Connected Average Net Porosity. The results of the connected average net porosity transfer function. The expected value, the connected average net porosity values where the probability of exceeding are 10% (the 0.90 quantile) and 90% (the 0.10 quantile) and the difference between the 0.90 and 0.10 quantile values are shown at each *X*-*Y* location in a 2-D map. The color scale used is shown immediately to the right of each 2-D map.

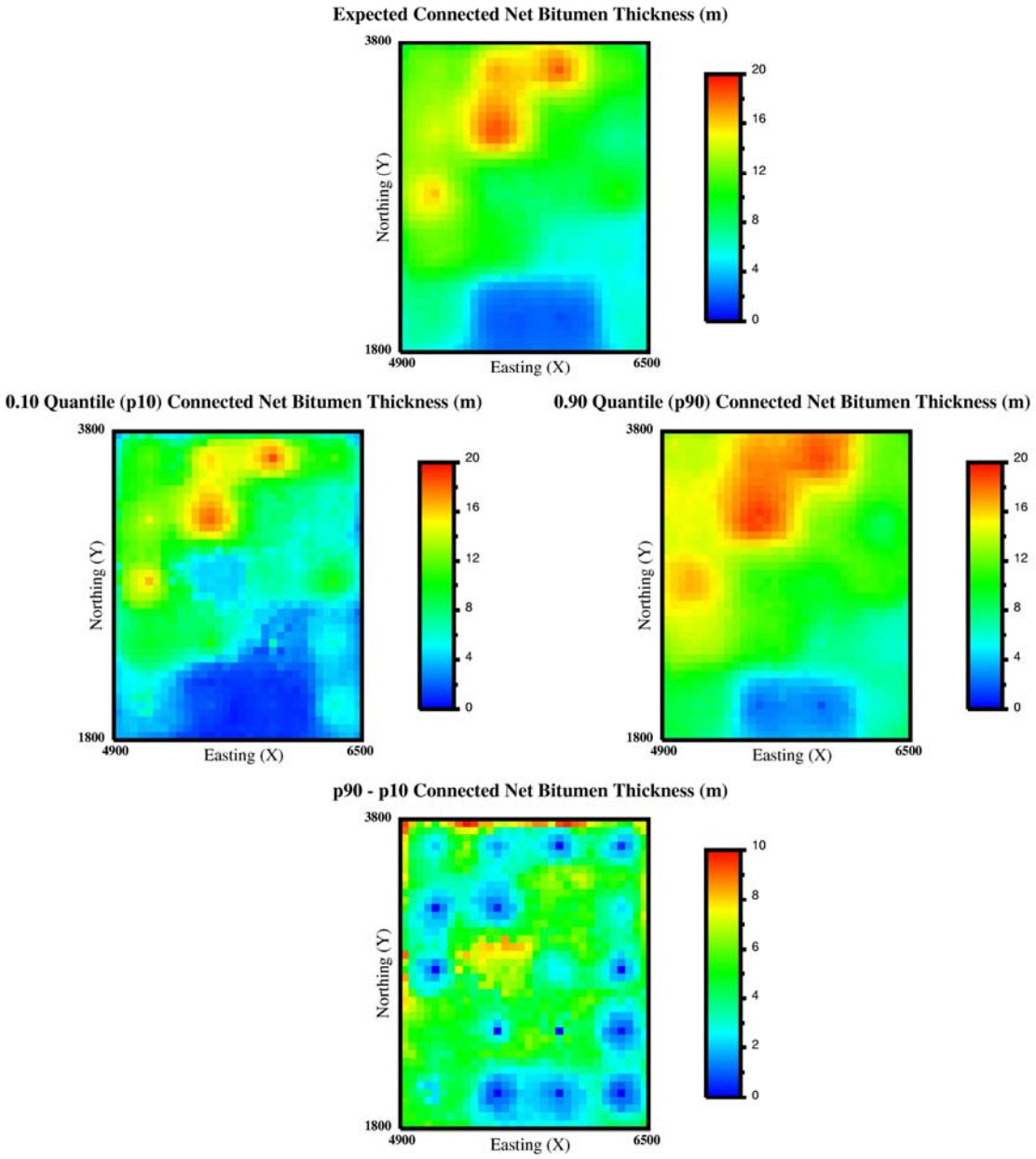

Figure 8.13 – Connected Net Bitumen Thickness. The results of the connected net bitumen thickness transfer function. The expected value, the connected net bitumen thickness values where the probability of exceeding are 10% (the 0.90 quantile) and 90% (the 0.10 quantile) and the difference between the 0.90 and 0.10 quantile values are shown at each *X*-*Y* location in a 2-D map. The color scale used is shown immediately to the right of each 2-D map.

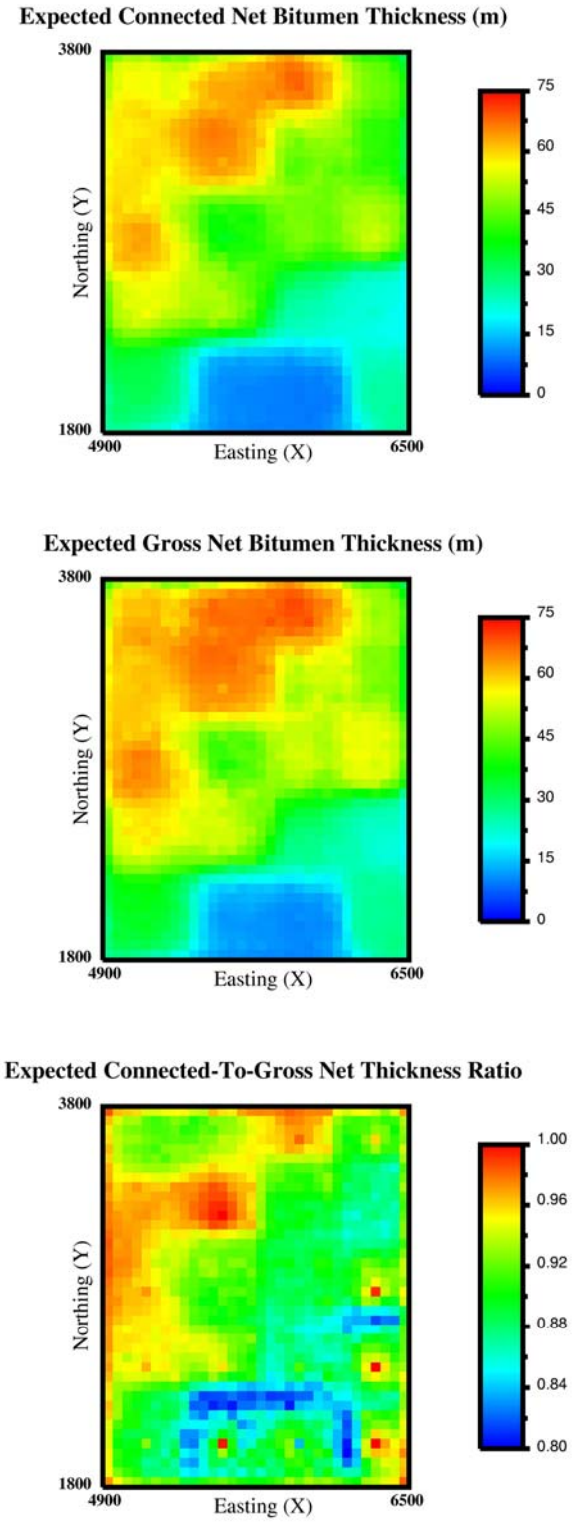

Figure 8.14 – Connected Net Thickness vs. Gross Net Thickness. An illustration of the connected net thickness and gross net thickness results calculated by the local connectivity program. The expected value of the connected net thickness, gross net thickness and connected-to-gross net thickness ratio at each *X-Y* location are plotted on a 2-D map. The color scheme used is shown directly to the right of each map.

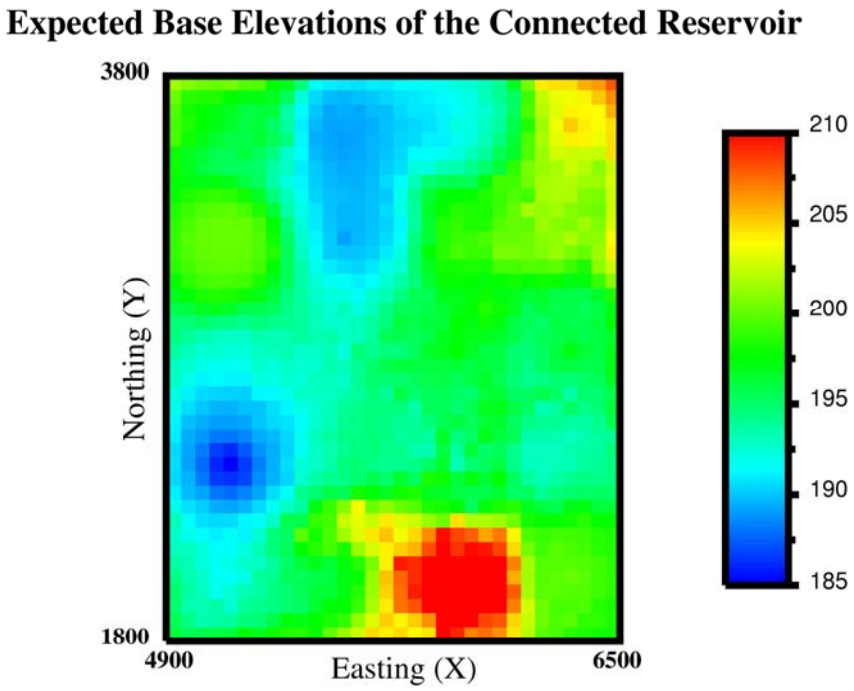

Figure 8.15 – Base of the Connected Reservoir. The results of the base of the connected reservoir calculated by the local connectivity program. The expected value of the elevation of the base of the connected reservoir is calculated at each *X*-*Y* location and summarized in a 2-D map. The color scheme used is shown directly to the right.

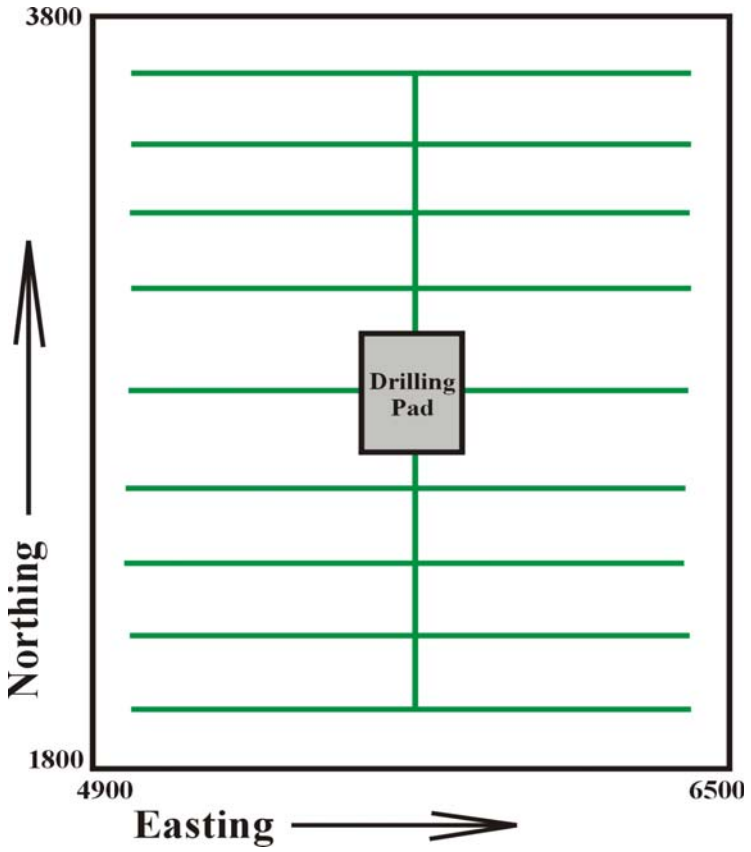

Figure 8.16 – Constrained SAGD Well Placement. An illustration of the likely aerial SAGD well positions if the reservoir were to be produced in practice. The drilling pad is located in the center of the reservoir to avoid the cost of multiple drill pads.

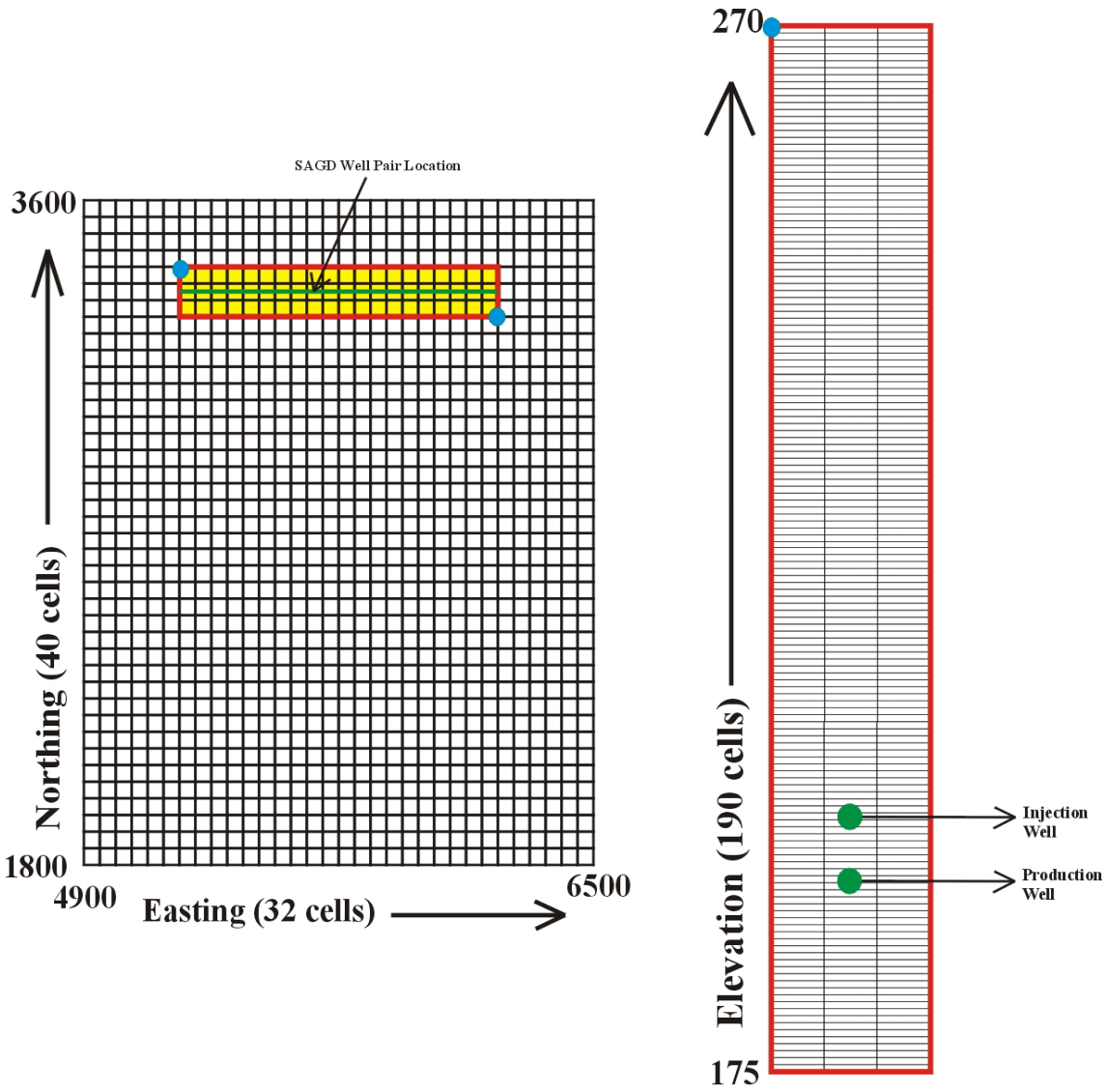

Figure 8.17 – SAGD Well Pair Location. An illustration of the aerial and vertical position of the SAGD well pair location. The Elevation cross section's orientation can be seen by either of the blue control points. The aerial and vertical location of the SAGD well pair is shown in green. The red outline in the aerial and vertical views shows the area around the SAGD well pair location making up the volume of reservoir that is input into the flow simulator.

9 MODEL EXTRACTION AND REGGRIDDING, RANKING, FLOW SIMULATION, AND ANALYSIS OF RESULTS

After multiple geological realizations have been constructed, they are used to create multiple reservoir characterization parameter realizations by way of various transfer functions. The transfer functions that are part of the final connected resource assessment characterize the amount and spatial location of net reservoir that will likely be heated and potentially recovered by the SAGD process. Based on the results of this type of assessment, optimal SAGD well pair positions can be established.

A transfer function to characterize SAGD reservoir performance must now be implemented, namely, flow simulation. With the multiple geological realizations of the candidate well pair locations as part of the input, flow simulation describes likely SAGD performance, for example, the cumulative SOR and oil production rate. Flow simulation provides the vital link between geological uncertainty and production uncertainty needed to make important SAGD reservoir engineering decisions.

This section describes some details involved in implementing flow simulation for SAGD reservoir performance characterization. This involves increasing geological detail of the nominal drainage volumes, but reducing the amount of input into the flow simulator.

Flow simulation requires the solution of complex equations and requires significant computer resources and relatively long implementation times; nevertheless, it is a necessary step to fully characterizing any potential SAGD reservoir. We will not actually perform flow simulation in this report; however, we will discuss the preliminary steps involved in preparing the multiple geological realizations for input and the techniques involved in analyzing the results.

SAGD well pair locations are often known even before reservoir characterization; however, it is useful to know the production potential. Initial capital costs, for example, can be recovered quickly by operating the most optimal SAGD well pairs first. Prior to flow simulation, the nominal drainage volume of each well pair should be established. The multiple geological realizations of the nominal drainage volume surrounding the candidate SAGD well pair location are actually part of the input to flow simulation.

The established drainage volume around each candidate well pair location must be extracted from the reservoir model. To implement flow simulation for the purpose of assessing SAGD performance, the amount of geological detail available from the extracted SAGD drainage volumes is deficient. The cell sizes used in the reservoir modeling process are too large for use in obtaining accurate SOR and oil production rate parameters. A technique to regrid the local drainage volumes is required. This regridding technique down-scales the larger coarsely spaced reservoir model cells into smaller finer

spaced SAGD flow simulation cells. The result is multiple fine-scale geological realizations.

Not all of the multiple fine scale geological realizations for the multiple candidate SAGD well pair drainage volumes can be transferred through the flow simulator. This is due to the large amount of processing time that would be required. A ranking technique based on a parameter that is well correlated with SAGD performance can be used to reduce the input. For the example of this report, we base ranking on the volume of connected net modeling cells within the local drainage volume. That is, the multiple fine scale geological realizations at the SAGD well pair location are ordered by increasing connected net volume and a few geological realizations that span the uncertainty are chosen for input into flow simulation.

Other ranking techniques can be implemented within the SAGD drainage volumes. The volume of sand, average sand thickness, average tortuosity, or average net porosity could also be calculated for each fine scale geological realization and then ordered in increasing order. In Norrena and Deutsch (2002), an optimization procedure is implemented to decide an optimal vertical position of the producer well. The fine scale realizations of the drainage volumes were ordered according to optimal vertical well position.

Flow simulation provides steam-to-oil ratio (SOR), oil production rate, as well as the time variation of other variables such as thermal efficiency, steam pressure, reservoir pressure, etc. The cumulative SOR and stabilized oil production rate are two summaries. Often, these two variables show excellent correlation between themselves, that is, as SOR decreases, production rate increases.

It is the good correlation between the SOR and oil production rate flow simulation outputs with the connected drainage volume ranking parameter that provides the link from geological uncertainty to production output uncertainty and allows us to make important SAGD production decisions. For example, production uncertainty can help determine the number of well pairs needed to produce a given amount of bitumen?

We chose one SAGD well pair location. Figure 8.16 shows the location in green as well as its surrounding reservoir volume to be extracted in red. Although multiple well pair locations will need to be considered in practice, this well location and surrounding volume is used as an example.

9.1 MODEL EXTRACTION AND REGRIDDING

SAGD well placement is usually based on drilling pad accessibility and producing the entire reservoir; and the connected resource assessment is done mainly to obtain the global recoverable reserves (Figure 8.10) rather than to infer optimal SAGD well locations. The aerial SAGD well locations must be known to extract and regridd the surrounding volumes for flow simulation – the vertical dimension can be taken as the full thickness of the model.

To predict the SAGD performance of a specific well pair location via flow simulation, only the nominal drainage volume of that well pair needs to be input. There are a few details in extracting these volumes from the reservoir model and preparing them for the flow simulator that need to be discussed.

9.1.1 EXTRACTION

The dimensions of the volume extracted for each well pair depends on a number of factors. The idea is to extract the volume as the expected cumulative steam chamber for that well pair. Additional volume or lack of volume might create inefficient or inaccurate flow simulation results. The window used for calculating connectivity, the required time to run flow simulation and the steam chamber volume of influence must also be considered in choosing the drainage volume dimensions.

In consideration of these details, we chose the nominal drainage volume shown in Figure 8.16 by the red outline in an *X-Y* (Easting-Northing) and *Z-Y* (Elevation-Northing) section (the blue control points are used to orientate the sections). This volume is now extracted from the reservoir. The size of the cells in the reservoir model is maintained in the extracted volumes. Figure 9.1 shows both the large scale reservoir model and the extracted drainage volume. The grid specification of each, including the center of the first cell location (*min*), the number of cells (*ncells*) and the size of cells (*siz*) in the Easting (*X*), Northing (*Y*) and Elevation (*Z*) directions, is also shown. The extracted volume spans twenty 50m cells in the Easting direction (1000m) by three 50m cells in the Northing direction (150m) by one-hundred and ninety 0.5m cells in the Elevation direction (95m). Written in terms of the full reservoir model cell indices in the Easting (*X*), Northing (*Y*) and Elevation (*Z*) directions (there are 32 x 40 x 190 cells, respectively, in total), the extracted volume spans cells 7 to 26, 34 to 36 and 1 to 190, respectively.

The volume shown in Figure 9.1 is extracted from each of the 100 sets of modeled reservoir parameters or geological realizations. That is, we now have 100 realizations of the bottom and top surface elevations, facies types and by-facies-porosity within the extracted reservoir volume at the resolution of the reservoir modeling scale. Figure 9.2 shows a central *X-Y* section through the 50^{th} facies and 50^{th} porosity extracted volume realization.

In practice, multiple volumes corresponding to multiple SAGD well pair locations will need to be extracted. The result is multiple geological realizations of the multiple nominal SAGD well pair drainage volumes at the resolution of the reservoir modeling scale.

9.1.2 REGRIDDING

The gridding scheme required for SAGD flow simulation is quite different than classical flow simulation for reservoir forecasting. Usually, due to large-scale flow interactions, flow simulation is performed on a larger scale than what is used for modeling reservoir parameters, that is, the cell sizes used to model the reservoir

properties needed for resource assessment and engineering decisions are often smaller than the cell sizes required to model the reservoir's flow responses. However, flow simulation for SAGD performance is an exception. Here, we are concerned with the physical SAGD steam interaction within the local connected net reservoir volume where the steam chamber is assumed to distribute through. For each established nominal drainage volume, therefore, we need to scale down the reservoir modeling resolution to a finer resolution appropriate for modeling SAGD flow responses.

Various techniques are available to scale coarse resolutions down to finer resolutions, such as mathematical scaling relationships or interpolation algorithms. For the well pair volume extracted in the SAGD example, we will use the coarsely spaced geological parameter realizations (see Figure 9.1) to condition a fine resolution simulation of the extracted volume. Similar to the workflow for creating geological realizations, only one fine grid realization is created per coarse grid conditioning data realization. We do not create multiple fine grid resolutions for one particular conditioning coarse grid. The result is multiple geological realizations of a finely gridded version of the extracted well pair volume appropriate for input into flow simulation.

Figure 9.3 illustrates the coarse conditioning data grid and grid specification, which is the extracted volume grid specification, and the final finely simulated grid and grid specification used in the SAGD example. The re-simulated fine grid, in the Easting (*X*), Northing (*Y*) and Elevation (*Z*) directions, has 100 10m cells, 150 1m cells and 190 0.5m cells. The re-scaling procedure described above is now implemented. We now have 100 fine-scale realizations of the geology within these drainage volumes. Figure 9.4 shows the same central *X*-*Y* cross section as Figure 9.2, but through the re-gridded version of the 50^{th} realization of facies and porosity. The resolution of the re-gridded drainage volumes is now appropriate fine enough for flow simulation for performance modeling and characterization.

In practice, the scale-down technique must be implemented on all of the extracted nominal well pair volumes and for all geological realizations of these volumes. After the regridding process, the result is, for each drainage volume, multiple geological realizations at a fine enough scale for flow simulation.

9.2 RANKING

Accounting for processing time constraints, not every fine scale realization for every drainage volume can be input into the flow simulator. The next section discusses a few post-processing techniques that can be implemented to reduce the input, collectively referred to as ranking.

Once the multiple realizations of the SAGD well pair location have been extracted and regridded, they are ready to be passed through the flow simulator. The realizations must be ranked to choose a few that span the SAGD potential. Depending on the parameter used for ranking, the correlation between it and the performance outputs from flow

simulation should be good, and, therefore, provide a means to infer the production performance for the realizations or locations not passed through the flow simulator.

In the SAGD example, for each of the 100 finely gridded geological realizations within the extracted SAGD volume chosen, we calculate the connected net drainage volume. A cell is deemed "connected" if it is a net facies type, that is, not shale, it is above a specified porosity threshold and it is beside at least one other cell that is also a net facies type above the specified porosity threshold. The set of 100 connected volumes realizations is a distribution of 0.01 quantile values. The geological drainage volume realizations with the 0.10, 0.50 and 0.90 quantile values (where the probability of exceeding is 90%, 50% and 10%, respectively) are selected for input into flow simulation. These three realizations are thought to span the SAGD potential of the drainage volume chosen. The connected volume parameter would be well correlated to the cumulative SOR and oil production rate outputs from flow simulation.

An alternative ranking measure is one based on optimal vertical production well position. The pore volume for all possible vertical well positions is penalized according to a straight line connectivity proportion calculated for each possible well position. The result is an optimal vertical production well position associated to a weighted or discounted pore volume for as many realizations of the geology exists. The realizations can then be arranged in increasing discounted pore volume order and the 0.10, 0.50 and 0.90 pore volume quantile realizations can be chosen to span the space of SAGD potential. Similar to the connected volume ranking measure, the optimal vertical production well position is a good ranking parameter because it should be well correlated to SAGD production performance parameters.

In practice, multiple well pair drainage volumes exist and, for each volume, the parameter values should be calculated for as many realizations of the geology exists. Ranking is then done on a *global* realization basis as well as a *local* drainage volume basis. In such a case, the 0.10, 0.50 and 0.90 quantile values for the global realizations specify the SAGD well pair locations to be input into the flow simulator and the 0.10, 0.50 and 0.90 quantile value realizations within each of these realizations can be said to span the SAGD potential of each of the chosen locations.

Many other ranking measures can be used as long as they are well correlated to SAGD performance. For example, the volume of sand or the volume of shale within each chosen drainage volume can be used to rank the realizations. The sand volume and shale volume are well correlated – positively and negatively, respectively – to the cumulative SOR and oil production rate. This correlation allows inference, with an attached uncertainty, of SAGD production performance at drainage volumes not actually run through the flow simulator.

9.2.1 CONNECTED VOLUME

For the SAGD well pair drainage volume chosen in the example, the connected drainage volume is calculated for each of the 100 re-gridded realizations. Unlike the local

connectivity calculations in section 8, the connectivity program used now is thought of as a global connectivity calculation. It is global in the sense that it is calculated for the entire local drainage volume, but really, it is local. For a particular realization, each cell within the fine-scale local drainage volume is assigned a binary code of 1 or 0 if the cell is connected or unconnected, respectively. The cell volume is now 10 x 1 x 0.5 = $5m^3$ and the same porosity threshold of 9% is used.

The distribution of 100 connected volume values is shown in Figure 9.5 in the form of a histogram and probability plot. The 0.10, 0.50 and 0.90 quantile values (where the probability of exceeding the connected contained net bitumen value is 90%, 50% and 10%, respectively) are 8.65 x 10^6 m^3, 9.09 x 10^6 m^3 and 9.58 x 10^6 m^3, respectively; the realization numbers corresponding to these three quantile values are 49, 68 and 03, respectively. These three finely gridded geological realizations, which span the space of SAGD potential (since connected volume is well correlated to SAGD performance output), are the input drainage volumes for flow simulation.

9.2.2 OPTIMAL PRODUCTION WELL ELEVATION

Here, the objective is to select an optimal vertical SAGD production well position for a particular aerial well pair location and nominal drainage volume. Shale above the producer well will reduce SAGD performance. The optimal vertical well placement is one that minimizes the probability of shale impeding performance. Visualization software such as GoCad helps our understanding of the shale variability and can assist in the well placement process.

The optimal vertical well placement procedure is based on a parameter much like the one used for ranking. In Norrena and Deutsch (2002), this parameter is connected pore volume above the producer well location. The calculation of this pore volume connectivity is not the same as the connectivity calculations in sections 9.2.1 or 8.2. Here, connectivity is calculated at each cell as the proportion of net reservoir that is encountered in a straight line of sight from a producer well location and the cell, see Figure 9.6. In this context, connectivity is a percent. The greater the fraction of net reservoir along this line of sight, the more likely the bitumen will be produced. A pore volume multiplicative factor is then considered as a function of this connectivity parameter. This penalty function is shown in Figure 9.7. There is no pore volume discount when the net percent is 100% and there is considered to be no pore volume when the net fraction is equal to or less than a threshold of 50% and a penalty factor of 0 is obtained. The result is a total weighted pore volume associated to each vertical producer well location.

Figure 9.8 shows the results of this procedure for the SAGD example of this report in the form of a plot of the vertical producer well elevation versus the weighted pore volume. The orange line corresponds to the 50% threshold penalty function, while the yellow and purple lines refer to less and more severe penalty functions with thresholds of 0% and 75%, respectively. In all cases, the optimal vertical producer well position is approximately 24m above the base of the reservoir. This optimal producer well position

corresponds to a pore volume of approximately 26, 000 m^3 for the 50% connectivity threshold. Although it is not done, multiple realizations of this pore volume for the 50% connectivity threshold can be created and ranked in increasing order. Similar to the connected volume ranking technique, the 0.10, 0.50 and 0.90 quantile realizations can be said to span SAGD uncertainty and be input into the flow simulator. This is possible because the weighted pore volume associated to the optimal vertical producer well positions would be well correlated to the SAGD performance parameters.

Using this method, not only can we reduce the input into the flow simulator and still span SAGD performance, but we can also decide on the best vertical position for the producer well within a particular nominal drainage volume.

9.3 FLOW SIMULATION

Once an appropriate number of well pair volumes that span the space of SAGD potential are established by whatever ranking measure/s, they are input into the flow simulator. Flow simulation provides the SAGD performance, that is, the cumulative steam-to-oil ratio and oil production rate for each of the well pair drainage volumes input. These are the final parameters that are used to characterize potential SAGD reservoirs. Flow simulation is not performed in our example; however, we discuss how to use the results in practice.

9.4 ANALYSIS OF FLOW SIMULATION RESULTS

Once flow simulation is implemented on the selected SAGD drainage volumes selected, the cumulative SOR and oil production rate are used to make some final engineering decisions regarding the production of the entire SAGD reservoir. Since we did not perform the flow simulation for the SAGD example of this report, a potential SAGD reservoir in Northern Alberta is explored in this context. Deutsch, Dembicki, and Yeung (2002) is applicable.

The potential Northern Alberta SAGD reservoir was geostatistically investigated using the same geostatistical procedure applied to the SAGD example of this report. Based on a volume of sand global and local ranking measure, the 0.25, 0.50, 0.75 and 1.00 quantile sand volume quantile drainage volume locations were chosen; then the 0.10, 0.50 and 0.90 sand volume quantile realizations (high, medium and low, respectively) within each of these locations was chosen. In this way, twelve SAGD well pair drainage volume geological realizations were input into the flow simulator. Flow simulation was implemented to get the SOR and cumulative oil production rate performance parameters for this reservoir.

9.4.2 CUMULATIVE SOR AND OIL PRODUCTION RATE

The cumulative SOR and oil production rate should be well correlated. For the Northern Alberta oil sands SAGD reservoir, Figure 9.9 shows the almost perfect negative

correlation between SOR and rate. Each SOR-rate point is one of twelve drainage volumes selected for input into a flow simulator. For this project, the ranking parameter is volume of sand. The numbers 1, 2, 3, 4 are used to indicate the well pair drainage volumes selected and the capital letters L (low), M (medium), H (high) indicate the p-90, p-50 and p-10 realizations, respectively, selected within each of the 4 drainage volumes.

The correlation between production performance calculated from flow simulation and the ranking parameter used to select the input drainage volumes is important. This correlation is the link between geology and production performance or between geological uncertainty and final production uncertainty. This correlation relationship allows us to infer the cumulative SOR and oil production rate at drainage volumes in between the ones input into the flow simulator based on the ranking procedure used. Figure 9.10 shows the relation between the flow results for the twelve drainage volumes and the volume of sand ranking parameter in the previously mentioned Northern Alberta reservoir.

In order to predict the production variables for any SAGD drainage volume, that is any value of the ranking parameter, the flow results of the selected drainage volumes must be filled in. This is based on the correlation between the flow results and the ranking parameter (Figure 9.10). Figure 9.11 shows the points in Figure 9.10 with synthetically created points in between. These infill points allow the production performance to be inferred at any sand volume value, that, is any SAGD drainage volume in the reservoir. Therefore, since every realization at each of the potential SAGD locations has an associated volume of sand, through Figure 9.11, every realization can also be associated to a cumulative SOR and oil production rate.

9.4.2 UNCERTAINTY ANALYSIS

An analysis of the final production uncertainty can now be made. Uncertainty in SAGD well production is linked to the underlying geological uncertainties, which are the variations in the geological model that are permissible while remaining consistent with all the available data. The differences in the realizations quantify uncertainty. This geological uncertainty can be transformed to uncertainty in SAGD well productivity with the link between geological uncertainty and production performance (see Figure 9.11).

One other engineering decision to be made is the number of wells needed to produce a given amount of bitumen. This is based on the final SAGD well production uncertainty as provided by the link between geological uncertainty and production. The sequencing of well pairs must be decided prior to this uncertainty analysis and is usually based on the most optimal locations being produced first.

For the potential SAGD reservoir in Northern Alberta discussed in this section, forty-eight non-overlapping SAGD well pair volumes that would produce the entire net reservoir volume were chosen. For every geological realization within each of the forty-eight SAGD drainage volumes, the volume of sand is calculated. The p-10, p-50 and p-90 volume of sand within each drainage volume is established and then the link between

geological uncertainty and production (Figure 9.11) is used to get the corresponding p-10, p-50 and p-90 SOR and oil production rate values.

Assuming the drainage volumes with the highest SAGD potential, that is the highest volume of sand, are first in the production sequence, the uncertainty in cumulative production rate for increasing well pairs is shown in Figure 9.12. Note that the uncertainty increases with more well pairs.

The value of additional exploratory core holes, seismic data or any other delineation information is that the final production uncertainty will be reduced. A geostatistical simulation exercise could be used to address the reduction in geological uncertainty due to additional delineation information.

9.5 CONCLUSIONS

The results in this report communicate the main features of SAGD reservoir characterization: (1) flow response is linked to geological variations characterized by geostatistical techniques, (2) production uncertainty is captured by the geostatistical methods and (3) it is possible to reliably assess uncertainty in flow response due to geological variability.

9.5 FIGURES

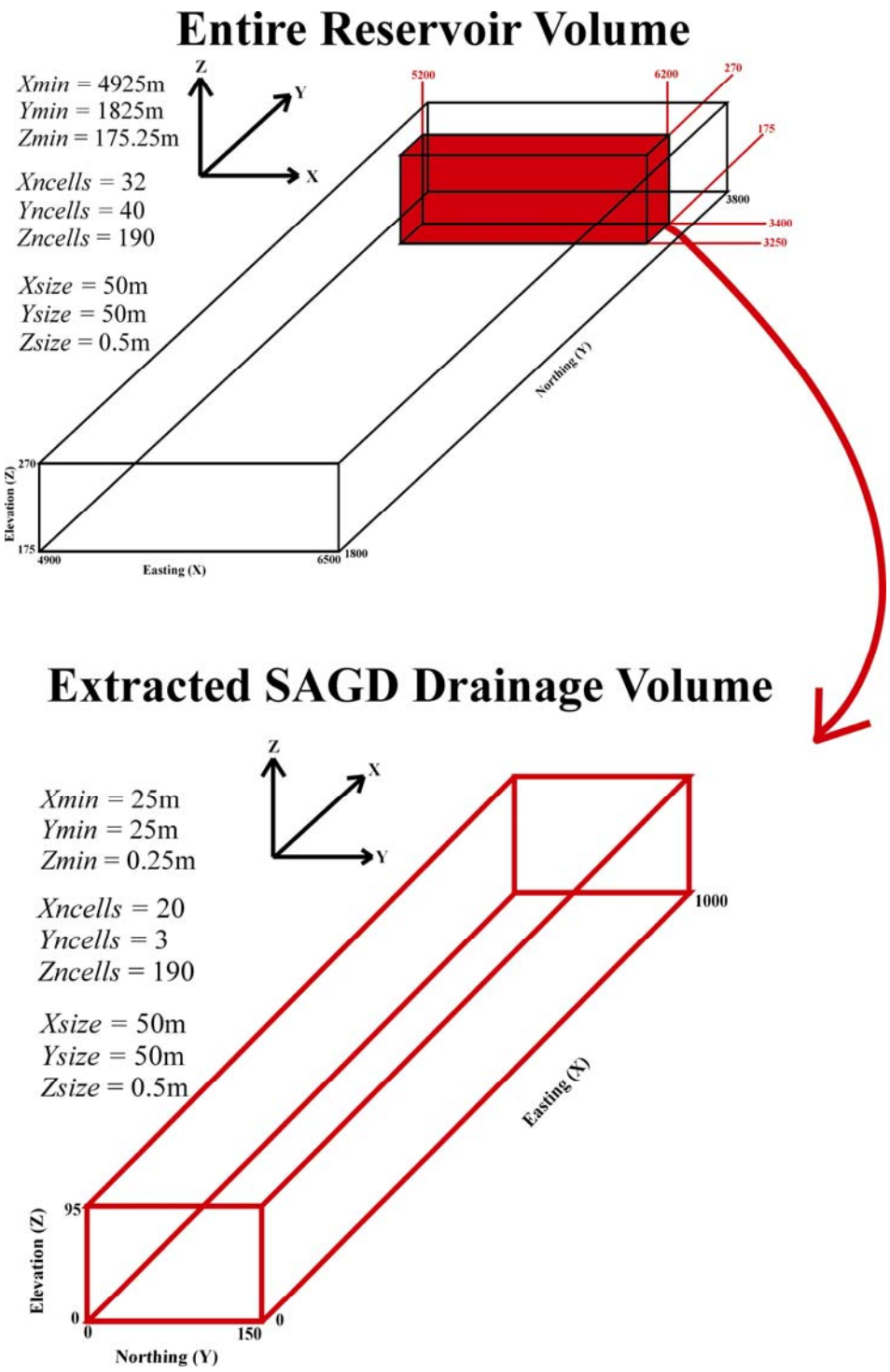

Figure 9.1 – Extracted SAGD Drainage Volume. An illustration of the volume that is extracted from the large reservoir model in the SAGD example. The extracted volume is shown in red. The grid specification for the reservoir model and the drainage volume are also shown. Note the *X*-*Y* coordinate direction reversal when sketching the extracted volume.

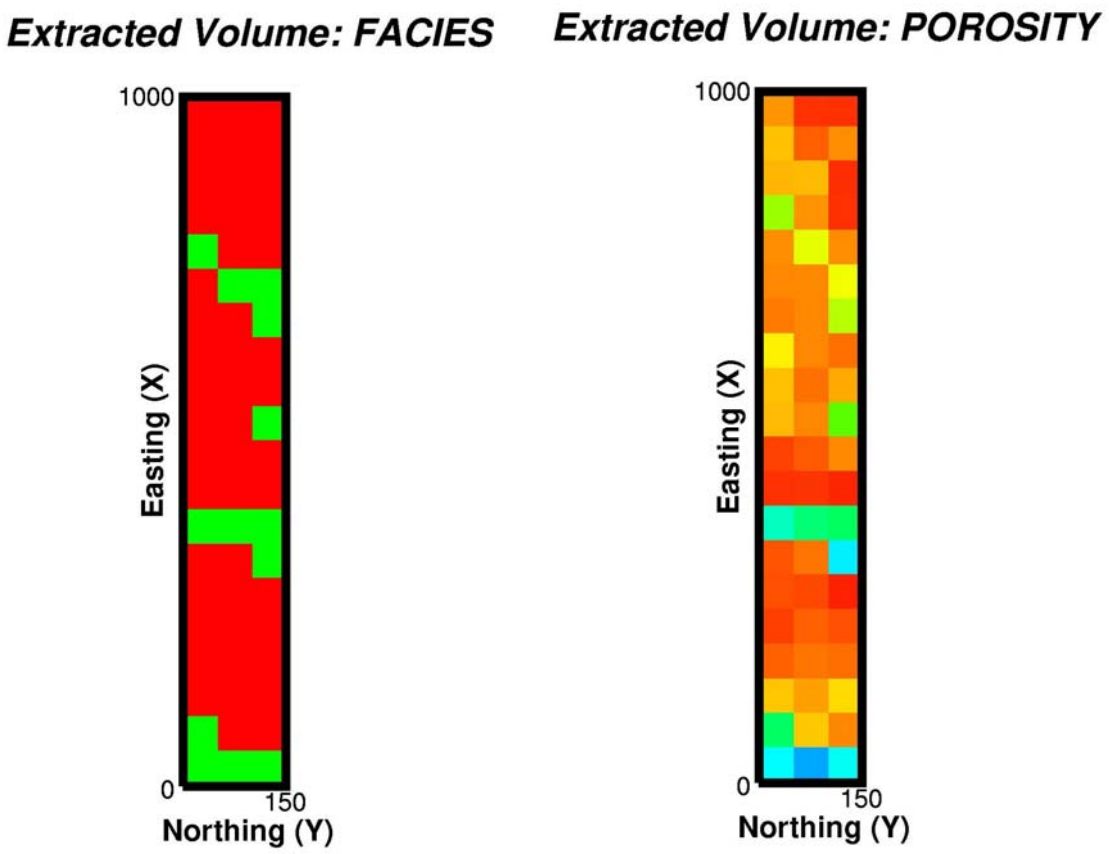

Figure 9.2 – Extracted Volume: Facies and Porosity. The central slice through the 50th facies (left) and 50th porosity (right) extracted volume realizations. The same color schemes used in Figures 6.1 (for facies codes) and 7.1 (for porosity) are used here. Only the porosity within sand and breccia need to be recalled for this particular section.

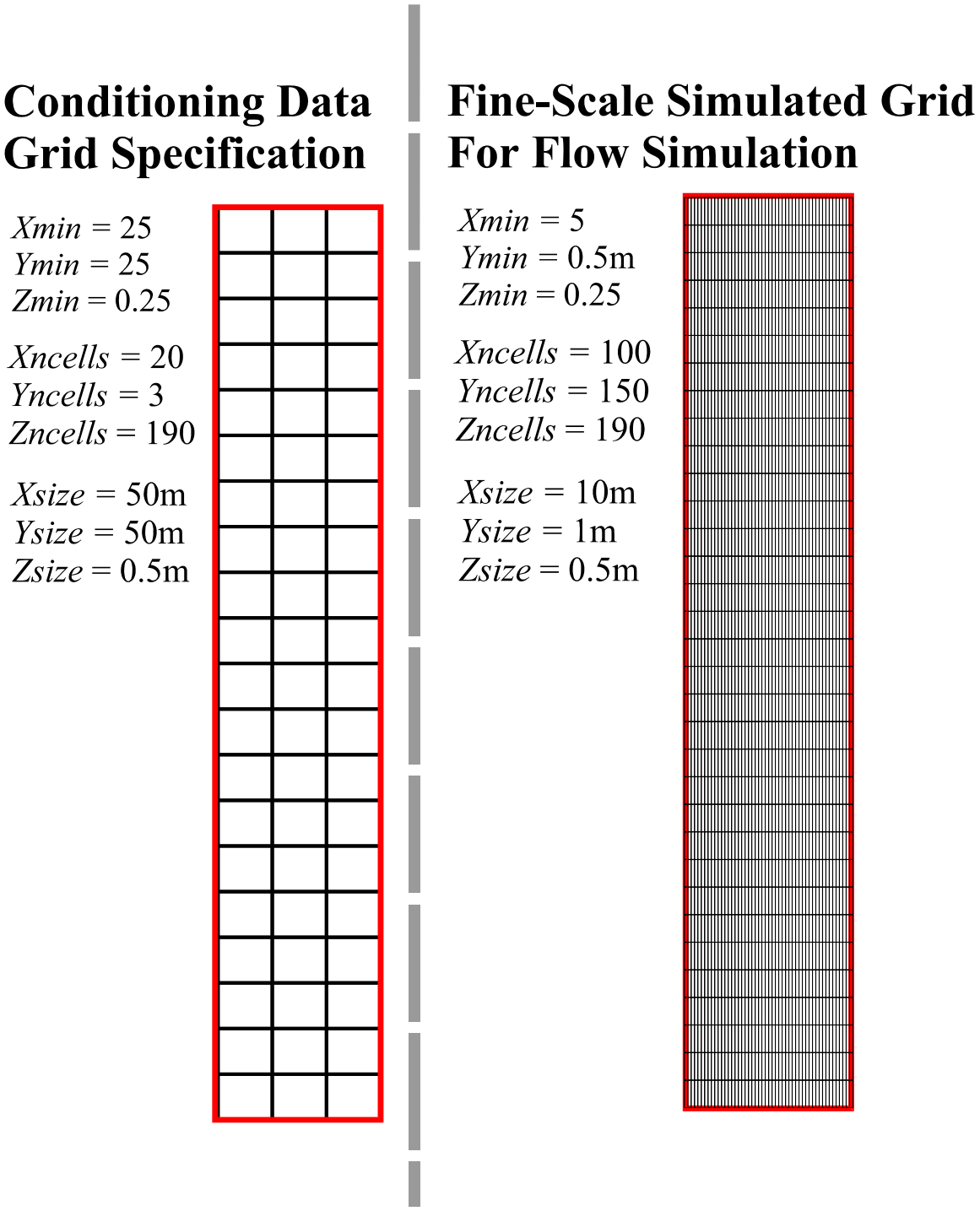

Figure 9.3 – Re-Gridding. An illustration of the grid specifications for the coarse conditioning data extracted and the fine grid to be simulated. Only 2-Dimensional *X*-*Y* slices are shown since the grid is the exact same in the elevation (*Z*) direction.

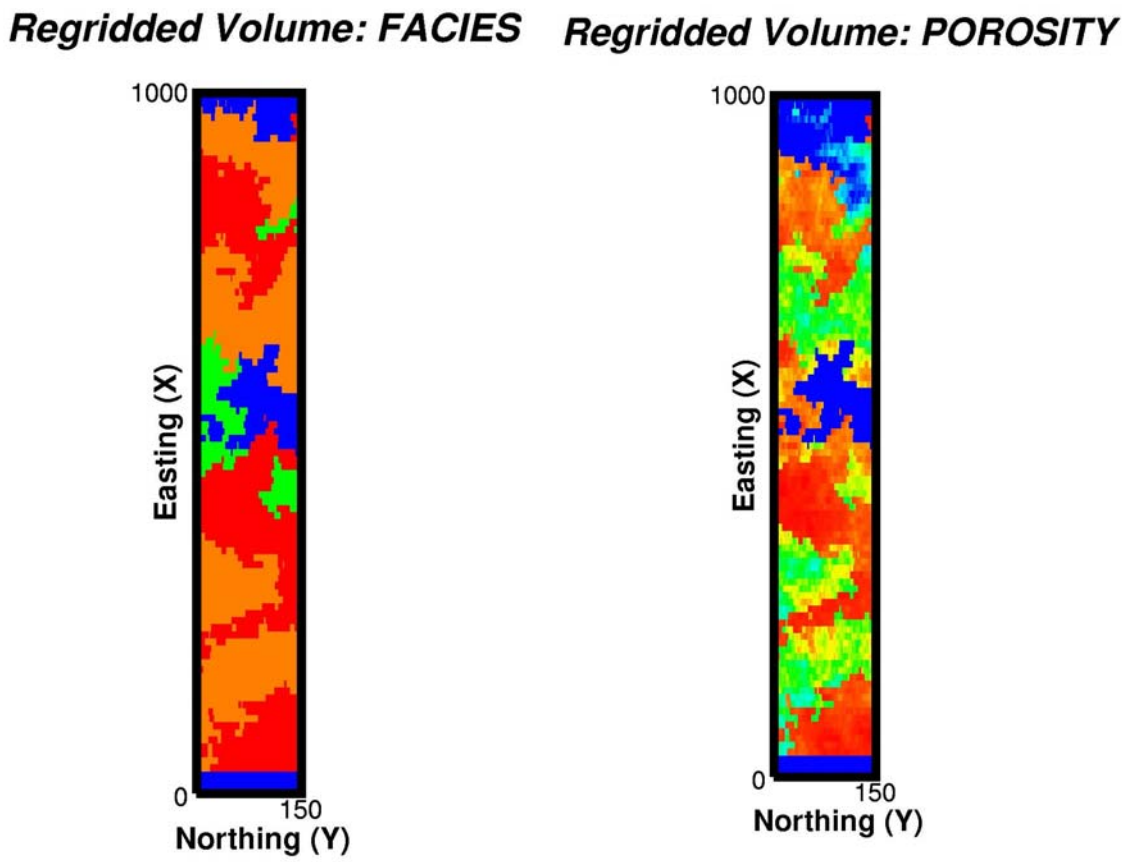

Figure 9.4 – Re-Simulated Facies Realization. An illustration of the 50th lithofacies and porosity realization after being re-simulated using the extracted conditioning data. The central *X*-*Y* section is shown. The same categorical color scheme used in Figures 6.1 and 7.1 are used in this figure.

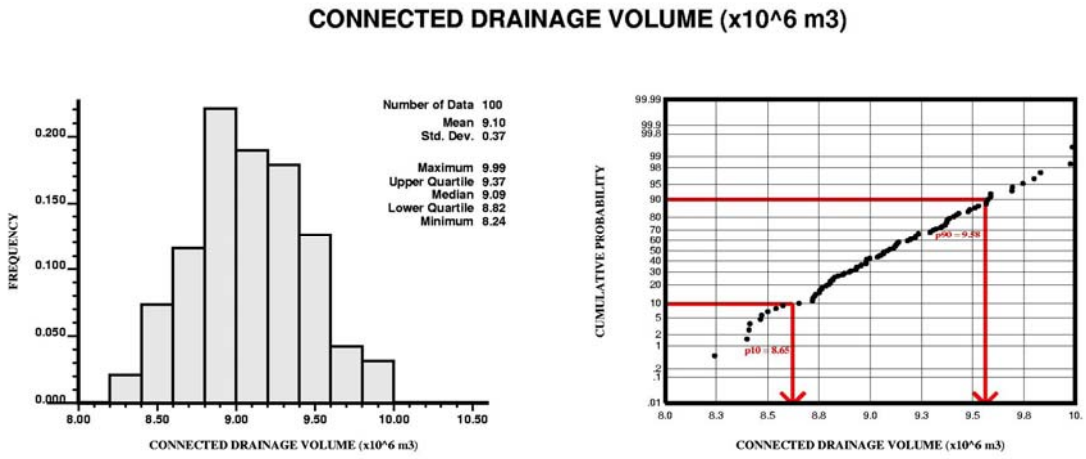

Figure 9.5 – Connected Contained Net Bitumen. The results of the connected contained net bitumen transfer function within the SAGD drainage volume. The histogram on the left shows the expected value and uncertainty in units of m^3. The probability plot on the right reveals the connected contained net bitumen values where the probability of exceeding is 90% (the 0.10 quantile), 50% (the 0.50 quantile) and 10% (the 0.90 quantile). The realizations corresponding to these quantile values are also specified.

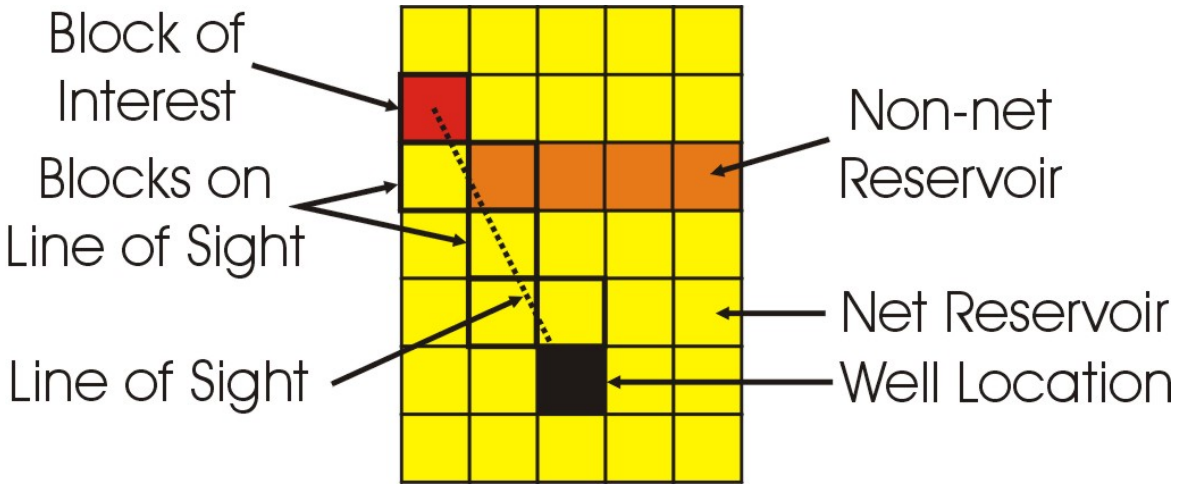

Figure 9.6 – Connected Pore Volume Calculation. An illustration of the method used to calculate connected pore volume for optimal vertical well placement. Connected pore volume is calculated by evaluating the fraction of non-net blocks on a line of sight path from a block of interest to the well location. The figure shows a straight line connectivity of 20% (1 out of 5).
(Source: *Norrena and Deutsch (2002)*)

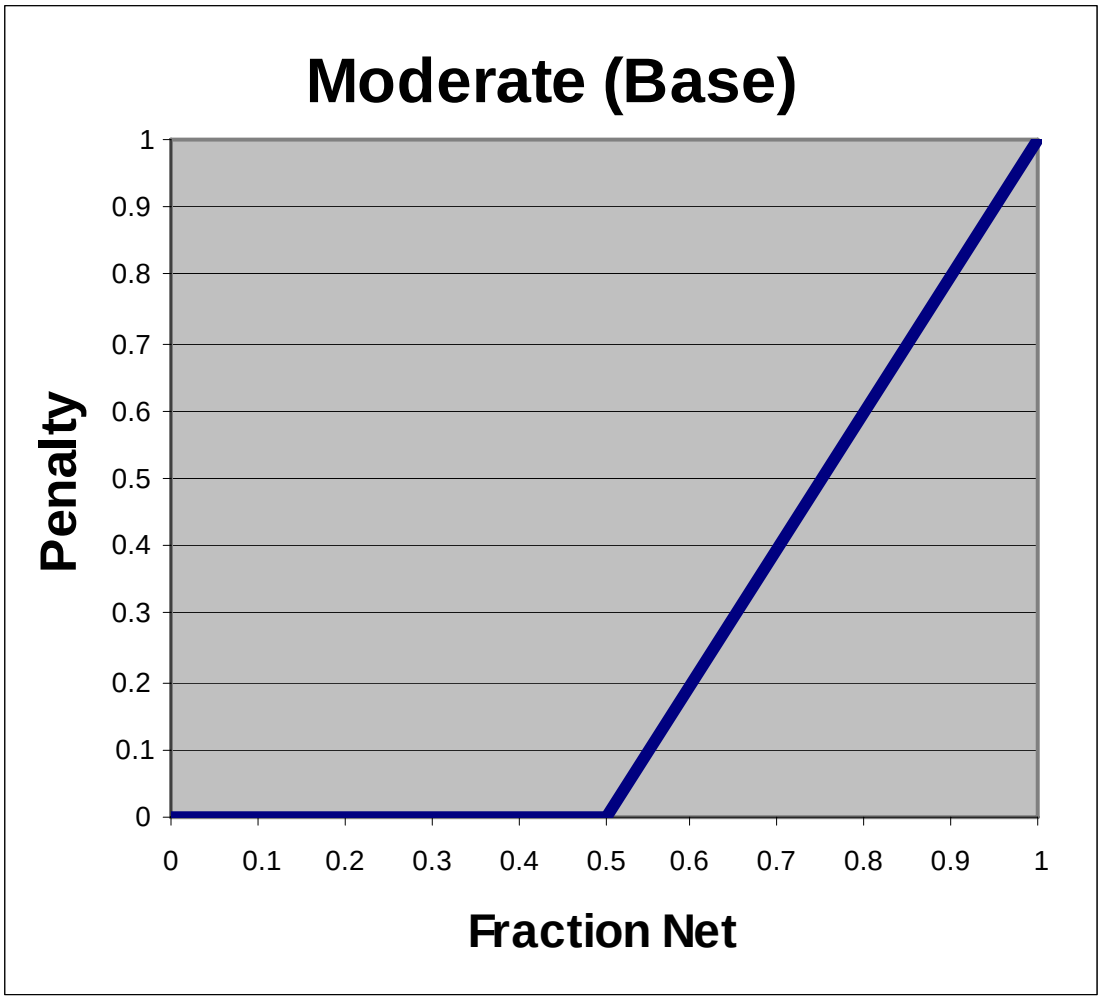

Figure 9.7 – Connected Pore Volume Penalty. An illustration of the penalty function used for ranking according to optimal vertical well placement. The weighted pore volume increases as the connected pore volume percent increases after a net straight line connectivity fraction of 50% is reached.
(Source: *Norrena and Deutsch (2002)*)

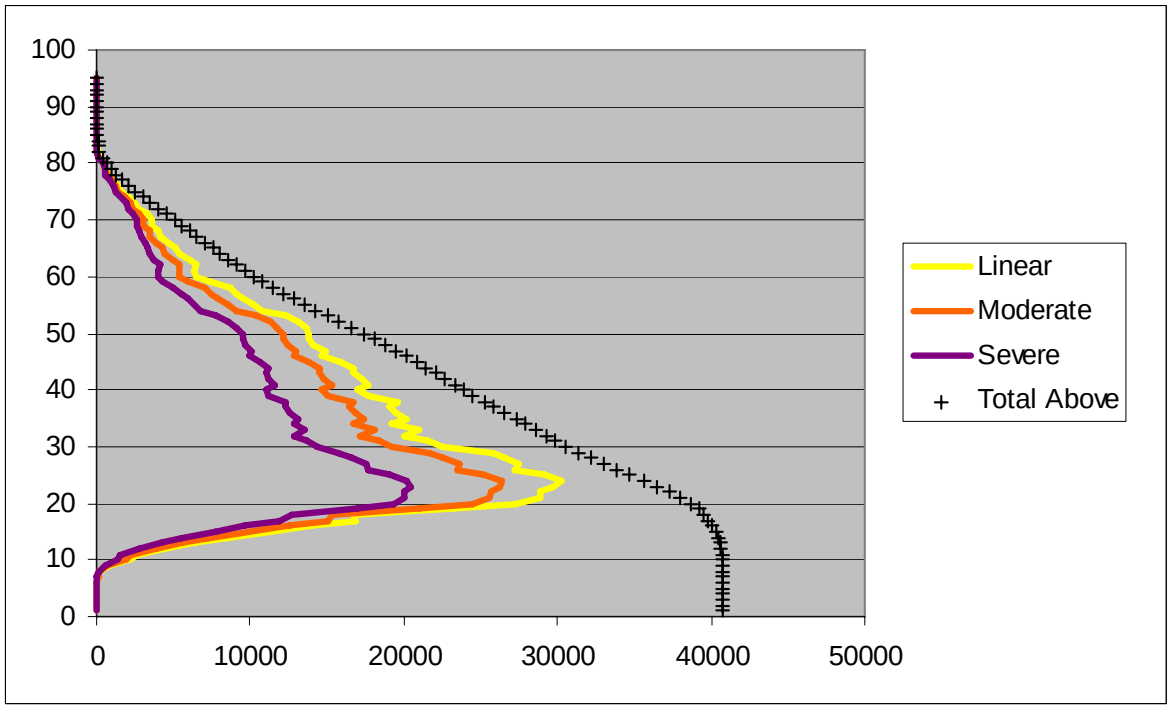

Figure 9.8 – Optimal Vertical Production Well Placement. A plot of the elevation vs. the weighted pore volume. The line is the average pore volume taken over all 100 finely gridded geological realizations within the chosen SAGD drainage volume. The optimal vertical SAGD well placement is at an elevation of approximately 24 m.
(Source: *Norrena and Deutsch (2002)*)

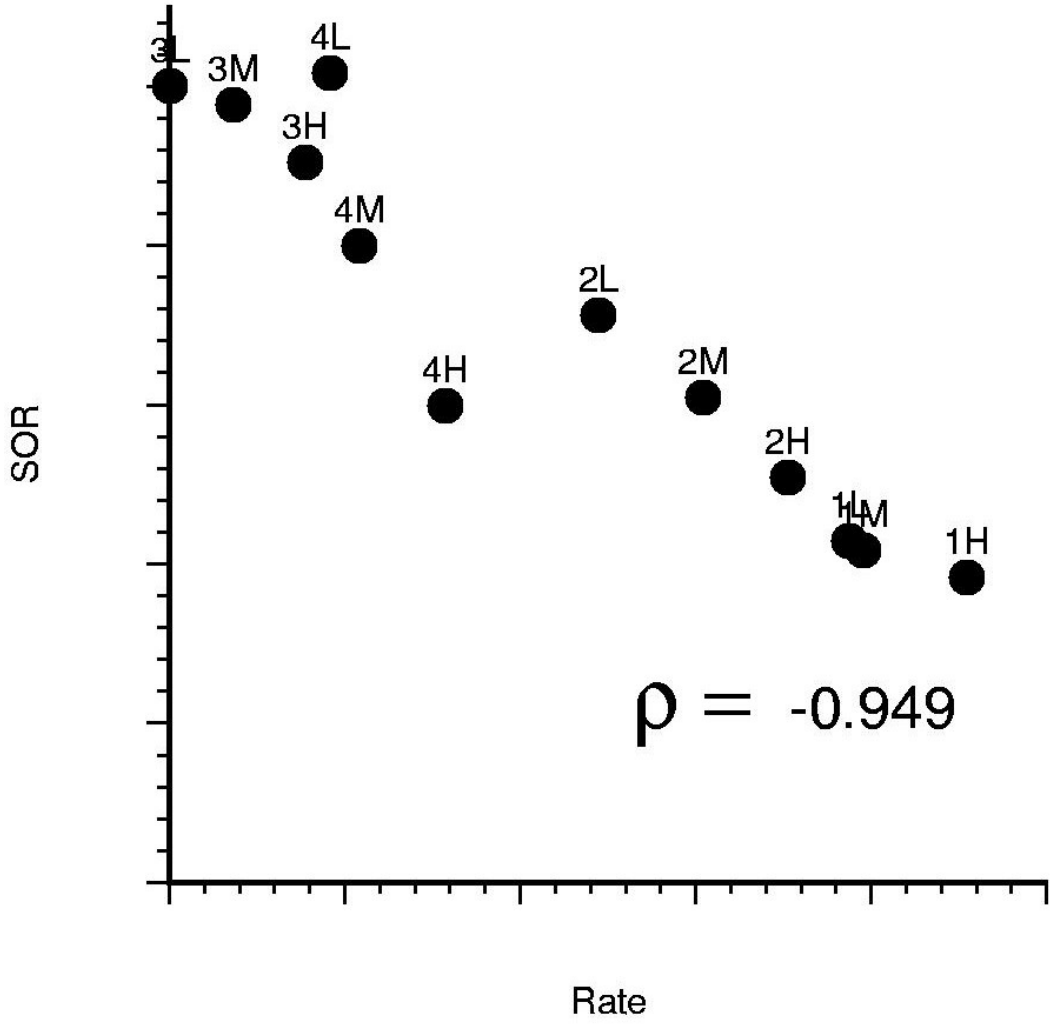

Figure 9.9 – SOR vs. Rate. A cross plot between SOR and oil production rate for a Northern Alberta potential SAGD reservoir. The four well pair drainage volume locations (1, 2, 3 and 4) are labeled with the p-90, p-50 and p-10 (L, M, H) realizations within each location. Note the excellent negative linear correlation.

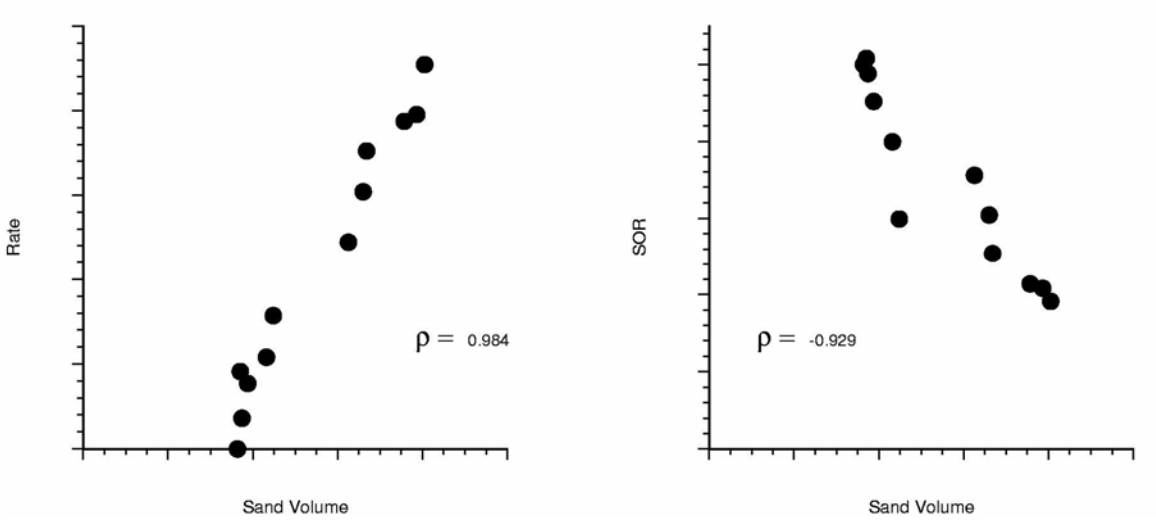

Figure 9.10 – Flow Results vs. Ranking Parameter. A cross plot between oil production rate and volume of sand and of SOR and volume of sand for the Northern Alberta potential SAGD reservoir. The twelve cases depicted in Figure 9.9 are used to construct the points. Note the excellent correlation in both SAGD production output cases.

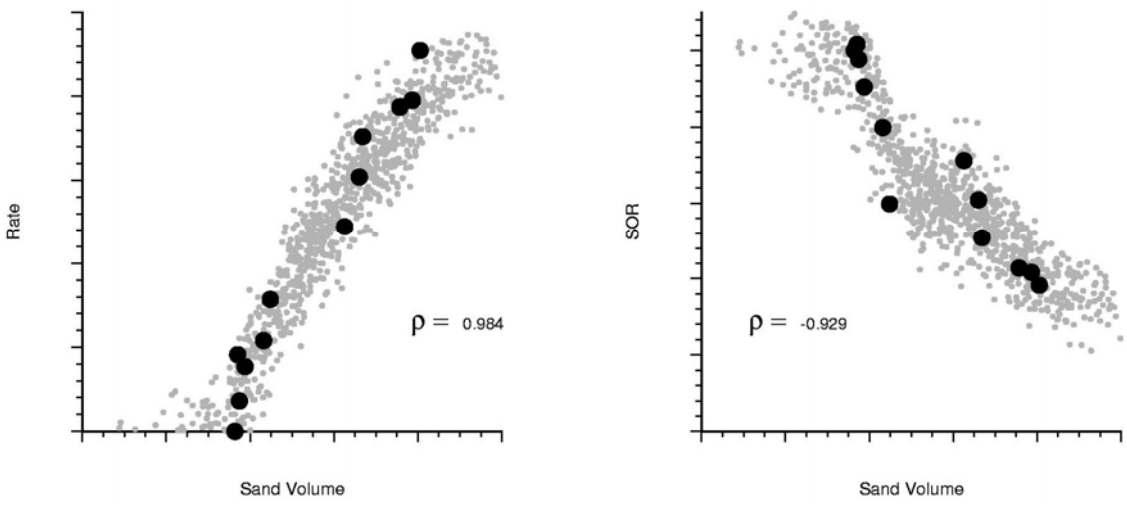

Figure 9.11 – Flow Results Inference. An illustration of the synthetically created data used to fill in the correlation between SOR and volume of sand and rate and volume of sand for the Northern Alberta potential SAGD reservoir. This allows the inference of production performance at the SAGD drainage volumes not input into the flow simulator. The correlation reported is that of the synthetic data sets.

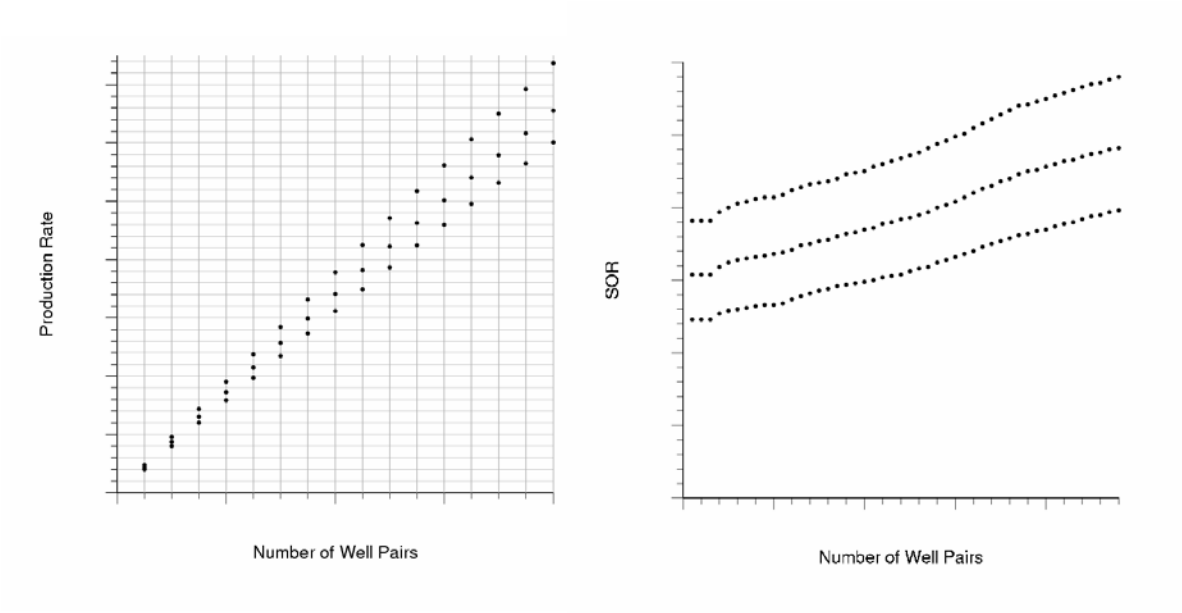

Figure 9.12 – Uncertainty in Oil Production Rate. An illustration of the uncertainty in cumulative oil production rate (left) and SOR (right) with the number of production well pairs. For each well pair number increment, the p-10, p-50 and p-90 rate is plotted.

10 REFERENCES

- Alberta Research Council (ARC) and Alberta Energy Research Institute (AERI), 2001.*Thermal Gravity Processes*, Power-point, AERI/ARC Core Industry Research Program.

- Denbina, E.S., 1998. *SAGD Comes of AGE!*, Journal of Canadian Petroleum Technology, 37(7):9-12.

- Pooladi-Darvish, M. and Matter, L., 2001. *SAGD Operations in the Presence of Overlying Gas Cap and Water Layer – Effect of Shale Layers*, Canadian Institute of Mining and Metallurgy (CIM), no. 178.

- Card, C.C., Woo, J. S., Wang, C. and Hu, Z., 1998. *CNPC Liaohe Dual Well SAGD – The Journey from Vision to Reality*, Canadian Institute of Mining and Metallurgy (CIM), no. 134.

- Komery, D. P., Luhning, R. W. and Pearce, J. V., 1998. *Pilot Testing of Post-Steam Bitumen Recovery from Mature SAGD Wells in Canada*, Canadian Institute of Mining and Metallurgy (CIM), no. 214.

- Shangqi, L., Yongrong, G., Zhimian, H., Naiqun, Y., Liping, Z. and Suning, H., 1998. *Study on Steam Assisted Gravity Drainage with Horizontal Wells for Super-Heavy Crude Reservoir*, Canadian Institute of Mining and Metallurgy (CIM), no. 217.

- Komery, D.P., Luhning, R.W. and O'Rourke, J.C., 1999. *Towards Commercialization of the UTF Project Using Surface Drilled Horizontal SAGD Wells*, Journal of Canadian Petroleum Technology, 38(9):36-40.

- Das, S.K., 1998. *Vapex: An Efficient Process for the Recovery of Heavy Oil and Bitumen*, Society of Petroleum Engineering (SPE), no. 50941, 3(30):232-236.

- Edmunds, N.R. and Sugget, J.C., 1995. *Design of a Commercial SAGD Heavy Oil Project*, International Heavy Oil Symposium, June 1995, Calgary, Alberta, Canada.

- Singhai, A.K, Das, S.K., Leggitt, S.M., Kasraie, M. and Ito, Y., 1996. *Screening of Reservoirs for Exploitation by Application of Steam Assisted Gravity Drainage/Vapex Processes*, International Conference on Horizontal Well Technology, November 1996, Calgary, Alberta, Canada.

- Palmgren, C. and Edmunds, N., 1995. *High Temperature Naptha to Replace Steam in the SAGD Process*, International Heavy Oil Symposium, June 1995, Calgary, Alberta, Canada.

- Edmunds, N., 1999. *SAGD: Present and Future Challenges*, APEGGA Professional Development Conference, April 1999, Calgary, Alberta, Canada.

- Llaguno, P.E., Moreno, F., Garcia, R., Mendez, Z., Escobar, E., 2002. *A Reservoir Screening Methodology for SAGD Applications*, Canadian International Petroleum Conference, June 2002, Calgary, Alberta, Canada.

- Gong, J., Polikar, M. and Chalaturnyk, R.J., 2002. *Fast SAGD Geomechanical Mechanisms*, Canadian International Petroleum Conference, June 2002, Calgary, Alberta, Canada.

- Akgun, F., 2002. *Drilling Stable Horizontal Wells – A Key Problem in Modern Oil Well Drilling*, Canadian International Petroleum Conference, June 2002, Calgary, Alberta, Canada.

- Deutsch, C. V., Dembicki, E. and Yeung, K. C., 2002. *Geostatistical Determination of Production Uncertainty: Application to Firebag Project*, Center for Computational Geostatistics (CCG), University of Alberta, Edmonton, Alberta, Canada.

- Norrena, K. P., Deutsch, C. V., 2002. *Automatic Determination of Well Placement Subject to Geostatistical and Economical Constraints*, SPE International Thermal Operations and Heavy Oil Symposium and International Horizontal Well Technology Conference, November 2002, Calgary, Alberta, Canada.